DYNAMIC AND SPATIAL PROPERTIES OF SATELLITES

IN ISOLATED GALACTIC SYSTEMS

by

ABEL B. DIAZ, B.S., M.S.

A DISSERTATION

IN

PHYSICS

Submitted to the Graduate Faculty
of Texas Tech University in
Partial Fulfillment of
the Requirements for
the Degree of

DOCTOR OF PHILOSOPHY

Approved

Ronald Wilhelm
Chairperson of the Committee

Lynn Hatfield

Beth Ann Thacker

Accepted

John Borrelli
Dean of the Graduate School

December, 2006

TABLE OF CONTENTS

ABSTRACT

Using the NYU Value-Added Galaxy Catalog (NYU-VAGC) I examine the line-of-site velocity dispersion, σ_v, of satellite galaxies orbiting larger, isolated, primary galaxies. The line-of-sight dispersion can be directly compared to the functional form of three models (NFW, MOND and a relic neutrino based model) that diverge at large distances allowing discrimination between models. The algorithm used to determine the primary and satellite samples yielded 2741 primary galaxies and 4966 possible satellites. After removing foreground/background interloper galaxies, I found the NFW model is the most probable. This agrees well with other published results which find that the density of the dark matter halo declines as $\rho \propto r^{-3}$. The neutrino model has large probabilities and cannot be completely excluded as a possible explanation of the observed velocity dispersions. The MOND model had small probabilities of fitting the velocity dispersion, and results of higher dispersions found for early type primaries than those found for late type primaries of the same luminosity make MOND unlikely.

From the data I find no evidence of the Holmberg Effect. Satellite galaxies tend to be isotropic both at small projected distances from the primary galaxy and at large projected distances (at the 1σ level) from the primary galaxy. However, I do find that the distribution of early type satellites tends to decline more steeply than the late type satellites in a high magnitude primary sample.

I was also able to examine the line-of-sight velocity dispersions in two directions: parallel to the plane of the galaxy and perpendicular to the plane of the galaxy along the axis of rotation. From sampling the velocity profiles of primary galaxies at different tilt angles relative to the axis of rotation, I find that the velocity distribution of satellites is isotropic about the primary, suggesting that the dark matter halo is spherical in shape.

Finally, I also find that the velocity dispersion of satellites within $125 kpc$ scales with the luminosity of late type primary galaxies as $\sigma \propto L^{0.22 \pm 0.02}$.

LIST OF TABLES

LIST OF FIGURES

CHAPTER I

SCIENTIFIC BACKGROUND

1.1 Introduction - Discovery of Dark Matter

The existence of dark matter has been a subject of debate for decades.

Investigating dark matter has been a tricky task because dark matter does not emit or

reflect light. Therefore the methods to study dark matter have involved observing its

effect on regular matter. The first observation that provided proof of dark matter was

made by Zwicky [1]. He found an unexpectedly large velocity dispersion,

$\sigma = 1019 \pm 360 km/s$ while studying the Coma Cluster. Zwicky concluded that the mean

density of the Coma Cluster would have to be 400 times greater than the density he

determined from the luminous matter for a velocity dispersion of $1000 km/s$. Six years

later, Babcock [2] obtained long-slit spectra of the Andromeda galaxy (M31), which

showed that the outer region of M31 was rotating with an unexpectedly high velocity.

This indicated either a high outer mass-to-light ratio or strong dust absorption.

These observations by Babcock indicated that the mass in the outer regions of the

Andromeda galaxy increased with distance from the center of the galaxy, even though the

optical luminosity of M31 did not. From these observations Roberts & Whitehurst [3]

concluded that the mass-to-light ratio had to be $\geq 200 \, (M/L)_\odot$ in the outermost regions of

the galaxy. From N-body simulations Ostriker & Peebles [4, 5] concluded that

instabilities in galaxy disks could be prevented by a massive spherical "halo" component

which showed that the mass of a galaxy increases with increasing radius. Today this "halo" is referred to as the "dark matter halo."

1.2 What is Dark Matter?

Ideas of what this dark mass could be range from massive black holes, to low-mass brown dwarfs, to sub-atomic particles. Possible candidates are divided up into two groups: Massive Astrophysical Compact Halo Objects (MACHOS) and Weakly Interacting Massive Particles (WIMPs).

MACHOS are comprised of ordinary matter such as brown dwarfs and black holes. Because of their relatively low mass, brown dwarfs do not have high enough internal temperatures and pressures to initiate thermonuclear reactions and, therefore, can not emit sufficient amounts of radiation to be detected by today's technology. Isolated black holes cannot be directly observed because the escape velocity for a black hole exceeds the speed of light.

As for the WIMPs, they include particles like neutrinos and axions. Axions are a hypothetical elementary particle proposed to explain the absence of an electrical dipole moment for the neutron [6]. The axion has no electric charge, no spin, and interacts with ordinary matter only weakly. If they exist, they should have only a tiny mass and would have been produced abundantly in the Big Bang, which make relic axions an excellent candidate for dark matter. There have been indirect searches for WIMPs with data from the Super-Kamiokande detector by looking for a high energy neutrino signal resulting

from WIMP annihilation events in the Earth, the Sun, and the Galactic Center. This technique has produced no significant results to date [7].

Neutrinos are also neutral, abundant, and interact weakly with matter. Currently their mass is uncertain. Best mass estimates to date are in the range $0.05\,eV/c^2 < m_{\nu_e} < 2.2\,eV/c^2$. Where their true mass falls within this range will decide if they significantly contribute to the dark matter problem.

In recent years there has been a growing number of black hole and brown dwarf discoveries but not enough to explain the mass discrepancies in the Universe. The EROS and MACHO [8] collaborations have each published upper limits on the amount of dark matter in the halo of the Milky Way obtained from gravitational microlensing searches. They showed that the MACHO's can account for no more than ~25% of the halo mass.

1.3 Dark Matter

1.3.1 Do We Need Dark Matter?

The evolution of structures in the Universe can be understood within a "bottom-up" scenario. In this type of scenario, smaller substructures (such as dwarf galaxies) combine to form larger structures (such as large galaxies) which further combine to form large scale structures (galaxy clusters, super clusters, and filaments). Observational evidence such as the impending collision of the Milky Way and M31, the infall of the Local Group into the Virgo cluster, and sub-clustering found in most galaxy clusters, all support the hierarchical scenario.

Because the aggregation of structures is driven by gravity, the overall density of the Universe over time is pivotal in how the Universe appears. In order for structures to form from gravitationally attracted matter, the density of local matter must be larger than the density of the Universe [9]. Contrary to the inadequate amounts of matter detected by observation to initiate structure formation, Plionis and Basilakos [10] found a strong indication that clusters develop in a hierarchical fashion. Because there exists evidence of clustering, there must be another form of undetectable matter (dark matter) that initiated structures in the early Universe.

1.3.2 Cosmological Models

During the past decade cosmological simulations have shown the need for a dark matter component to mimic the hierarchical scenario process. Hoffman [11] pointed out that the structure of dark matter halos should depend on the value of the baryon density, Ω_B. Based on a systematic N-body study of halo formation in a range of hierarchical clustering cosmologies, Navarro, Frenk, and White (NFW) showed that the density profiles of Cold Dark Matter (CDM) halos can be fitted to a "universal" profile, independent of the halo mass [12, 13, 14, 15]. The issue is critical because the density profile that gives rise to a flat rotation curve ($\rho \propto r^{-2}$) is different from that predicted by cosmological models at larger distances ($\rho \propto r^{-3}$).

The NFW profile takes the form

$$\rho(r) = \frac{\delta_c \rho_{crit}}{(r/r_s)(1 + r/r_s)^2},$$
(1)

where $r_s = r_{200}/c$ is a characteristic radius, r_{200} is

$$r_{200} = 1.63 \times 10^{-2} \left(\frac{M}{h^{-1} M_{sol}} \right)^{1/3} \left[\frac{\Omega_0}{\Omega(z_0)} \right]^{1/3} (1+z_0)^{-1} h^{-1} kpc, \qquad (2)$$

where c is a dimensionless parameter, ρ_{crit}, is the critical density,

$$\rho_{crut} = \left(\frac{3H_0^2}{8\pi G} \right)(1+z_0)^3 \left[\frac{\Omega_0}{\Omega(z_0)} \right] \left(\frac{\delta_c}{cx(1+cx)^2} \right) \qquad (3)$$

and where x = r/r$_{200}$, and δ_c the characteristic density,

$$\delta_c = \frac{200}{3} \frac{c^3}{[\ln(1+c) - c/(1+c)]}. \qquad (4)$$

In this study $\Omega_0 = 1$. This corresponds to an Einstein-de Sitter cosmology and $z_0 \sim 0$ because the galaxy sample has low redshifts (z << 1).

1.4 Detecting Dark Matter

1.4.1 Gravitational Lensing

The delicate process of measuring dark matter is not limited to galaxy rotation curves. Zwicky [16] points out that "gravitational lensing" might provide useful information on the mass distribution of galaxies. Gravitational lensing is a consequence of general relativity which predicts that warped spacetime will bend light from a more distant source as it passes near a massive object.

Consider a bright object such as a quasar that is far away from the Earth. If there is nothing between it and us, we see one image of the quasar. Now consider figure 1.1. It

illustrates an example of a massive galaxy along the line-of-sight to the quasar. The light will be bent by the gravitational field around the galaxy and will produce twin images of the quasar as seen from Earth. This is called "gravitational lensing" since the intervening galaxy acts as a lens to focus the image of the distant quasar to a new location.
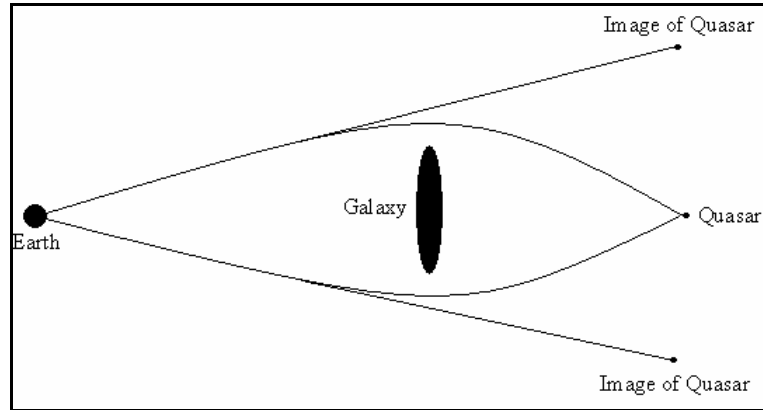
Figure 1.1: Basic Gravitational Lensing - A large galaxy between the observer and the source will bend light in such a way as to create a double image of the source.

According to general relativity, light passing at a distance r from a mass M is bent by an angle

$$\alpha \approx \frac{4GM}{rc^2} = \frac{2R_s}{r},$$
(5)

where R_s is the Schwarzschild radius $2GM/c^2$. Measuring α is a direct measurement of the halo mass interior to the distance r. This method does not rely on dynamical measurements of a tracer population (e.g. stars, gas, satellite galaxies) making it a powerful tool for measuring halo masses.

While gravitational lensing is a good method for probing the halos at large distances from the center of galaxies, this technique is complicated because lensing is inherently a multi-deflection problem. In an analysis of the first significant detection of lensing, Brainerd et al. [17, 18] found that more than 50% of their source galaxies should have been lensed by at least two or more foreground galaxies. That is, for a given source galaxy, it was clear that the closest lens on the sky to any given source was not necessarily the only lens, and neither was it necessarily the strongest lens. The uncertainty introduced by this multi-scattering severely limits the usefulness of this process.

1.4.2 Rotation curves

Estimates of the dark matter halo of galaxies can be made with rotation curves [2, 3, 19, 20]. The dark matter within disk galaxies can be estimated by plotting the Doppler velocity of the stars as a function of their distance from the center of the galaxy. The fact that the velocity curve does not decrease (Keplerian decline) as distance increases indicates the presence of more mass beyond the luminous component. These rotation curves can rarely be measured beyond twice the optical radius because of the lack of dynamical tracers. Satellite galaxies can provide a unique dynamical probe well beyond the optical radius of the central primary galaxy. While the inner parts of galaxy halos have been well studied and have density distributions that yield approximately flat rotation curves (example shown in figure 1.2), our understanding of the rotation curve at larger distances is much more uncertain.
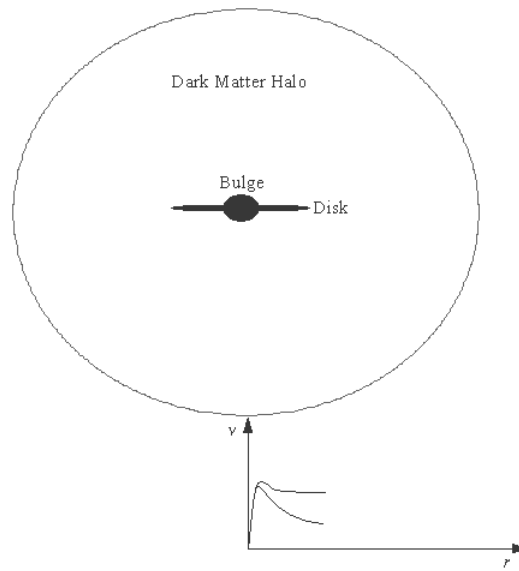
Figure 1.2: Example of a rotation curve relative to the galaxy above, showing that the rotational velocity deviates from a Keplerian decline and becomes constant at large radii.

One method to probe the mass distribution at large radii is to look at the velocity dispersions of satellites of a galaxy. Unlike the rotation curve for a disk galaxy where the stars are in uniform circular motion, the line-of-sight velocity for satellite galaxies only measures one component of the true satellite velocity. It is therefore necessary to characterize the velocity dispersion of the satellite system. A simple prescription for determining the velocity dispersion is to fit the radial velocity differences (radial velocity of the satellites minus the radial velocity of their primaries) with a Gaussian plus constant function. To study the mass distribution of galaxies in this way, a large number of satellites have to be used to accumulate enough statistics.

1.5 Possible Dynamic Explanations

1.5.1 Relic Neutrinos

The Universe is filled with relic neutrinos that were produced during the early stages of the Big Bang and have survived to the present day. These neutrinos have been affected by the expansion of spacetime and have slowed down enough to be influenced by the gravitational potential of individual galaxies [21, 22]. As galaxies form in a cluster, each of their gravitational wells becomes steeper and narrower over time. This changing of the potential can slow down or trap relic neutrinos as they pass through the forming galaxy. Consider the situation in the diagram below (figure 1.3 [23]). It shows the gravitational wells of several galaxies in a cluster. The longer arrows indicate the direction of relic neutrinos accelerating toward the galaxies. The shorter arrows indicate the direction of relic neutrinos decelerating away from the galaxies.
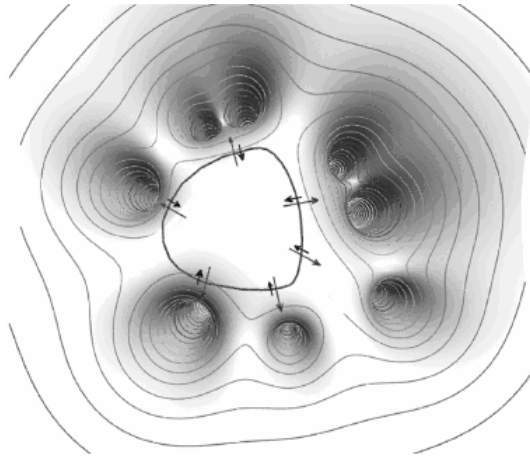
Figure 1.3: Diagram illustrating the gravitational wells of several galaxies in a cluster. The longer arrows show the direction of relic neutrinos accelerating toward the galaxies. The shorter arrows show the direction of relic neutrinos deceleration.

If a neutrino is traveling toward a forming galaxy, it will gain energy as it "falls" into the potential well. Over time the galaxy's mass has condensed causing the walls to become steeper than when the neutrino entered, so by the time the neutrino reaches the other end it cannot escape the galaxy's potential. This leads to an increase in mass within the galaxy's potential well. The mass density of the neutrino component beyond the disk is expected to scale as $\rho \propto r^{-3/2}$ [21].

1.5.2 Modified Newtonian Dynamics (MOND)

In the early 1980's Milgrom [24, 25] considered an alternative to dark matter for explaining the flat rotation curves in disk galaxies. Known as Modified Newtonian Dynamics (MOND), it describes the motion of bodies in a gravitational field by assuming that in the limit of small accelerations ($a \approx 2 \times 10^{-10} \, m/s^2$) Newton's second law does not accurately describe an object's motion. At galactic scales, the acceleration of a gravitationally bound object can approach the MOND limit.

Consider a modified form of Newton's law,

$$F = m\mu(x)a ,\qquad (6)$$

where $\mu(x)$ is a function that for

$$\begin{array}{ll} x \gg 1 & \mu(x) = 1 \\ x \ll 1 & \mu(x) = x \end{array},$$

and a is the acceleration of the object.

Now if an object such as a star exists at a great distance from the center of the galaxy, the modified equation for circular motion is

$$\frac{mv^2}{R} = \frac{GMm}{R^2} = m\mu\left(\frac{a}{a_0}\right)a \; . \tag{7}$$

If we assume that $a \ll a_0$ then $\mu\left(\frac{a}{a_0}\right) = \frac{a}{a_0}$ then (7) becomes

$$\frac{GMm}{R^2} = m\frac{a^2}{a_0}$$

$$\frac{GM}{R^2} = \frac{a^2}{a_0}$$

substituting $a = v^2/R$ for the acceleration and solving for velocity, we find

$$v^2 = \sqrt{GMa_0} \; , \tag{8}$$

where a_0 is $\approx 2 \times 10^{-8} \, cm/s^2$ [24]. This tells us that the velocity is constant which is consistent with observational evidence. Even though MOND does resolve some issues, it is only an empirical relation, and there is, as yet, no underlying physical principles why it should be correct.

1.6 Discussion

In the three models introduced above each has a unique velocity dispersion profile that can be directly compared to velocity dispersion results. The NFW models predict a velocity profile that goes as $\sigma \propto r^{-1/2}$ at large distances, the neutrino model predicts a velocity profile that goes as $\sigma \propto r^{1/4}$, and the MOND model predicts a constant velocity profile beyond the disk. Given the functional forms of these models, they will diverge at large distances, allowing discrimination between models if an appropriate sample can be found.

11

CHAPTER II
SCIENTIFIC RESEARCH

2.1 Galaxy System Rotation Curves

2.1.1 Selecting Primaries

Around any single large galaxy there are insufficient numbers of satellite galaxies

to determine the velocity dispersion as a function of distance. It was established early in

this type of work that to probe dark matter around galaxies, a large number of satellites

from many different host (or primary) galaxies were needed to do a statistical analysis.

With the large data bases such as Sloan Digital Sky Survey (SDSS) [26], CfA Redshift

Catalog [27], Uppsala General Catalog [28], and 2dFGRS [29] that are now available,

gathering enough data is possible.

To investigate the gravitational potential in the outer regions of galaxies, it is

significantly less problematic to explore galaxies that are the dominate source of

gravitation for the system, therefore providing a system for which the center-of-mass

coincides with the center of the galaxy. This condition eliminates binary systems and

galaxy clusters and can be met if a galaxy is sufficiently isolated. To be truly isolated, a

galaxy should have insignificant external forces acting on it, which means that the

measured redshift is only due to cosmological expansion. In binary systems and clusters

the gravitational forces between galaxies cause an additional redshift, the Doppler

redshift, which is independent of the cosmological redshift. In selecting primaries it is

important for them to have significantly smaller satellites so that the center-of-mass is

located within the primary galaxy; therefore, the primary can be considered at rest relative to the system.

Prada et al. [30] defined primary galaxies as having an absolute magnitude brighter than $M_B = -19.0$. Furthermore, their criteria to be an isolated primary required no neighboring galaxies within a specific magnitude difference, ΔM (or difference in mass), projected separation, ΔR (or separation on the sky), and a radial velocity separation of ΔV (or difference in distance). If ΔM, ΔR, or ΔV are too small, it is possible that the galaxy in question is part of a binary system or a cluster. Prada used SDSS data to compile a list of isolated galaxies. Prada's sample set of over 3000 primaries, and his selection criteria are shown in table 2.1.

Table 2.1: Data summary from Prada et al. [30].

SELECTION AND ISOLATION CRITERIA FOR SDSS SAMPLES			
Parameters	Sample 1	Sample 2	Sample 3
Maximum depth of the sample (km s^{-1})	10000	60000	60000
Constraints on bright neighbors:			
Magnitude difference, ΔM	2.0	2.0	0.75
Minimum projected distance, ΔR (h^{-1} kpc)	500	500	2000
Minimum velocity separation, ΔV (km s^{-1})	1000	1000	1000
Constraints on satellites:			
Minimum magnitude difference, δm	2.0	2.0	1.5
Maximum projected distance to primary, δr (h^{-1} kpc)	350	350	500
Maximum velocity separation with primary, δv (km s^{-1})	500	500	1000
Number of isolated galaxies	1278	88603	26807
Number of satellites	453	1052	2734
Statistics of isolated galaxies with at least one satellite:			
Number	283	716	1107
Mean distance (km s^{-1})	7100	14700	23170
Mean distance for $-19.5 < M_B < -20.5$ (km s^{-1})	7244	9785	11076
Mean distance for $-20.5 < M_B < -21.5$ (km s^{-1})	7697	15917	20854
Limiting magnitude M_B	-16.4	-18.0	-19.0

The criteria for selecting primary galaxies change slightly from author to author [17, 18, 30, 31, 32, 33, 34, 35, 36, 37, 38], but do not vary much from the above criteria.

2.1.2 Selecting Satellites

Prada defined his satellite galaxies (also in table 2.1) as all galaxies within a projected distance δR, velocity difference δV, and being at least δM magnitudes fainter than the primary galaxies. This assumes that if a satellite was not within δR, then it was too far to be gravitationally bound to the primary. Similarly if a satellite was not within δV, then it was either well beyond or well in front of the primary galaxy. And finally, if a satellite was within δM, then it was too large and would gravitationally affect the primary galaxy. The criteria for satellites also change slightly for different authors.

Although there is a difference between the criteria adopted by Prada et al. [30], Brainerd [17, 18, 31], Zaritsky [32, 33, 34, 35, 36], McKay [37], and Sales and Lambas [38], their investigations conclude that there is no statistical difference between results. That is, as long as one adopts "sensible" criteria for selecting primary galaxies and their satellites, the resulting samples are consistent with the change in criteria.

2.2 Interlopers

2.2.1 The Problem

In this type of research it is difficult to determine "true" satellites of a primary galaxy. The distances to the satellites are determined using the Hubble Law, which relates cosmological redshift to distance. However, the observed redshift is composed of

both the cosmological redshift and the Doppler redshift resulting from the satellites' peculiar velocity. The peculiar velocity arises from the gravitational attraction of the primary galaxy and can be on the order of $400 km/s$. To examine the mass distribution of a primary galaxy, it is necessary to analyze the peculiar velocities of the satellites. This requires the observed radial velocity range, relative to the primary, to extend out to $\pm 500 km/s$. This range in radial velocity causes a distance uncertainty of $\pm 7 Mpc$ along the line-of-sight.

The uncertainty in distance along the line-of-sight will cause a loss of distance information within the search volume. This loss restricts our information to two-dimensions and removes the ability to determine the "true" positions of the candidate satellites. This specifically makes differentiating true satellites (which should be within $500 kpc$ of the primary) from interloper galaxies (foreground/background galaxies) difficult.

<p style="text-align:center">2.2.2 Relative Velocities</p>

Zaritsky's method for testing the fraction of interlopers involved looking at the distribution of receding candidate satellites vs. approaching candidate satellites [32]. Zaritsky found that candidate satellites exhibit a tendency to have radial velocities that exceed that of their associated primary galaxy [39]. When dealing with a system of bound objects, the assumption can be made that their recessional velocities will split between satellites approaching and satellites receding. In reality the volume searched for possible satellites represents a solid angle, which is a cone truncated by the velocity constraints.

This volume difference introduces a bias of having more satellites in the volume behind the primary than in front of the primary. Zaritsky used the number of satellites with positive Δv divided by the total number of satellites (P/T) of multiple samples and determined the excess in positive radial velocities for candidate satellites. This excess was then interpreted as due to the volume bias. With this information Zaritsky found an interloper background fraction of approximately 0.1.

2.2.3 Velocity Distributions

McKay et al. [37] removed interlopers by fitting the velocity distribution of satellites in bins of primary luminosity by a Gaussian plus constant function. The idea was that the Gaussian component models the velocity distribution of satellites, and the constant component describes the distribution of interlopers. Using this method, McKay assumed that the interloper fraction was constant with projected distance from the primary.

2.2.4 Adaptive Velocity Distributions

Prada et al. [30] and Brainerd [17, 18, 31] point out that from the geometry of the system the fraction of interlopers is a function of projected distance. This is because the search volume for satellites increases with projected distance from the primary. If the interlopers are foreground and background galaxies relative to the primary galaxy, then they should be randomly spread out in the sky analogous to random "noise." This would mean that as projected distances increase, the interloper fraction will also increase.

Using simulations, Prada et al. [30] showed that the velocities of the true satellites are indeed well approximated by the Gaussian distribution and that the width of the distribution (velocity dispersion) changes with radius. From this result Prada extended McKay's method by making the Gaussian plus constant fit for separate radial bins within the bins of primary luminosity. They tested this by using a standard Λ (dark energy) Cold Dark Matter cosmological model with no interlopers present. They next constructed an interloper sample using the SDSS field luminosity function [40] and then introduced interlopers into the simulation. Their results showed that the number of interlopers must increase as a function of projected radius in order to produce the observed rotation curves. Brainerd [17, 18, 31] also came to this conclusion using a Λ Cold Dark Matter GIF simulation.

2.3 Density Profiles of Galaxy Systems

2.3.1 Density Profile Within the Disk

Rotation curves within the disk of galaxies have been made for years with one common outcome: the velocity curve becomes flat (constant velocity) in the outer disk region. So how is the velocity curve related to the density of the system? From Newton's second law, the velocities of the stars are related to the mass within their orbit by equation,

$$v = \sqrt{\frac{GM}{R}} \ .$$
(9)

The mass is proportional to the density,

$$M \propto \rho R^3 ,$$
(10)

17

so in equation (9) if v is to become constant, the density must go as $\rho \propto R^{-2}$. Although all rotation curves are not ideally flat, in general, they do not follow Newtonian mechanics if all the galactic mass is in the form of luminous matter.

2.3.2. Density Profile Beyond the Disk

Determining the density profile beyond the disk of a galaxy becomes complex due to the fact that one can only get the Doppler line-of-sight velocities of the satellites. As mentioned in 1.4.2, the line-of-sight velocity for satellite galaxies only measures one component of the true satellite velocity. It is therefore necessary to obtain the velocity dispersion of satellites as a function of projected distance to probe the mass distribution of the primary.

To obtain the velocity dispersion of satellites, we need to compile enough satellites to obtain good statistical results. This is done by obtaining an ensemble of primary galaxies with similar mass. Figure 2.1 shows how galaxy ensembles of primary galaxies with different masses can give different rotation curves. The three thinner lines represent the velocity dispersion as a function of distance for three galaxies. This sketch shows that increasing the mass of the ensemble of galaxies results in a larger velocity peak. The thicker green line is the average of all three ensembles, which is quite different from the individual velocity curves. It has been shown that the luminosity of a galaxy is proportional to its mass [30]. Therefore galaxies of similar luminosity can be used to construct ensembles.
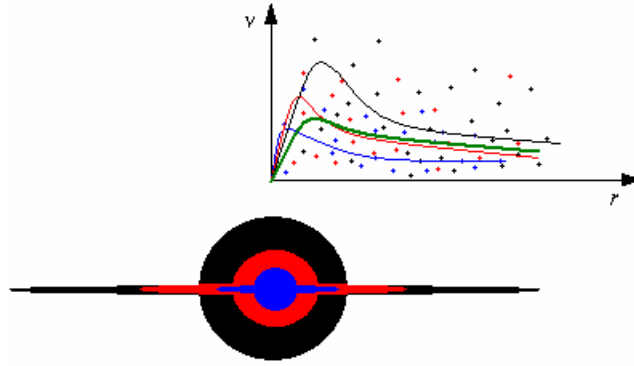
Figure 2.1: A sketch of ensembles of different size galaxies showing how galaxy ensembles of differing mass can give very different rotation curves. The curves correspond to the size of the galaxies. The green curve corresponds to the average of all galaxies.

2.4 Other Properties of Satellite Galaxies

2.4.1 Holmberg Effect

The Holmberg Effect deals with the locations of satellites around a primary galaxy relative to its rotational plane. Holmberg found that satellites tend to inhabit the polar region around the primary in greater numbers than in the planar region [41]. This effect can give clues as to how the hierarchal scenario progress over time. This type of density can arise from either dynamical interactions [42, 43] or from the initial mass distribution in the early Universe [43].

It has been shown that satellites in planar orbits spend greater amounts of time influenced by the gravitational potential of the primary galaxy's disk and are, therefore, more susceptible to tidal orbital decay than their polar orbiting counterparts [42, 44, 45].This results in planar satellites being preferentially destroyed, decreasing the numbers in the planar region.

19

Dynamical processes cannot account for these effects at large distances from the primary galaxy because the orbital periods are comparable to the Hubble time [43]. Finding the Holmberg Effect at large distances would indicate a preferential distribution of matter in the early Universe [36, 43, 44].

2.4.2 Stellar Properties as a Function of Distance

The stellar populations of satellite galaxies may depend on where their orbits are located with respect to the primary galaxy. This could be closely related to the Holmberg Effect. Star formation in satellite galaxies can be induced by the gravitational interaction with the primary [43]. This is caused by tidal interactions with the primary, which induces an increase in the velocity dispersion in the satellite and results in an increase in cloud-cloud collisions (initiating star formation). The significance of this tidal interaction can vary as a function of distance to the primary and also as a function of orbital orientation relative to the plane of the disk.

It might be expected that bluer (star forming) satellites will be found closer to their primaries and in the plane. Zaritsky et al. [33] looked at this effect and found bluer satellites at small distances, but his small sample size made this result marginally significant. Contrary to this finding, Koch and Grebel [45] discovered that satellites in the Local Group, with low star formation, are found near the primary. This result may be due to the satellites having used up their available gas in early star forming epochs. Sales and Lambas [38], having a larger sample than Zaritsky, published a more detailed analysis and found that satellites with low star formation are found, preferentially, in polar regions

(co-planar orbits). This could be a sign that satellites with high star formation have a more spatially isotropic distribution. The Koch and Sales results are consistent if the assumption that the nearer satellites use up their gas more rapidly and are more susceptible to orbital decay in the plane of the galaxy is accepted.

2.4.3 The Tully-Fisher Relation

An observed relationship between the luminosity of spiral galaxies and their maximum rotational velocity, known as the Tully-Fisher relation, tells us that the brighter (or more massive) the galaxy is the faster it rotates. This is an empirically-derived relation that states that the luminosity of a galaxy is directly proportional to the fourth power of its rotational velocity,

$$L \propto v^4. \tag{11}$$

One way to think about this relation is that, if stellar velocities in a galaxy were to increase, the required mass of the galaxy would likewise have to increase in order to keep the stars bound. Therefore, measuring the rotational velocity of stars in the disk of a galaxy gives an idea of how much mass the galaxy contains. Since the galaxy's mass is related to its luminosity, there exists a relation between luminosity and rotational velocity. The Tully-Fisher relation can be used as a standard candle (distance estimator) to relate galactic distance to the rotational velocity.

There is debate as to whether the "Tully-Fisher" relationship exists for the primary galaxy luminosity and the velocity dispersion of its satellites. Because the luminosity is related to the absolute magnitude, which is found using Hubble's law, we

21

can determine the Tully-Fisher relation for a system of satellites. Prada et al. found a relationship between the velocity dispersion and luminosity of $\sigma \propto L^{0.3}$ [30]; as where, McKay found a relationship of $\sigma \propto L^{0.5}$ [37].

It is interesting to note that MOND shows the Tully-Fisher relation quite straight forwardly from equation (8) if $M \propto L$. With the mass interior being proportional to the luminosity, we get equation (11), the Tully-Fisher relation, $v^4 \propto L$.

<div align="center">2.5 Research Discussion</div>

From previous work, authors [34, 36] have noted that a comprehensive measurement of the satellite velocity dispersion profile should combine two main elements: (1) a large number of primary galaxies and satellite galaxies and (2) a cosmologic model-independent, robust, and testable rejection of interloper galaxies. With these criteria in mind, I used the SDSS galaxy data from New York University and searched for primary galaxies and satellite galaxies from a data set of ~50,000 galaxies in order to fulfill element (1). Then with these data and the use of MatLab® [46] and ROOT, I carried out robust statistical analyses to determine interlopers. This fulfills element (2).

CHAPTER III

METHODOLOGY

3.1 OBSERVATIONAL DATA

3.1.1 The Value-Added Galaxy Catalog

The New York University Value-Added Galaxy Catalog (NYU-VAGC) [47] is a catalog of local galaxies. Most of these galaxies are below z = ~ 0.3 and based on a set of surveys matched to the SDSS Data Release 4 [48]. The photometric catalog consists of 693,319 galaxies, QSOs, and stars. For the following project I used the catalog of the low-redshift galaxies (lowz), a sub-sample consisting of 49,889 galaxies. The sample consisted of galaxies with redshift between $0.005 < z < 0.05$ that correspond to distances in the range of $21 \leq d \leq 214 Mpc$. Distances were derived assuming a smooth Hubble flow with $h = 0.70 (H_0 = 100 km/s/Mpc)$ [30].

This sample is significantly improved over the SDSS sample by the use of a more independent set of reductions than those used in the SDSS pipeline. This catalog is conveniently small and is specifically designed for studying galaxy properties and large-scale structure. Most catalogs or surveys contain data for everything that was imaged: stars, quasars, galaxies, asteroids, etc. This made gathering data for galaxy studies inconvenient. The specifics can be found in Blanton et al. [47].

3.1.2 The Samples

To obtain a sample of isolated primaries (no restrictions on Hubble type) and their satellites, I restricted primary galaxies to those with absolute blue magnitudes equal to or brighter than $M_B = -18.0$, using the conversion given by Yasuda et al. [49],

$$M_B = 0.482 \times (M_g - M_r) + 0.169 + M_g, \tag{12}$$

where M_g is the green absolute magnitude, and M_r is the red absolute magnitude from the lowz catalog.

From this set I defined isolated primary galaxies as Prada et al. [30], with no neighboring galaxies within a magnitude difference of $\Delta M > 2$, projected separation of $\Delta R > 500 kpc$, and a radial velocity separation of $\Delta V > 1000 km / s$. The satellite candidates were chosen to have a magnitude difference relative to their primary of $\Delta M > 2$, projected separation relative to their primary of $\Delta R < 350 kpc$, and a radial velocity separation relative to their primary of $\Delta V < 500 km / s$. The MatLab$^{\circledR}$ program I wrote for this procedure is found in Appendix A. A flow chart that represents the process is shown in figure 3.1.
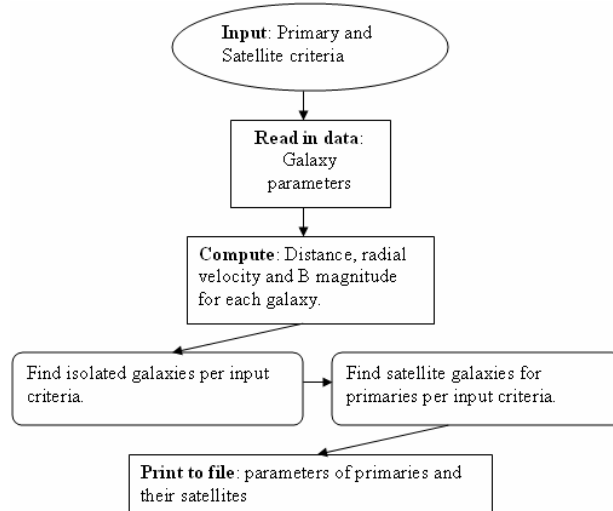
Figure 3.1: Flow chart of the code that determines primaries and their satellites from the NYU data.

Table 3.1 gives the parameters used to define two different samples with the number of primaries and satellites found in those samples, thereby comparing the results from using two different criteria.

Table 3.1: Selection criteria for finding primary galaxies and satellite galaxies. *Same as sample 1 in Prada et al. [30].

sample 1*		sample 2	
primary (2076)		primary (2741)	
$\Delta M >$	2	$\Delta M >$	2
$\Delta R >$	500kpc	$\Delta R >$	700kpc
$\Delta V >$	1000km/s	$\Delta V >$	1000km/s
satellites (3318)		satellites (4966)	
$\Delta M >$	2	$\Delta M >$	2
$\Delta R <$	350kpc	$\Delta R <$	500kpc
$\Delta V <$	500km/s	$\Delta V <$	500km/s

Figure 3.2 shows the distribution of primary and satellite brightness, differences in brightness, and number of satellites per primary for sample 1. This was similar to Prada et al. [30], Zaritsky et al. [33, 34, 35], and McKay et al. [37]. Figure 3.3 shows the distribution of primary and satellite brightness, differences in brightness, and number of satellites per primary for sample 2.
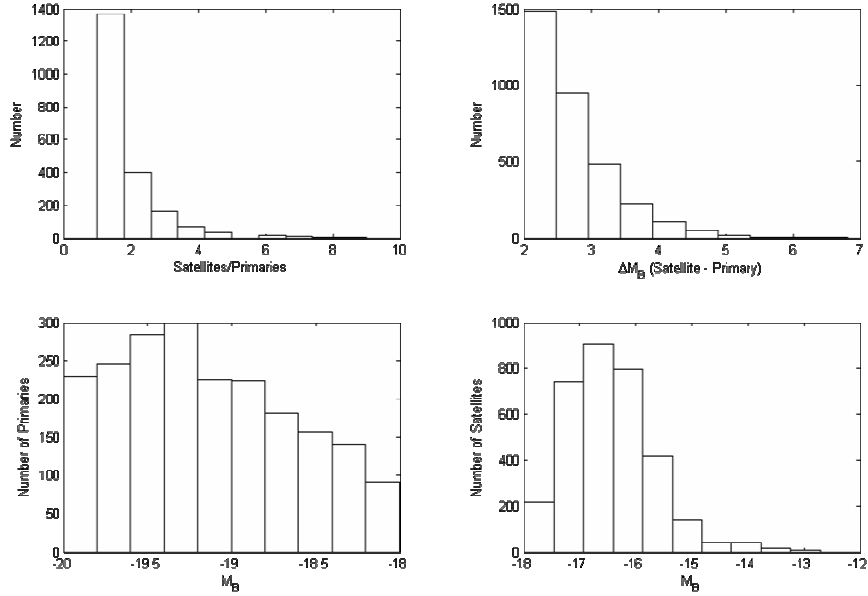
Figure 3.2: Statistics of primary galaxies and their satellites in sample 1. The top left panel shows the number of satellites per primary. The top right panel shows the absolute blue magnitude differences between the primaries and the satellites. The bottom left and right show the distribution of absolute blue magnitudes, M_B, of isolated primaries and satellites respectively.

Sample two resembles sample one with the exception of having larger numbers. This was to be anticipated from the increase in the search volume.
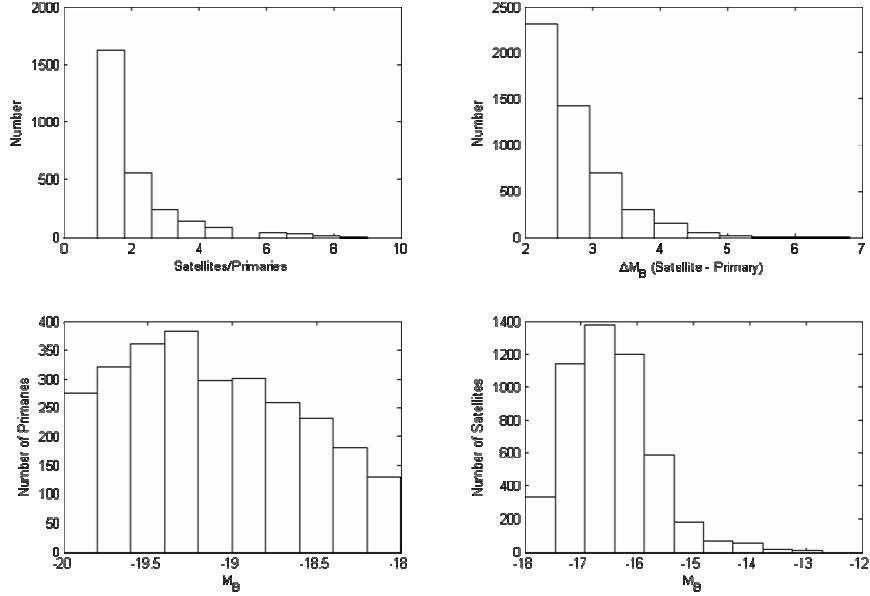
Figure 3.3: Statistics of primary galaxies and their satellites in sample 2. The top left panel shows the number of satellites per primary. The top right panel shows the absolute blue magnitude differences between the primaries and the satellites. The bottom left and right show the distribution of absolute blue magnitudes, M_B, of isolated primaries and satellites respectively.

3.2 DEALING WITH INTERLOPERS

3.2.1 The Consequence of 3-D Space

Recall that the uncertainty in distance between the primary and its satellites along the line-of-sight is due to the peculiar velocity of the satellites relative to their primary (see section 2.2.1). This ambiguity will cause a loss of distance information within the search volume. This lack of dynamical information forces us to model and analyze a 2-D environment to explain an actual 3-D environment. Figure 3.4 demonstrates how satellites around a galaxy (center of sphere) can appear to be true satellites from the line-of-sight (part A) direction. The true situation, part B, is that satellites that appear to be part of the primary system actually lie in front of the primary or behind the primary and

27

are not truly part of the system. This dilemma specifically makes differentiating true

satellites from interlopers difficult.
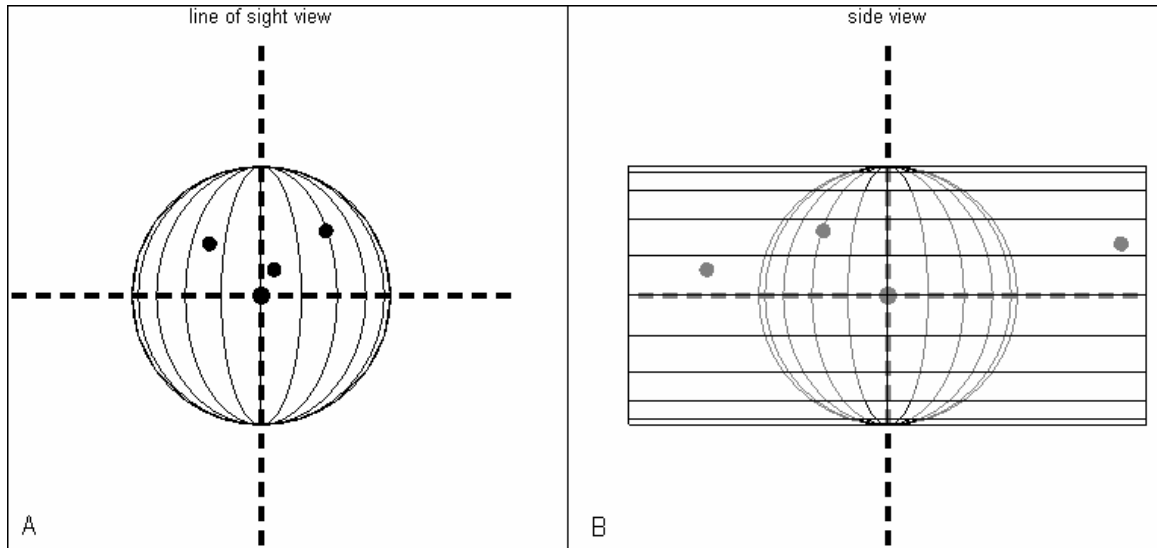
Figure 3.4: A - Line of sight view of primary galaxy and possible satellites. B - Side view of primary galaxy and possible satellites.

The interloper problem cannot be completely alleviated due to lack of dynamical

information. One can only be cautious in modeling and estimating fractions of galaxies

that are not part of a given system.

3.2.2 Interloper Contamination

As mentioned in section 2.2.4 the fraction of interlopers comes from a geometric

effect due to the volume searched. This volume is determined from the criterion of

maximum projected distance, ΔR, the maximum distance a satellite galaxy appears to lie

from its primary galaxy. Because ΔR was my choice, I could calculate the percentage of interlopers expected in a given projected radius. The "line-of-sight" view of the volume searched is illustrated in figure 3.5. This shows that the volume of each radial bin increases with the increase of projected distance from the primary. If the interlopers are uniformly distributed on the sky, then the number of interlopers in each radial bin will be proportional to the volume of that bin.
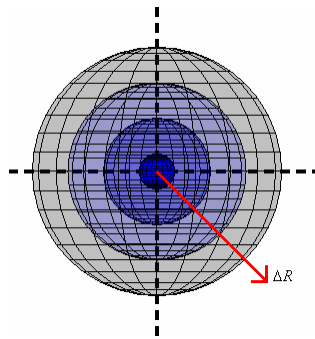
Figure 3.5: Line-of-sight view of the volumes for four radial bins.

For example, if we are looking within a projected distance, ΔR, the percentage of interlopers in the total interloper sample is 100%. If we now split the sample into four equal radial bins, the first radial bin would contain about 6% of the total number of interlopers. The second radial bin would contain 19%, the third 31%, and the fourth 44%. The sample was also broken up into four equal radial bins and should have these percentages in each bin.

3.2.3 Interloper Subtraction - Adaptive Sigma fit

I adopted the Gaussian plus constant method used in a few studies [17, 18, 30, 31] that took into account that interloper contamination increases with projected distance. Figure 3.6 illustrates how to determine the velocity dispersion by accounting for interlopers from the line-of-sight velocities of possible satellites. A histogram for the differences of the line-of-sight velocity between satellites and their primaries was made. This velocity difference is the peculiar velocity of the satellites relative to the primary galaxy. From the assumption of isotropy in the velocity distribution, I was able to fold the velocity sample by taking the absolute magnitude of the velocity difference. This was fitted by a Gaussian plus constant function. In the figure, open circles with error bars represent the number of satellites in each "sub-bin", and the solid black line is the best Gaussian fit. The sigma (width) measurement of the Gaussian represents the velocity dispersion of the satellites, and the constant represents the interloper contamination in this radial bin.
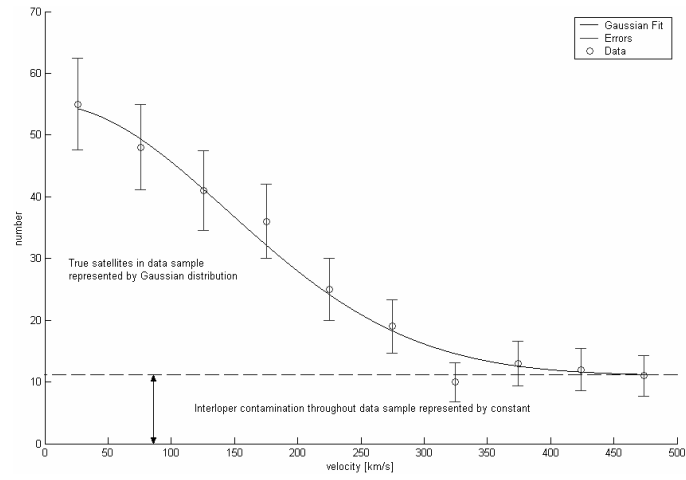
Figure 3.6: Illustration of modeling satellite velocities and interlopers with a Gaussian plus constant.

The analysis described above was done in C++ using the ROOT system. Details about ROOT can be found on the World Wide Web at http://root.cern.ch/. The C++ code can be found in Appendix A under "Gaussian fit with ROOT".

CHAPTER IV

ANALYSIS AND RESULTS: VELOCITY PROFILES

4.1 Programs

Routines that required doing a fit were written in C++. All other routines and

functions specific to do this research were written with MatLab®. MatLab® is a software

package for technical computing and model-based design. It is used by engineers,

scientists, and mathematicians for performing mathematical calculations, analyzing and

visualizing data, and writing new software programs. MatLab® is a sophisticated

language and interactive environment that enables the user to perform computationally

intensive tasks faster than with traditional programming languages such as C, C++, and

FORTRAN. MatLab® can be used in a wide range of applications, including signal and

image processing, communications, test and measurement, and computational biology.

The programs and functions that I describe in this study can be found in Appendix A.

4.2 Velocity Dispersion

4.2.1 Velocity Profiles

Using the results of the ROOT program, I plotted the Gaussian plus constant fit

for four radial bins for a subset from sample 1 (shown in figure 4.1). Only satellites of

primary galaxies in the range $-18.5 > M_B > -19.5$ are shown. The closed circles with

error bars show the velocity distribution of satellites in the subset. The solid curve is the

best Gaussian plus constant fit. Each of these plots also shows best fit values for the

Gaussian plus constant function (i.e. width (σ), height (h), and constant (K)) along with

the chi squared per degrees of freedom (χ^2/DF) value.
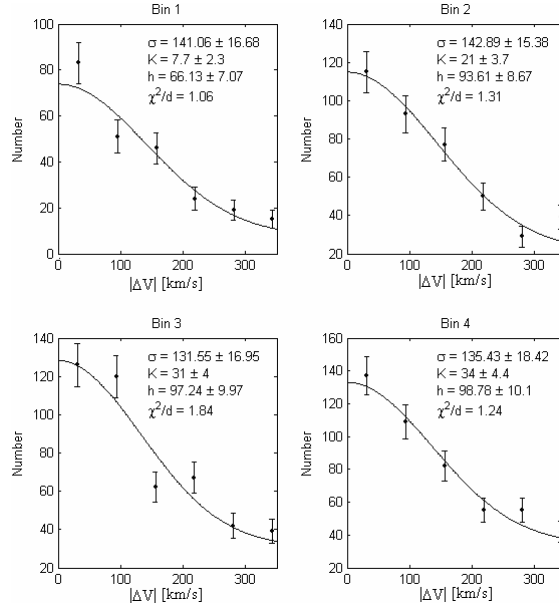
Figure 4.1: The Gaussian plus constant fit for four radial bins of a subset from sample 1. Only satellites of primary galaxies in the range $-18.5 > M_B > -19.5$ are shown. The closed circles with error bars show the velocity distribution of satellites in the subset. The solid curve is the best Gaussian plus constant fit. Each of these plots also shows best fit values for the Gaussian plus constant function along with the χ^2/DF.

From the outcome of the Gaussian plus constant fits, above a velocity dispersion

vs. projected distance plot was made. The velocity dispersion, after removing interlopers,

(figure 4.2) is constant within the error bars with projected distance (a straight line was

drawn to show this).
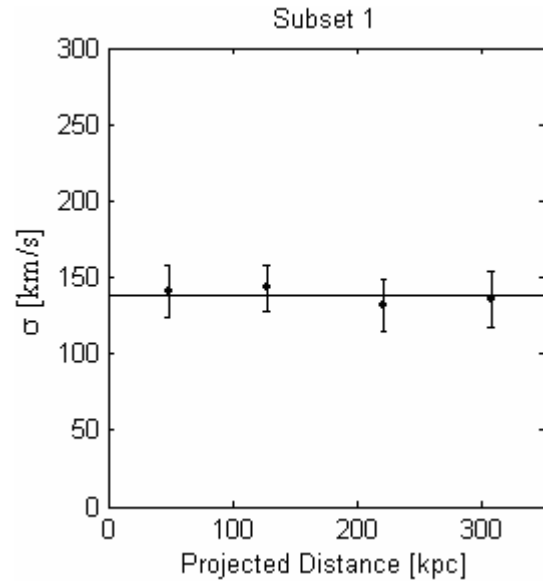
Figure 4.2: The velocity dispersion profile of satellites belonging to primary galaxies in a subset from sample 1 in the range $-18.5 > M_B > -19.5$.

Figure 4.3 shows an equivalent plot to figure 4.2 but for a subset of sample 2 in the same magnitude range. This plot extends out to $500kpc$ in projected radius as compared to the previous one of $350kpc$. The velocity dispersion within error bars is also constant with projected distance.
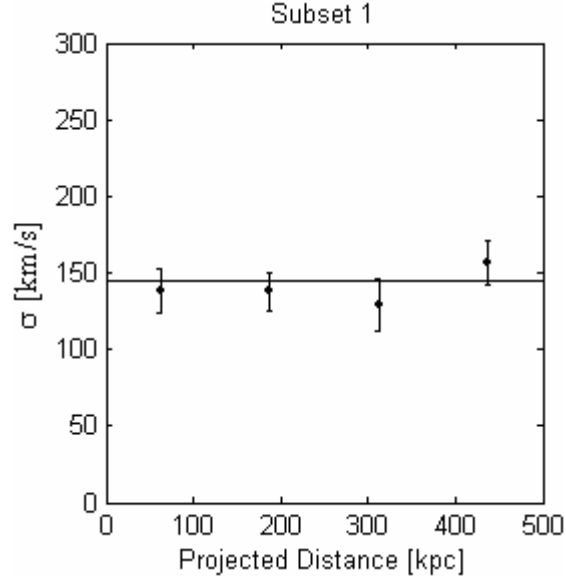
Figure 4.3: The velocity dispersion profile of satellites belonging to primary galaxies in a subset from sample 2 in the range $-18.5 > M_B > -19.5$.

The only difference in the second sample is the increase in the projected radius criterion for both the primary galaxies and the satellite galaxies. This change extends the search area around the primary galaxy, which adds satellites to the sample but only beyond $350kpc$. The similarities between samples show that changing the projected distance criterion does not change the result of the analysis. To examine the situation further, I divided sample 2 into multiple subsets (or ensembles). The subsets were defined by the primary galaxy type, early type, late type, or both types, and then divided into magnitude ranges. The type was determined by the u - r color index cutoff described in Strateva et al. [50]. Galaxies that have u - r color ≥ 2.22 are classified as being early type galaxies (E, S0, Sa), and those that have u - r color < 2.22 are classified as late type galaxies (Sb, Sc, Irr).

4.2.2 The Subsets

As discussed above in section 2.3.2, the velocity profiles of satellites depend on the luminosity of their primary galaxy. Therefore, I proceeded by creating various subsets of primary luminosity (magnitude).

The information in table 4.1 shows how sample 2 was divided. The subsets 1 - 7 are for all primaries (both early and late types), subsets 8 - 14 are for early type primaries and 15 - 21 are for late type primaries. The subsets for each type of primary are split up into different magnitude ranges as well. The subsets 1 - 4, 8 - 11, and 15 - 18 all have ranges of 0.5 magnitudes. The remaining subsets, 5 - 7, 12 - 14, and 19 - 21 all have ranges of 1.0 magnitude. The subsets that have magnitude ranges of 1.0 are the combination of two subsets with magnitude ranges of 0.5.

Table 4.1: Subsets of Sample 2.

Primary Magnitude Range	Early & Late Primaries	Early Primaries	Late Primaries
$-18.0 > M_B > -18.5$	subset 1	subset 8	subset 15
$-18.5 > M_B > -19.0$	subset 2	subset 9	subset 16
$-19.0 > M_B > -19.5$	subset 3	subset 10	subset 17
$-19.5 > M_B > -20.0$	subset 4	subset 11	subset 18
$-18.0 > M_B > -19.0$	subset 5	subset 12	subset 19
$-18.5 > M_B > -19.5$	subset 6	subset 13	subset 20
$-19.0 > M_B > -20.0$	subset 7	subset 14	subset 21

Primary and satellite counts for each subset are listed in table 4.2. The first column is the primary magnitude range, the second refers to both early and late type primaries, the third refers to the early primaries, and the last column refers to late

36

primaries. For both primary types the satellite number increases with the increase of the

primary magnitude. When looking at primaries, the number of satellites detected depends

on how faint they are, so when looking at bright primaries, there will be a larger number

of fainter satellites (relative to the primary) that can be detected. For the two primary

types, separately, there are about twice as many satellites for early types than there are for

late types.

Table 4.2: Percentages of Primary galaxies and their satellites for early, late and both types of primaries.

Primary Magnitude Range	All (Early & Late) Stats		Primary	Early Primary Stats (% of total)			Late Primary Stats (% of total)		
	subset	primaries	satellites	subset	primaries	satellites	subset	primaries	satellites
$-18.0 > M_B > -18.5$	1	439	753	8	56%	63%	15	44%	37%
$-18.5 > M_B > -19.0$	2	665	1151	9	55%	64%	16	45%	36%
$-19.0 > M_B > -19.5$	3	862	1497	10	63%	69%	17	37%	31%
$-19.5 > M_B > -20.0$	4	777	1564	11	68%	75%	18	32%	25%
$-18.0 > M_B > -19.0$	5	1103	1904	12	56%	63%	19	44%	37%
$-18.5 > M_B > -19.5$	6	1526	2648	13	60%	67%	20	40%	33%
$-19.0 > M_B > -20.0$	7	1638	3061	14	66%	72%	21	34%	28%

4.2.3 Robust Adaptive Sigma fit

Analyzing each radial bin multiple times for a different number of "sub-bins" in

the Gaussian plus constant fit will provide a robust technique to show if the results are

realistic. This is shown in figure 4.4 for the first radial bin of subset 1. If the velocities of

the true satellites follow a Gaussian distribution, their velocity dispersion will be

independent of the number of "sub-bins" used in the Gaussian plus constant fit. The

constant on the other hand should fall off linearly, and the number in each sub-bin will

double if the number of sub-bins is cut in half. Therefore, the background fraction will

be independent of the number of sub-bins.
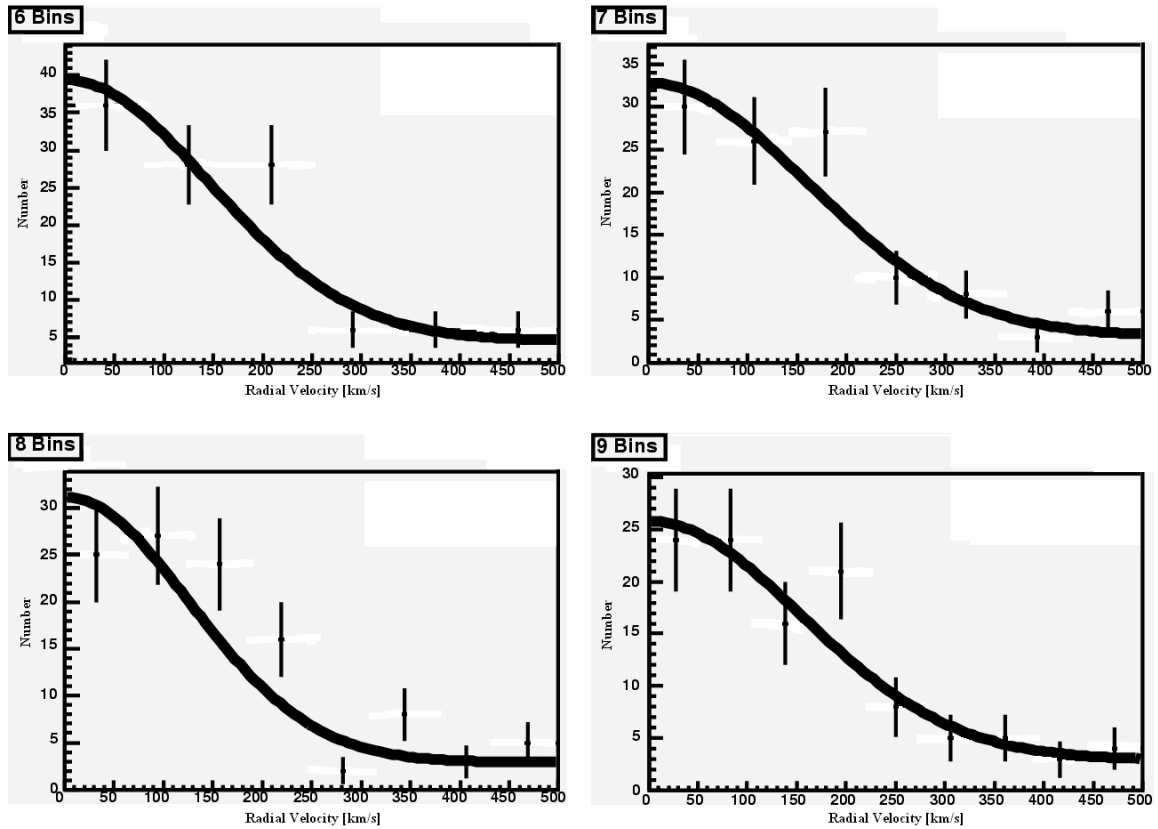
Figure 4.4: The Gaussian plus constant fit for four different numbers of sub-bins for the first radial bin of subset 1.

When running the Gaussian plus constant fits, I forced the sub-bins to range from

4 to 13 giving 10 different bin sizes. The smallest number of sub-bins used was 4. This

lower limit was set by the having three constraints (sigma, height, and constant) in the

analysis.

Figure 4.5 shows the results found from the Gaussian plus constant fit for the

different number of sub-bins in radial bin 1 of subset 1. The plot in the upper left shows

the velocity dispersion for each fit, the upper right shows the interloper fraction for each

fit, and in the lower left, the probabilities determined from the χ^2 for each fit along with

the 0.05 and 0.01 significant levels. The red line is a reference to check whether the

results can be considered independent of bin number (or bin size) within the uncertainty.

The Pass value above the top two graphs indicate whether the results are independent of

bin number (Pass = 1) and whether the results are dependent of bin number (Pass = 0).

The Pass value above the χ^2 graph indicates if the all the fits were above the 0.05

significant level or the 0.01 significant level.
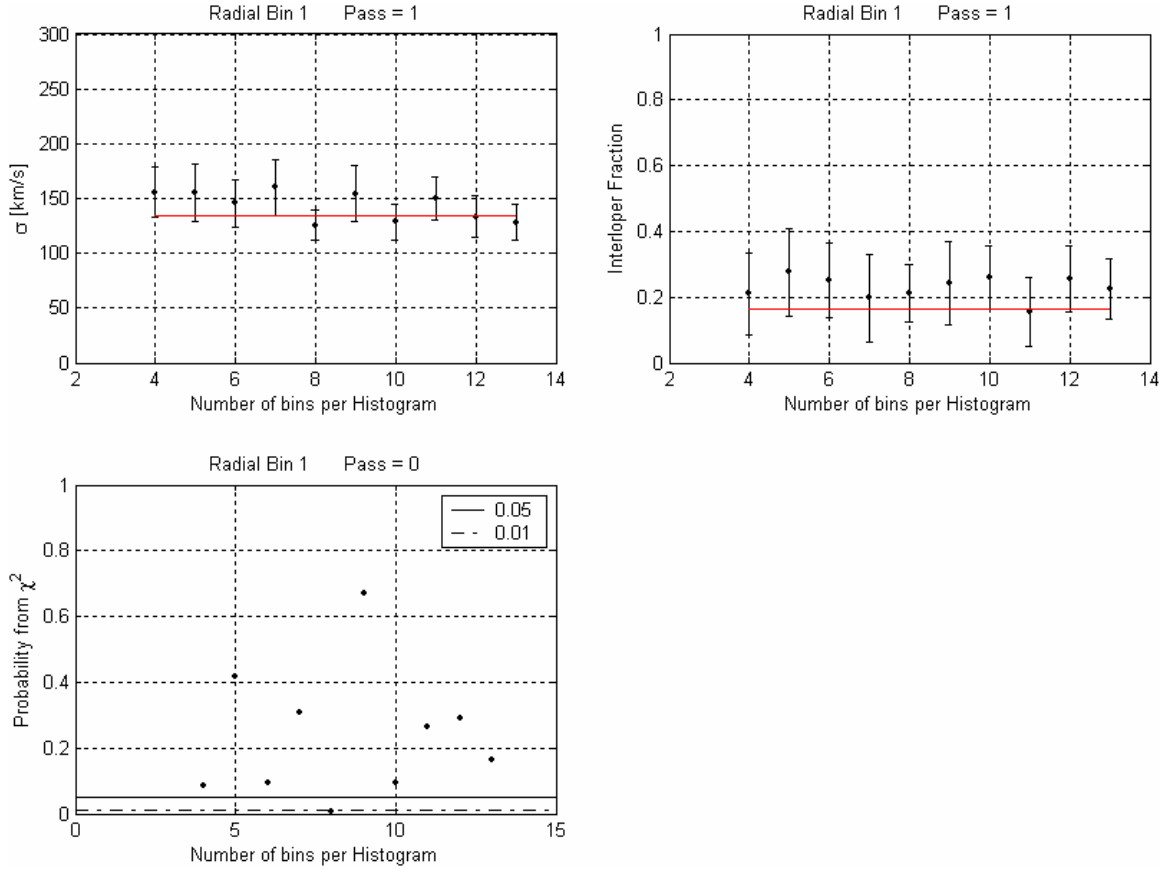
Figure 4.5: Results from the Gaussian plus constant fit for the different number of sub-bins in radial bin 1 of subset 1. The red line is a reference to check if the results can be considered independent of bin number (or bin size) within the uncertainty.

Using the χ^2 can help determine whether the data should be rejected or not. If the value of χ^2 is of the order 1 or less, then the data follows a Gaussian plus constant function. This is made quantitative by calculating the probabilities that the data follow the model. The probabilities are calculated from the integral,

$$P = \frac{2}{2^{d/2}\Gamma(d/2)} \int_{\chi_0}^{\infty} x^{d-1} e^{-x^2/2} dx \qquad (13)$$

where d is the degrees of freedom. If P is large, the observed and expected distributions are consistent; if it is small, they probably disagree.

4.2.4 Geometric Effect - Interloper Fractions

Section 3.2.2 explains how the fraction of interlopers increases due to the geometry of the volume searched showing that the number of interlopers per bin should be proportional to the volume of that bin. By dividing the sample into four radial bins, each $125 kpc$ wide, the number of interlopers in each bin will increase with distance from the primary. As determined in the earlier section, the first bin, $0 kpc$ to $125 kpc$, will have roughly 6% of the total number of interlopers in the sample. The second bin, $125 kpc$ to $250 kpc$, will have roughly 19% of the total number of interlopers in the sample. The third bin, $250 kpc$ to $375 kpc$, and the fourth bin, $375 kpc$ to $500 kpc$, have 31% and 44% of the total number of interlopers respectively.

Figure 4.6 shows the rotation curve of the data in subset 1 along with the three cosmological models, and the expected interloper fraction per bin is compared to the interloper fractions found in the data. The diamonds represent the expected fraction due to the geometry of the situation. The data points with error bars in both graphs are the average values found in each radial bin of the robust analysis.
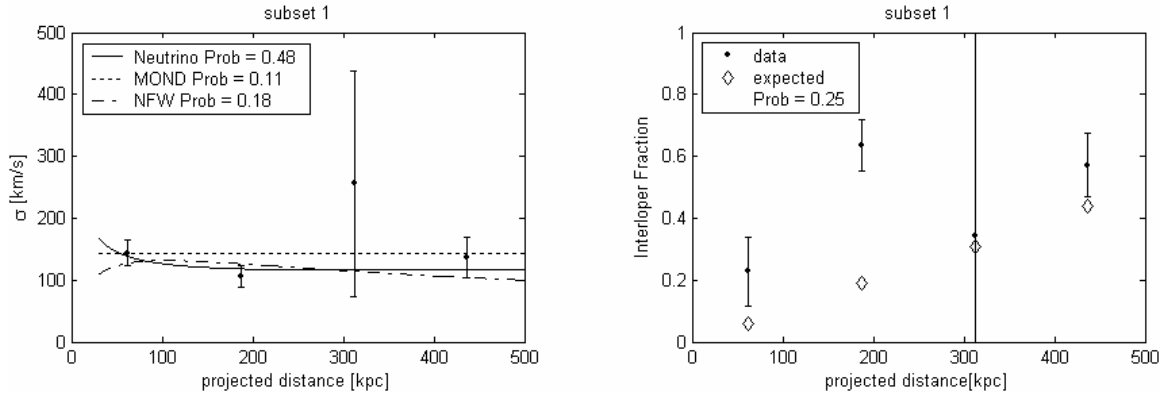
Figure 4.6: Velocity dispersion profile plotted with the three cosmological models and interloper fraction of subset 1.

The results of the analysis of subset 1 are shown in table 4.3. The first column is number of sub-bins. The second and third columns are the velocity dispersions and errors found from the Gaussian plus constant fit. The forth and fifth columns are the interloper fractions and errors found from the Gaussian plus constant fit. The sixth and seventh columns are the χ^2 values and the probabilities for each fit.

Table 4.3: Results of the robust analysis of subset 1.

	bin number	sigma	sigma error	fraction	fraction error	chi2	probability
Radial Bin 1	4	155.6742	22.6678	0.2096	0.1252	2.9403	0.0864
	5	155.2599	26.3995	0.2759	0.1334	1.7498	0.4169
	6	145.6067	21.3438	0.2508	0.1151	6.386	0.0943
	7	160.3394	25.5135	0.1983	0.133	4.7966	0.3088
	8	125.7091	14.2283	0.2124	0.0881	15.5261	0.0083
	9	154.4373	25.5788	0.2431	0.1273	4.0583	0.6688
	10	128.4858	16.7989	0.2611	0.0964	12.1779	0.0949
	11	149.9975	20.222	0.1543	0.1056	9.9862	0.266
	12	133.2149	18.8223	0.2564	0.0996	10.8009	0.2896
	13	128.2359	16.406	0.2261	0.092	14.1828	0.1648
	average	143.6961	20.7981	0.2288	0.1116		
Radial Bin 2	4	98.9095	18.7412	0.6368	0.0835	4.166	0.0412
	5	98.1733	17.2842	0.6701	0.083	3.3854	0.184
	6	119.8738	21.2661	0.6411	0.0916	4.9159	0.1781
	7	102.4851	16.4834	0.6569	0.083	7.4129	0.1156
	8	99.8378	15.6044	0.6127	0.0799	10.7217	0.0572
	9	109.8867	19.8828	0.6611	0.0873	6.8057	0.3392
	10	107.2403	16.323	0.6144	0.0824	12.6367	0.0815
	11	105.0753	19.3091	0.6609	0.0838	14.6693	0.0659
	12	111.358	16.8486	0.5762	0.0815	22.0794	0.0086
	13	109.1783	17.8121	0.6317	0.0837	15.6343	0.1106
	average	106.2018	17.9555	0.2288	0.084		
Radial Bin 3	4	190.9873	131.5838	0.6111	0.3214	2.5186	0.1125
	5	208.8118	89.1239	0.5573	0.2739	0.3348	0.8459
	6	353.0519	333.7149	-0.0853	1.7849	3.4309	0.3298
	7	378.5442	484.0419	-0.1755	2.6624	1.3634	0.8505
	8	233.3468	138.8004	0.4757	0.4408	4.8558	0.4337
	9	204.9779	81.4799	0.5078	0.2503	9.4285	0.1509
	10	226.2113	114.9035	0.5018	0.3567	4.3197	0.7423
	11	235.2873	131.3751	0.4723	0.4119	6.8098	0.5573
	12	223.1068	104.6922	0.4501	0.3353	11.2881	0.2565
	13	308.09	215.755	0.1022	0.9669	15.7925	0.1057
	average	256.2415	182.5471	0.3417	0.7804		
Radial Bin 4	4	167.7841	41.8117	0.5219	0.1418	0.2135	0.6441
	5	137.3106	36.1513	0.5795	0.1082	1.7627	0.4142
	6	121.1813	34.0939	0.6262	0.0959	5.6597	0.1294
	7	128.5881	30.8706	0.5952	0.0969	1.3814	0.8474
	8	150.9349	37.5559	0.5583	0.1176	3.6354	0.603
	9	119.5427	26.1707	0.5791	0.0854	12.3745	0.0541
	10	142.8314	31.5183	0.5356	0.104	5.8346	0.5592
	11	131.7484	28.7285	0.5757	0.0946	6.6901	0.5704
	12	137.5861	32.721	0.5673	0.1015	9.0654	0.4313
	13	128.3606	28.6119	0.5789	0.0927	7.2698	0.6997
	average	136.5868	32.8234	0.5718	0.1039		

4.3 Results

4.3.1 Velocity Profile Results: 0.05 significant level

After applying the robust analysis to all 21 subsets all but one are rejected for being dependent on bin size. At the 0.05 significant level, only subset 11 followed a Gaussian plus constant form that is independent of bin size for all four radial bins. The data following this form is only the first restriction in this analysis. The next restriction is that the sigma values and the constant values must be independent of bin number. This will provide additional support that the signal is real.

The velocity dispersion profile of subset 11 in figure 4.7 shows each model plotted along with the data and probabilities associated with each fit. This result shows that the NFW profile has the highest probability of following the data. The neutrino model has the next highest, and finally the MOND model has the smallest probability of fitting the data. The decline in the velocity dispersion as the projected distance increases is similar to what Prada et al. [30] and Brainerd [17, 18, 31] found in their analysis. Figure 4.7 also shows the interloper fraction in each radial bin, and it follows the expected fraction of interlopers per bin which adds support to the consistency of the data.
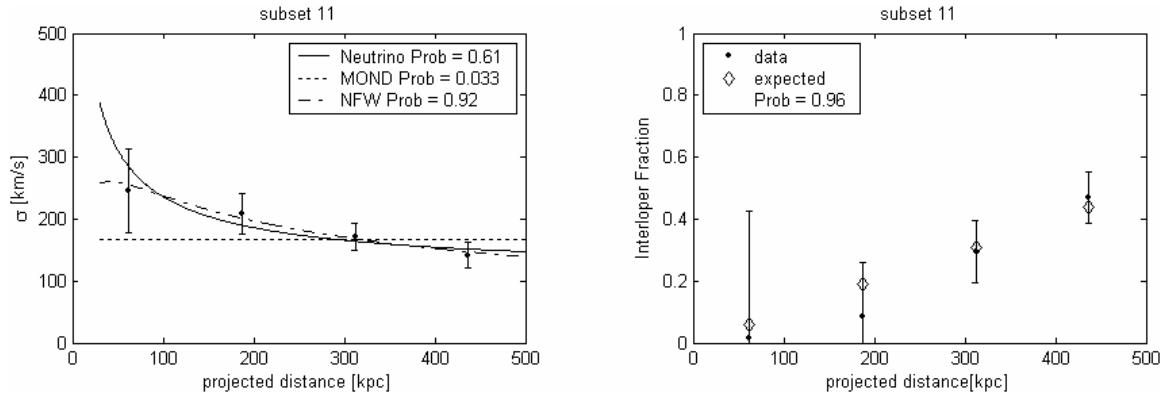
Figure 4.7: Velocity dispersion profile plotted with the three cosmological models and interloper fraction of subset 11.

4.3.2 Velocity Profile Results: 0.01 significant level

I repeated the process above at the 0.01 significant level, and subsets 2, 4, 7, 11, and 14 passed the robust analysis. Figure 4.8 shows the velocity dispersion profile of subset 2 along with each model and probabilities associated with each fit. These results are the same as the results of subset 11: that the NFW profile is most probable, then the neutrino model, and finally the MOND model. The difference is that in this subset all the models have relatively high and similar probabilities.
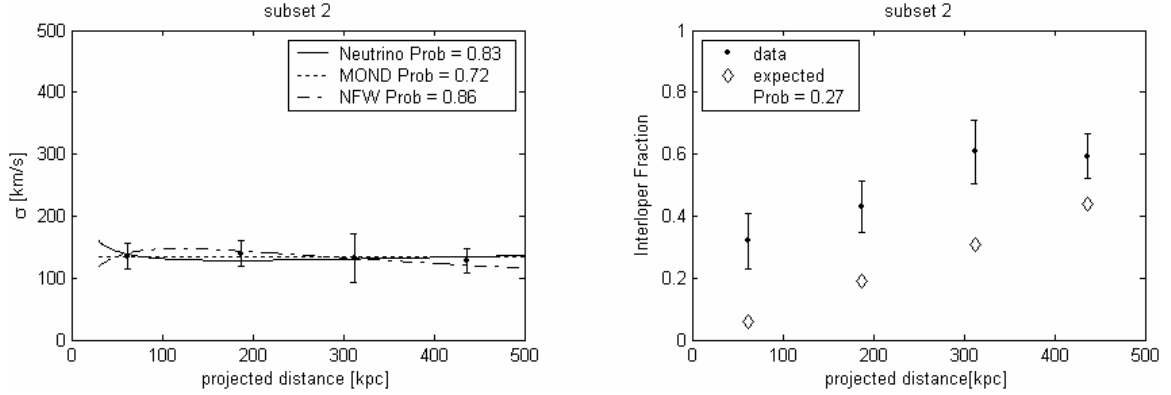
Figure 4.8: Velocity dispersion profile plotted with the three cosmological models and interloper fraction of subset 2.

Figure 4.9, similar to 4.8, shows the velocity dispersion profile of subset 4. This result again shows that the NFW profile has the highest probability of following the data, the neutrino model the next highest, and finally the MOND model has the smallest probability of fitting the data.
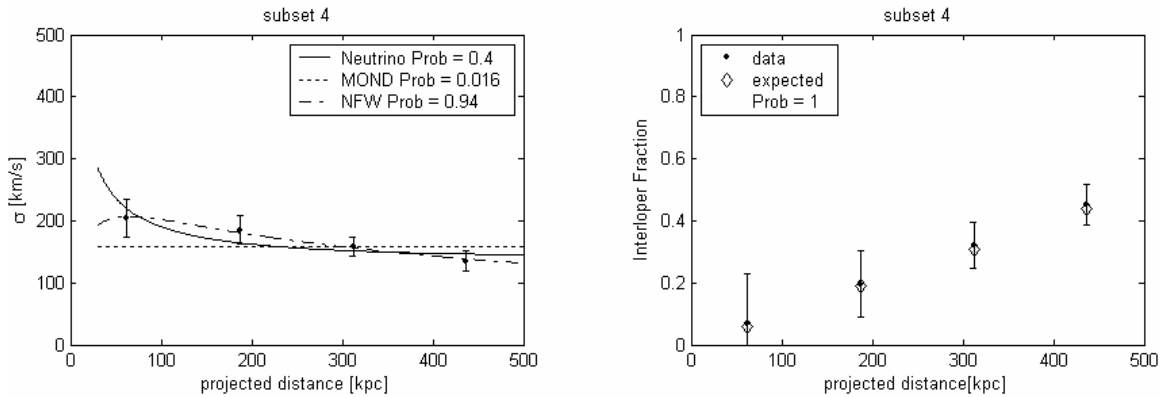
Figure 4.9: Velocity dispersion profile plotted with the three cosmological models and interloper fraction of subset 4.

The difference in subset 2 and 4 is the interloper fraction of subset 2 has a smaller probability (0.27) when compared to the probability of subset 4 (1.0) of following what is expected. The same trend is seen when looking at all the subsets, 2, 4, 7, 11, and 14. The velocity dispersion profile plots of these subsets are found in Appendix B.

4.3.3 Result Comparison

The NFW and neutrino probabilities are more similar in value to one another in subsets 2, 7, and 14 than in subsets 4 and 11. The probabilities for the MOND model vary for each of these subsets but are consistently the lowest of three models. The trend we see is that when the probability for the interloper fraction is > 0.90 the probabilities between models vary more than when the interloper fraction is < 0.90. From this analysis the NFW model is the most probable, but the neutrino has fairly large probabilities and cannot be excluded as a possible explanation of the observed velocity dispersion.

The sample from NYU consists of satellites fainter than that of Brainerd [18, 31] and Prada et al. [30]. There is a slight overlap with this sample (subset 4) at the bright end ($-19.5 > M_B > -20.0$) and with Prada's sample in the faint end ($-19.5 > M_B > -20.5$). Within this overlap the velocity dispersion I found peaked at $\sim 200 km/s$, while Prada's sample peaked at $\sim 120 km/s$. If Prada's sample contained primaries in a larger magnitude range ($-19.5 > M_B > -20.5$), then the velocity dispersion should have been higher than what I measured. This discrepancy between maximum dispersion is possibly due to the small numbers, under 300 satellites in Prada's sample at this magnitude range. After dividing these into four bins, there would be < 75 satellites per bin to do the

Gaussian plus constant fit. These low numbers would make the statistical analysis weak, which would make the results less accurate. The sample I used, subset 4 alone, had ~1570 satellites in a 0.5 magnitude range as compared to Prada's 1.0 magnitude range.

While Prada's sample was from the SDSS, Brainerd's [18] sample was from the 2DFGRS and was in the magnitude range ($-18.9 > M_B > -21.5$). This sample consisted of almost 2500 satellites and covers a magnitude range five times larger than mine. Considering that the radial velocity errors in 2DFGRS are on the order of $85 km/s$ and that she combined such a wide range of primaries (magnitude range), her results are an average (as discussed in section 2.3.2) of different size halos, possibly making them unreliable.

4.3.4 Early vs. Late Type Dispersions

To get an idea of what the velocity dispersions would look like for different primary types separately, the velocity dispersion from the first radial bin of each subset was taken from the robust analysis and plotted against the average magnitude of that subset (this is shown in figure 4.10). Only subsets of early and late types were used. Recall that subsets 1-7 are both early and late type primaries, 8-14 are early type primaries, and 15-21 are late type primaries. The early types (red) either have a larger dispersion than their late type counterparts (blue), or have the same dispersion within the uncertainty, but they never fall below their late type counterparts.
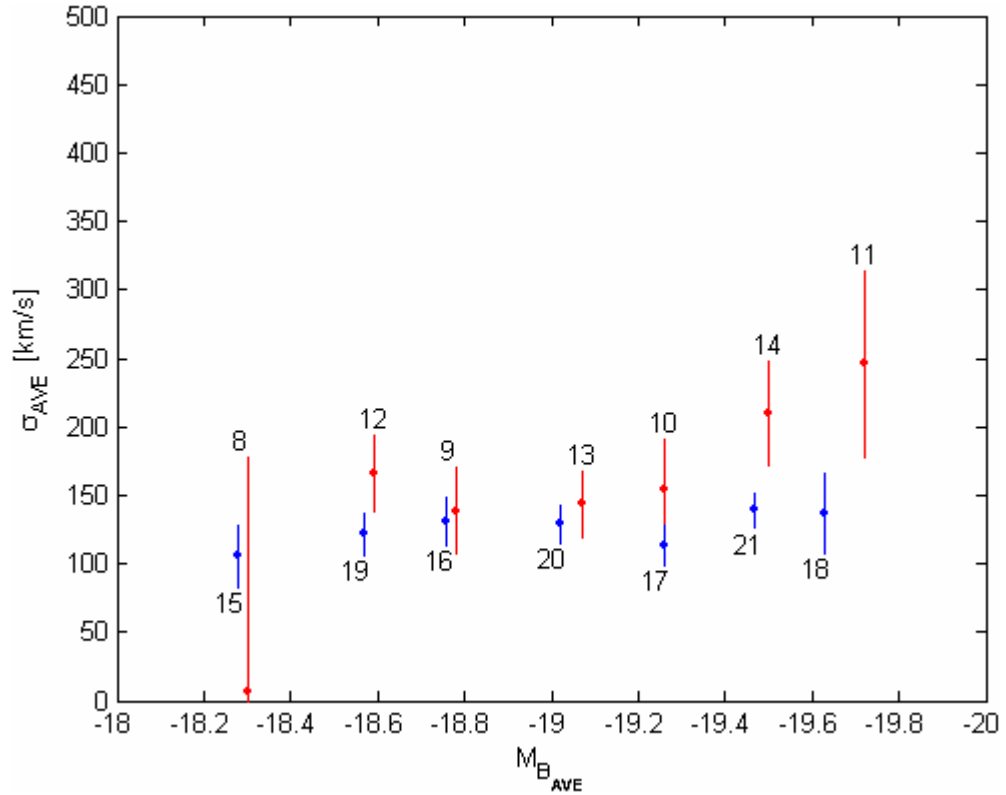
Figure 4.10: The velocity dispersion of the first radial bin for all subsets and plotted against the average magnitude of that subset. The subsets are for only early and late type systems.

This is what Brainerd [19] reported, but this was found from looking at the velocity dispersion profiles of early and late type systems for a wide range of primary magnitudes. Her sample did contain a large fraction of giant ellipticals that could drive the velocity dispersion this high ($297km/s$). These dispersions are high, which may be due to mixing the wide range of primaries and/or to the incorrect estimates of the fraction of interlopers. In her sample she shows that for the first bin she has an interloper fraction of ~0.12 and in the last bin ~0.25. Both of these bins are $150kpc$ in width, and according to the geometric effect that was discussed in section 3.2.2, she should have found ~0.09

in the first and ~0.51 in the last. Another explanation for the inflated dispersion is that her early type primaries could have had, on average, larger magnitudes as compared to the late type galaxies, making the dispersion higher. She did not report the magnitudes of these early and late type primaries; therefore, this cannot be verified.

To get a better look at what was seen in figure 4.10, I made a similar plot (figure 4.11) for the subsets that are greater than the 0.01 significance level.
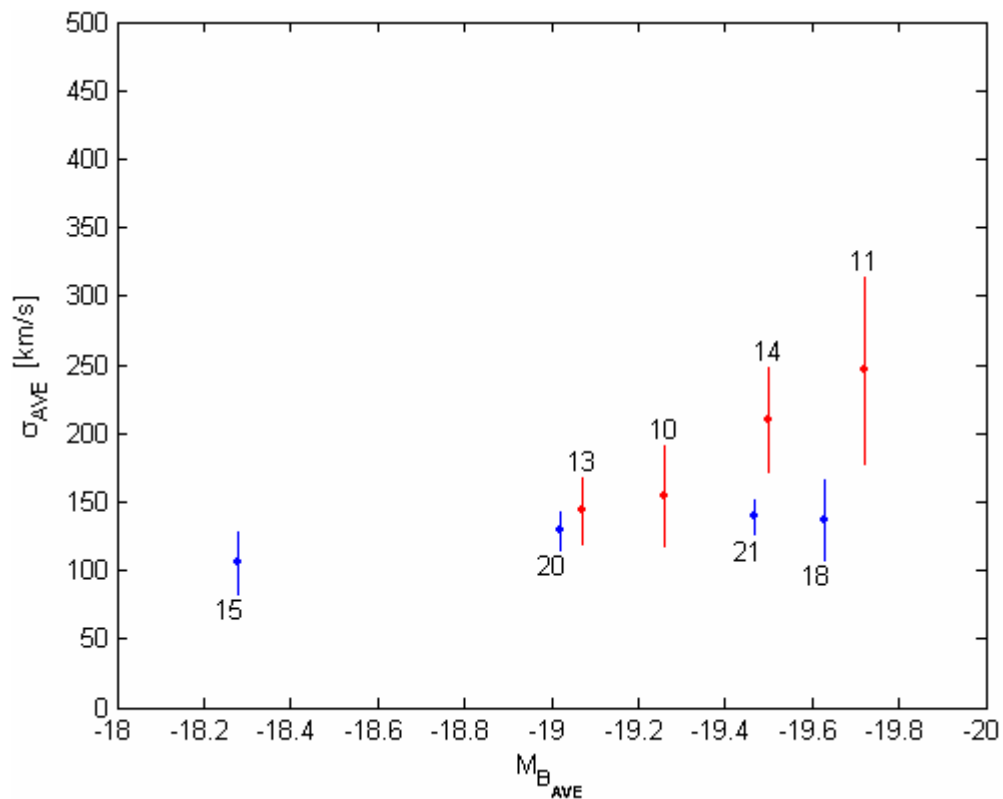
Figure 4.11: The velocity dispersion of the first radial bin for subsets that have a significance level greater than 0.01 and plotted against the average magnitude of that subset. The subsets are for only early and late type systems.

Subset 10 does not have its late type counterpart to be compared to, and similarly subset 15 does not have its early type counterpart to be compared to. The others pair up

as 13-20, 14-21, and 11-18. This shows that satellites with high mass primaries have significantly different velocity dispersions depending on primary type. Satellites for early type primaries have a larger dispersion than the satellites for the late type primaries.

There are two possible explanations for these satellites to have different dispersions around primaries with virtually the same magnitude (luminosity or mass). The first is that the satellites with the larger dispersion are found (on average) closer to their primary. Secondly, if the satellites (on average) are at the same distance from their primary, this would suggests that the early type primaries have a more massive dark matter halo than the late type primaries.

I next calculated the average distance for satellites relative to their primary (late and early) and found that regardless of primary type, satellites are found at $\sim 276 kpc$. If the distance is roughly the same for satellites with different dispersions, the mass interior to their orbit is larger for the satellites with a larger dispersion. This corresponds to a larger dark matter halo.

The fact that these primaries are similar in mass but show different velocity dispersions is evidence against MOND. With MOND, all the dynamics are due to the luminous matter of the galaxy, which means that beyond the galaxy's disk satellites should have the same dispersions. The fact that the satellites have different dispersions well beyond the disk is difficult to explain within the MOND model.

The larger dark matter halo for early type primaries happens from having a larger primordial dark matter halo at birth than that of the late type primaries. When a galaxy is forming, the infall rate of the baryonic matter depends on how large the dark matter halo

51

is. The larger the dark matter halo, the faster the infall, and the faster the galaxy forms. By initially having a larger dark matter halo, a galaxy can evolve from a late type galaxy to an early type galaxy relatively faster than a galaxy that initially has a smaller dark matter halo.

ANALYSIS AND RESULTS: OTHER SATELLITE PROPERTIES

5.1 Stellar Properties as a Function of Primary Type

5.1.1 Early Type Primaries

I next looked at how the satellites themselves are distributed relative to the primary type. Below is a histogram (figure 5.1) of the satellites in subsets 8-14. These belong to early type primaries. The histograms in figure 5.1 show the normalized number of satellites per area as a function of projected distance for two types of satellites (blue-late and red-early). The late types are likely star forming satellites, and early types are ones that have gone through this process and lack gas to form any new stars. The type was determined by the color cut off $u - r$ of 2.22 from Strateva et al. [50] as used previously. Each of the radial bins is $50kpc$ in projected distance in width, starting with bin 1 at $0kpc - 50kpc$ and so on to bin 10 at $450kpc - 500kpc$.

The data (points with error bars) was fitted to a power law function (solid line) of the form $N/A \propto r^{\rho}$. The fit for early type satellites decreases more rapidly than the late type satellites with projected distance in the high magnitude $(-19.0 > M_B > -20.0)$ range primaries. This effect could be the result of the gravitational influence of the primary that induces star formation in the closer satellites, which causes them to use up their gas more rapidly.
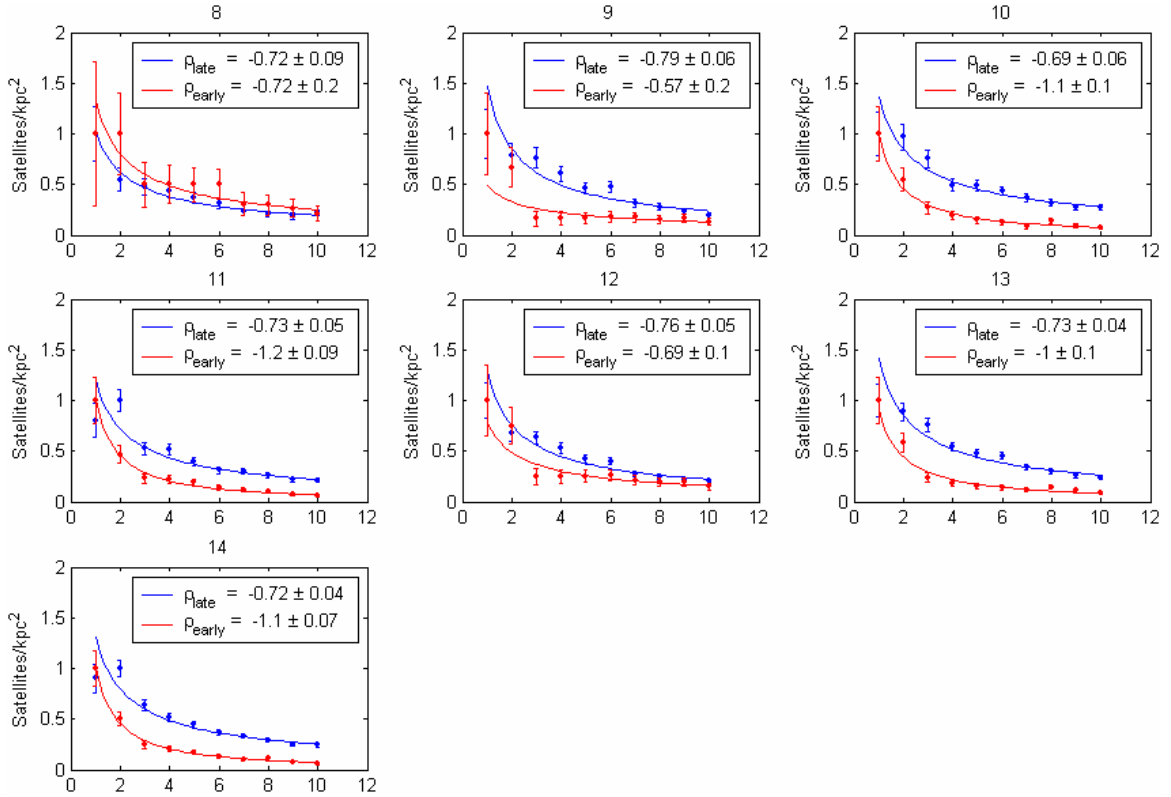
Figure 5.1: Histograms of the number of satellites per area on the sky for the subsets 8-14. These have early type primaries. The data (points with error bars) was fitted to a power law function (solid line). These are color coded: red – early type and blue – late type.

5.1.2 Late Type Primaries

Figure 5.2 shows a similar plot as in 5.1 except for the subsets 15-21. These subsets have satellites with late type primaries. From the power law fit, the early and late type satellites decrease at the same rate. This likeness could be the result of the lack of gravitational influence of the primary on its satellites. These primaries may not be large (lower magnitude range $-18.0 > M_B > -19.0$) enough to cause much effect gravitationally.
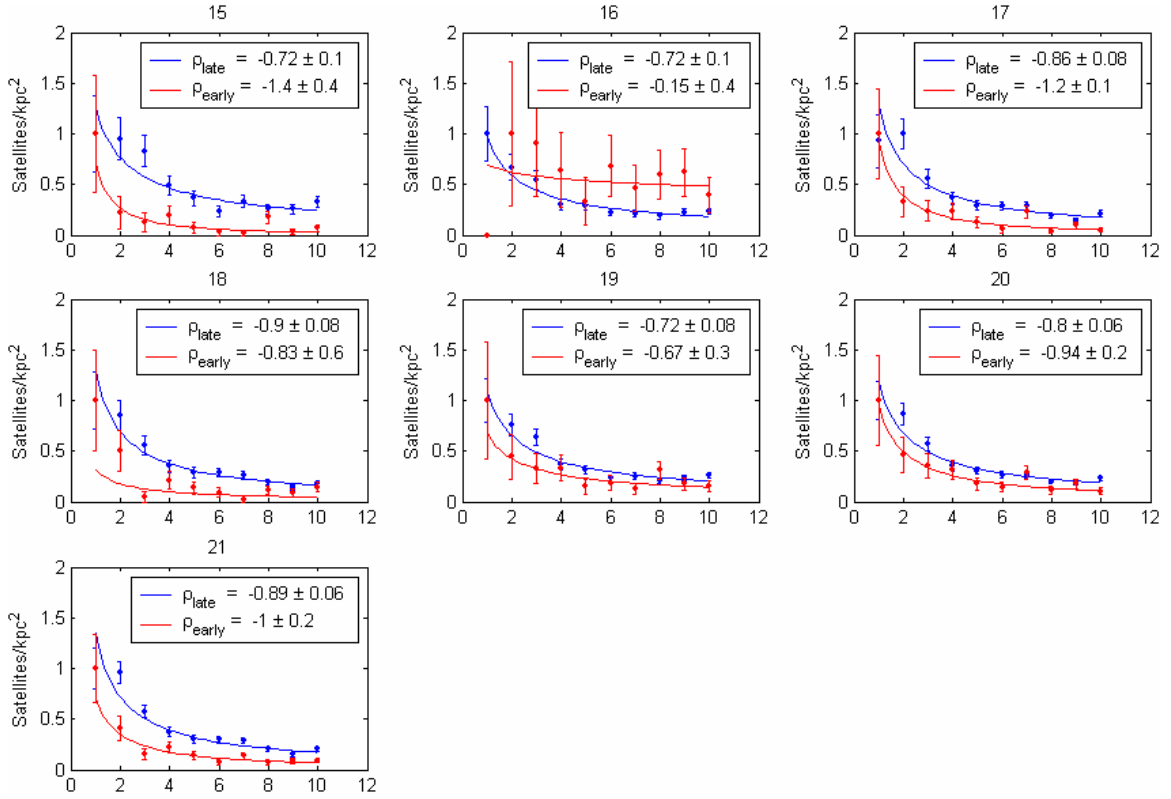
Figure 5.2: Histograms of the number of satellites per area on the sky for the subsets 15-21, these have late type primaries. The data (points with error bars) were fitted to a power law function (solid line). These are color coded: red – early type and blue – late type.

The results between the two types of primaries are shown below in table 5.1. The table shows the value of ρ for each type of satellite and the difference of ρ for each type of satellite. This is determined for both types of primaries in each magnitude range. The differences in early and late type satellites only appear significant for the early type primaries with the high magnitude range. These differences suggest that the primaries with higher magnitude (mass) interact more with their satellites than primaries with lower magnitude. So why is a significant change not seen in the late type primaries with high magnitudes? The results in 4.3.4 that early type primaries form faster due to the larger

dark matter halo than the late type primaries could explain this. If the early types form

faster, they will be able to affect their satellites much sooner than a late type galaxy can.

Affecting the satellites sooner also means that this interaction takes place over a longer

period of time for the early type primaries than for the late type primaries. This would

explain why the satellite types for early type primaries are different and why for late type

primaries they are not.

Table 5.1: Table showing how ρ does not change at low magnitude or with primary type but does change substantially at larger magnitude for early type primaries.

Early Type Primaries $-18.0 < M_B < -19.0$	Early Type Primaries $-19.0 < M_B < -20.0$
$\rho_{late} = -0.76 \pm 0.05$ $\rho_{early} = -0.69 \pm 0.1$ $\|\Delta\rho\| = 0.068 \pm 0.1$	$\rho_{late} = -0.72 \pm 0.04$ $\rho_{early} = -1.1 \pm 0.07$ $\|\Delta\rho\| = 0.43 \pm 0.07$
Late Type Primaries $-18.0 < M_B < -19.0$	Late Type Primaries $-19.0 < M_B < -20.0$
$\rho_{late} = -0.72 \pm 0.08$ $\rho_{early} = -0.67 \pm 0.3$ $\|\Delta\rho\| = 0.053 \pm 0.3$	$\rho_{late} = -0.89 \pm 0.06$ $\rho_{early} = -1 \pm 0.2$ $\|\Delta\rho\| = 0.12 \pm 0.2$

If satellites are dynamically influenced by their primary, the distributions of

satellite types should be an indication. The change in ρ for the low magnitude range

primaries shows that their satellites do not change (use their gas in star formation and go

from late to early type) and may indicate that there is little influence between them. The

change in ρ for the higher magnitude range early type primaries may indicate an influence on the satellites from their primary. This would cause the late type satellites closer to the primary to use their gas, to form stars, and to become early type satellites.

The projected density profiles of early type satellites for the high mass primaries fall off as r^{-1}. This radial distribution of satellites is consistent with the results of the spatial distribution of satellites around bright galaxies in an independent study by Lorrimer et al. [51].

Kosh and Grebal [45] found that early type galaxies tend to lie at closer proximity to M31 (primary) than do the late type galaxies. This is what I found in my analysis with the NYU data.

<div align="center">5.2. Holmberg</div>

<div align="center">5.2.1 Modeling Holmberg</div>

The Holmberg Effect deals with the locations of satellites around a primary galaxy relative to its rotational plane. Details of this effect were described in section 2.4.1. When Holmberg first recognized this effect, he defined the region within 30 degrees above and below the plane of the primary as the planar region and the remaining region as the polar region [41]. Figure 5.3 is a polar plot showing the polar region and planar region as defined by Holmberg. In the plot the primary galaxy is located at the center with the plane of the disk lined up at zero degrees. The black outlined area above and below the primary is the polar region. This region is defined as 60 degrees clockwise and 60 degrees counter clockwise from the axis of rotation (above and below) of the galaxy.

The area 30 degrees above and below the plane of the galaxy is the planar region. At this 30 degree split, the volume of the polar region and the volume of planar region are equal to each other.
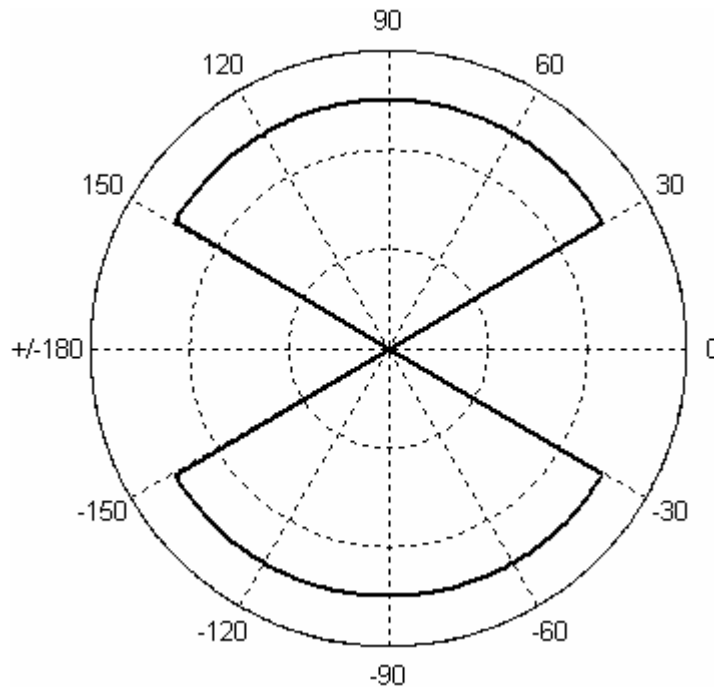
Figure 5.3: Polar plot distinguishing the polar region from the planar region.

Modeling the Holmberg Effect brings up the issue of analyzing a three dimensional situation in two dimensions. This satellite analysis is different from that of the velocity dispersion. In this examination I needed to look at the distribution of satellites in position space not velocity space. Interlopers, once again, played an important role in how this was done.

In this study there are two types of interlopers. The first type are ones that do not belong to the galactic system but only appear to be part of the system because of

projection effects. Previously we used velocity space to account for this type of interloper and to determine the non-spatial value of velocity dispersion, which has no dependence on spatial position. This velocity method cannot be effectively used to remove interlopers in position space because if interlopers are uniformly distributed, there would be no way of knowing which specific satellites to remove. Furthermore, if the goal is to determine an over density in particular regions, then removal of a uniform distribution of interlopers will not affect the results.

The second type of interloper comes from examining the two different 3-D regions in 2-D space. It is possible that satellites in one region appear to be in another. This type of interloper will be called "contaminates." In this situation, 3-D models should be examined as 2-D projections, thereby determining the contamination effect of one region on another.

Because we are looking at a spherical volume on a projected surface, some satellites that are truly in planar orbit (hereafter these satellites will be simply referred to as "planar") could appear to be in polar orbit (hereafter these satellites will be simply referred to as "polar"). Consider the image below, figure 5.4. It consists of 10,000 points. The red points and the black points are randomly distributed inside the polar regions of the sphere and inside the planar region of the sphere respectively. This is a true 3-D plot that has been projected onto this 2-D plane. The 30 degree cut off can be seen between the polar regions and the planar region. Also there are some black points that appear to lie in the polar regions. These points "contaminate" the polar regions. When studying the Holmberg Effect, one must consider the contamination of one region onto the other.
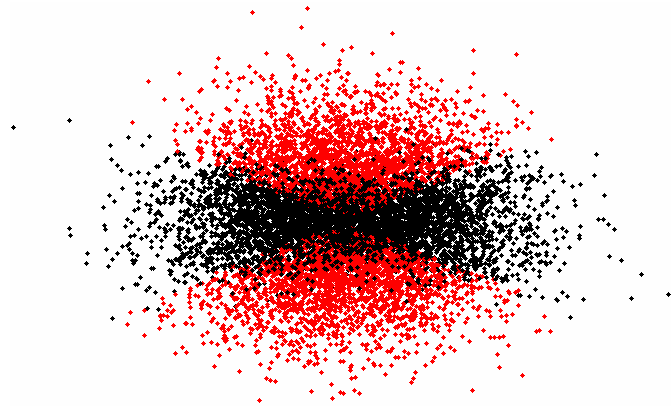
Figure 5.4: A 3-D image of randomly distributed points projected on a 2-D surface to illustrate contamination of satellites in one region onto the other.

Equally the argument can be made that there are some red points that appear to lie in the planar region. Depending on viewpoint this contamination does apply both ways but must be incorporated when deciding how to count the number of satellites in each region. Figure 5.5 is similar to that of 5.4 with the exception that it contains only 1000 points. In this simulation of 1000 points, there were 490 red points in the polar region and 510 black points in the planar region. Recall that each region is of equal volume, and it makes sense that the number in each would be close if not equal to one another in a random 3-D distribution. In this study I am counting the number of points that appear in the 2-D polar region. In this example, there were 184 points that appear in the polar region, but are planar. In reality, I find the fraction of points that appears in the polar region is 0.67.
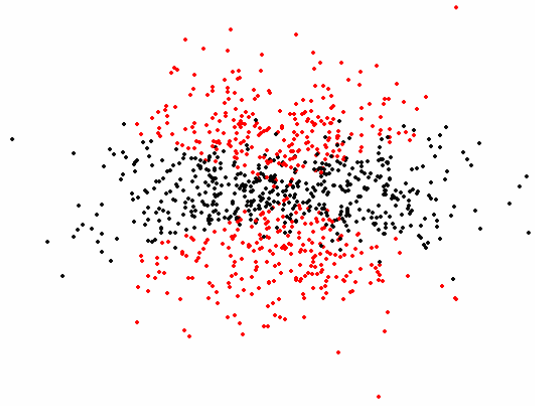
Figure 5.5: A 3-D image of randomly distributed points projected on a 2-D surface to illustrate contamination of satellites in one region onto the other.

I ran my model for various numbers of satellites. Each run uses 10 iterations of randomly generated points to get an average polar count. Figure 5.6 shows 12 histogram, each fit with a Gaussian to show the most likely fraction that makes up the polar points. The bins that make up each histogram are the mean polar count for each of the 10 iterations. The total number of satellites ranges from 25 to 1125 in step sizes of 100. The peaks in each histogram are roughly 0.7. With this wide range of total satellites there is clear support that the contamination is a geometric effect.

From the model, the fraction of points that appears polar is 0.69 ± 0.03 regardless of the total number of points in the system. From the model, I also determined the standard deviation of the Gaussian for the changing number of points that appeared polar. This deviation gives the errors in the model and fits the power law equation,

$$\sigma_{model} = N_{polar}^{-0.51 \pm 0.01} \tag{14}$$

61

where N_{polar} is the number of satellites that appear polar, and σ_{model} is the deviation from the most likely fraction.

A geometric effect that I also used to determine if the system is isotropic was to rotate the system and check to see if isotropy was preserved. If a system of points is isotropic, from the analysis above, the fraction of polar satellites in 2-D is ~0.70 of all satellites. This means that from any angle the fraction of polar satellites will still be ~0.70 of all satellites. With this in mind, if a system is not isotropic, more polar than planar, then as the tilt angle changes from perpendicular to the plane (more face-on), an increase in the planar region due to the over density in the original polar region would be seen. So if in the data we look at galaxies, edge-on through face-on, and if we see a change in the polar fraction, then this can help determine the true distribution of the satellites.

This process gives an idea of what to look for when running the real data. If a ~0.70 polar favor of the distribution is seen, then the true distribution is definitely not planar. The true distribution could be isotropic, and the over density is only due to the geometric effect of looking at a spatial distribution projected onto a plan.

Another method to determine if the distribution is isotropic or not is to find the average angle, ϕ, between the plane of the primary and the line joining the satellite to the center of the primary. If $\phi = 0$, this indicates that a satellite orbits in the plane of the primary, and if $\phi = 90°$, this indicates that a satellite orbits perpendicular to the plane (polar) of the primary. Then if the satellite orbits are isotropic, the mean value of ϕ should be 45 degrees. Following this method Brainerd [52] found that satellites have a

strong preference for being aligned with the plane of the primary at small radii and become isotropic at larger scales.
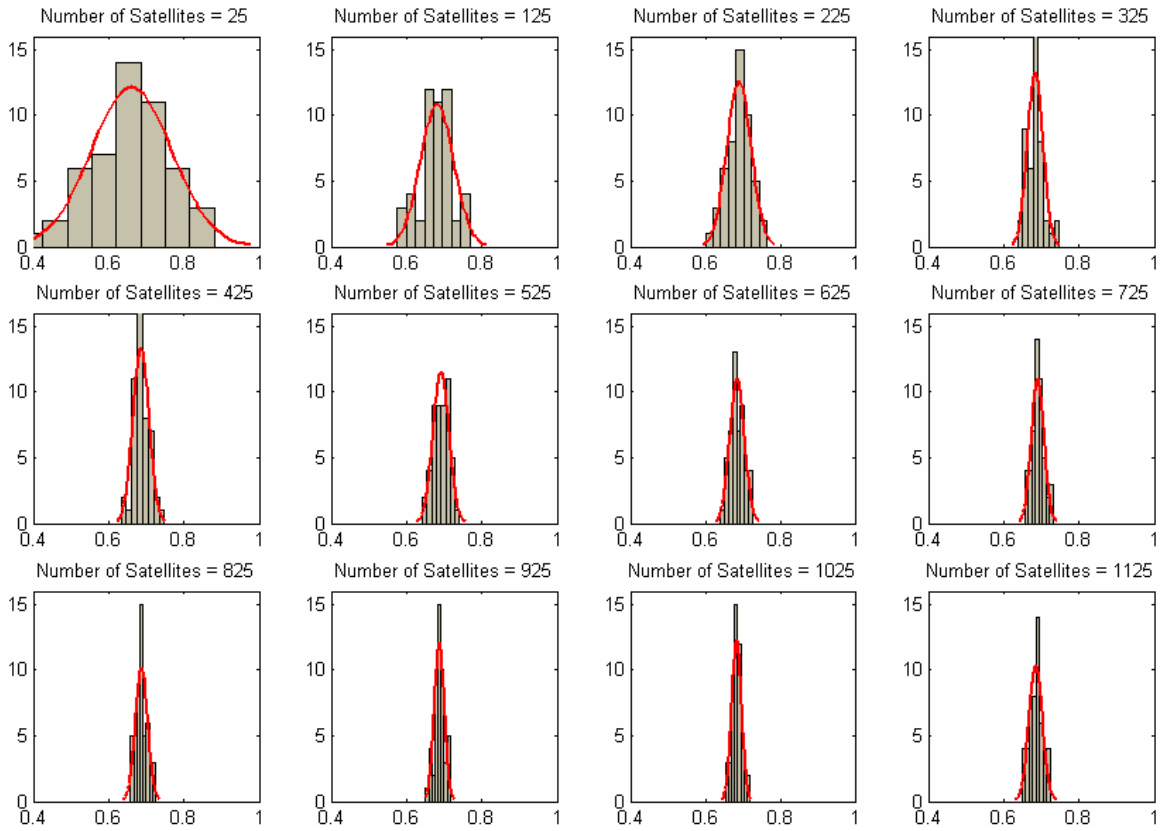
Figure 5.6: Histograms fit with a Gaussian to show the most likely fraction of the total points that are in the polar region. The bins that make up each histogram are the mean polar count for 10 iterations.

The procedure described above can determine if a system of satellites is isotropic or not, but how does having interlopers (type 1) affect this outcome? Since they cannot be "taken" out of the sample, the next best thing is to determine how many interlopers there are in the sample. Interlopers act as "noise" in the actual sample and spread out evenly. If the fraction of interlopers is small, then they do not change the situation significantly.

But if the fraction is large, it could lead to having an over density in the planar region. This is because if interlopers act as "noise" in the actual sample, then on the projected 2-D surface there will be equal numbers of satellites in the polar and planar region. Taking the geometric effect into account would mean that in 3-D space there are more satellites in the planar region than in the polar region. So to measure how affected a data set is by interlopers, Zaritsky's method of determining interloper contamination is used.

Recall that the method (section 2.2.2) by Zaritsky [16, 23] of determining the fraction of interlopers in a sample was by looking at the distribution of receding satellites vs. approaching satellites. The value P/T, which is the number of satellites with positive recessional velocity relative to the primary divided by the total number of satellites, is a useful quantitative measurement of the degree of interloper contamination. If a sample is significantly contaminated by interlopers, P/T >> 0.5 would be found.

5.2.2 Holmberg Results

For this investigation I did not have to limit myself to the three subsets previously used. Because I am examining the data in position space where the interlopers can be handled differently, as explained earlier, I am able to make one large sample with magnitude ranging from $-18.0 > M_B > -20.0$. I first examined the whole sample and then divided the sample into four equal radial bins. One sample was the only way to ensure sufficient statistics for this analysis. In figure 5.7 the angle ϕ that each satellite makes with respect to the plane (positive x - axis) of the primary for the sample is plotted. The primaries in this set are those that have a tilt less than 30 degrees from the axis of

rotation (edge-on galaxies). For this data set 0.65 ± 0.02 of all satellites were polar, the

P/T was 0.51, and the mean value of ϕ was 45.5 degrees. The error on the polar fraction

was determined from equation (13). These values correspond to a system that has an

isotropic distribution of satellites. A Kolmogorov-Smirnov (KS) test was applied to

$P(\phi \le \phi_{max})$ for this sample, and an isotropic distribution was favorable at a 0.9999

probability. Figure 5.8 shows the cumulative probability distribution plot for the position

angle of each satellite with respect to the plane of the primary.
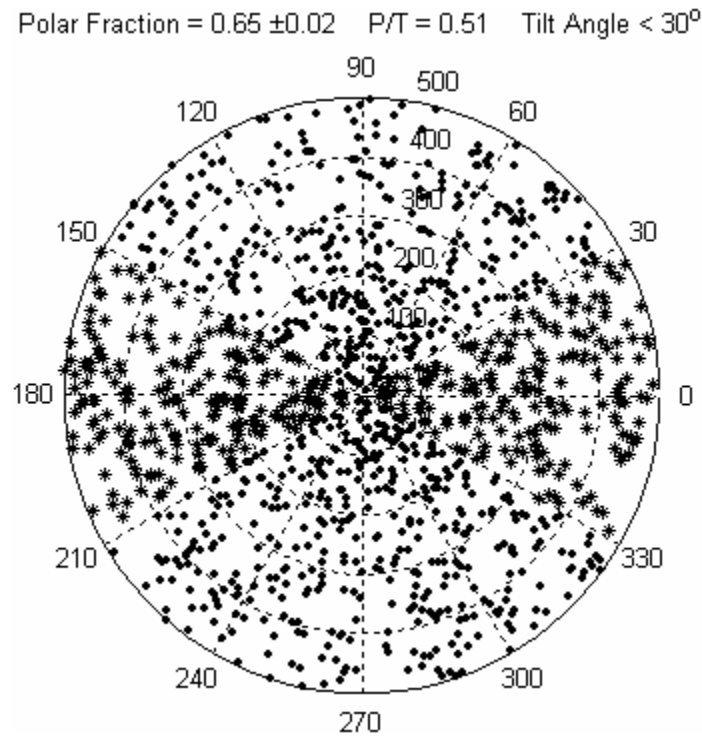
Figure 5.7: Polar plot of position angles of satellites with respect to the plane of primaries that are tilted < 30 degrees from the axis of rotation.
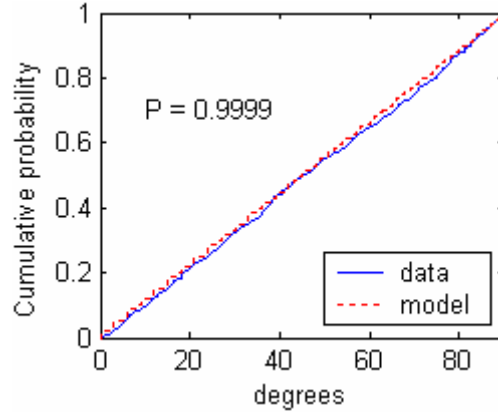
Figure 5.8: Cumulative probability distribution for the position angles of the satellites relative to the plane of the primary. Confidence level from the KS test for the data being isotropic is shown in the figure.

Next I checked what effect the tilt of the primary has on being isotropic. The range of tilt angles was divided into three different intervals: 90 degrees to 60 degrees (edge-on), 60 degrees to 30 degrees, and 30 degrees to 0 degrees (face-on). Angles are measured from the axis of rotation of primary relative to line-of-sight. Figure 5.9 shows two plots: the one on the left shows the fraction of satellites that appears polar along with the value of P/T for primary systems in the three different tilt intervals, and the one on the right shows the mean ϕ angle for these three different tilt intervals. The solid straight line is the polar fraction determined from the model, 0.69, with errors of ± 0.03 shown as the shaded grey area. The idea here, as stated above, is that if the distribution can be examined at different tilt angles, this will give an idea of what the 3-D distribution is. The polar fraction and the P/T do not change much with tilt angle. This shows that they are independent of the tilt angle, suggesting that the satellite distributions are isotropic around primary galaxies.

66

The plot of the mean angle, ϕ, is shown in figure 5.9. A KS test was applied to $P(\phi \le \phi_{max})$ for each of the intervals used to determine the mean phi in figure 5.9. The probabilities that these samples follow an isotropic distribution are also shown on this plot. These are acceptable at the 5% significance level (P > 0.05).
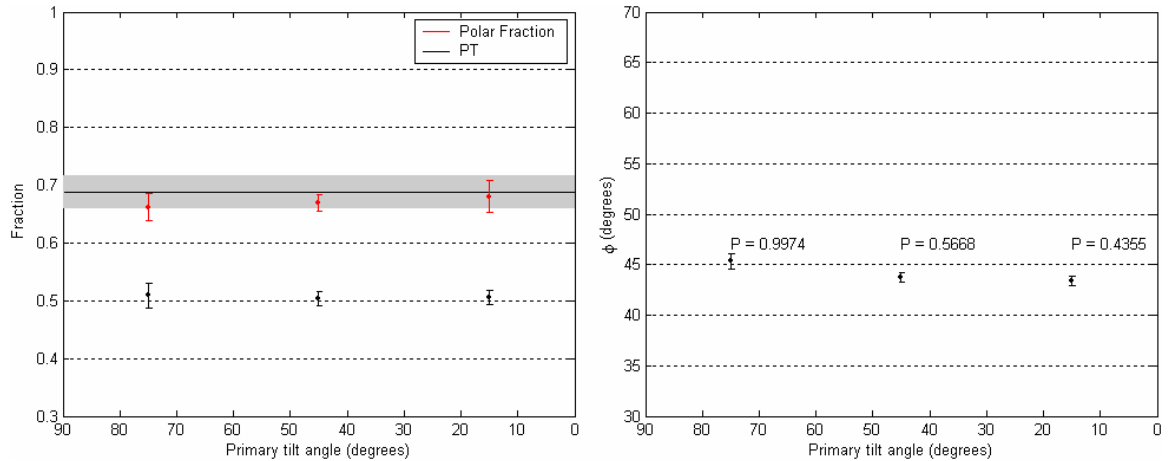
Figure 5.9: Left plot shows the fraction of satellites that appear polar along with the value of P/T for early and late type primary systems at different tilt angles. The solid straight line is the polar fraction determined from the model, 0.69 with errors of ± 0.03 shown as the shaded grey area. The plot on the right shows the mean angle, ϕ, for early and late type primaries at different tilt angles.

The results for early type primaries and late type primaries separately are shown in figure 5.10 and figure 5.11 respectively. The polar fraction and PT for early type primaries (figure 5.10) fits the model within the error bars, and the mean phi angle for early type primaries looks similar to that of the combined systems. The KS test gives probabilities that are acceptable at the 5% significance level (P > 0.05).

The late type primary system does seem to show isotropy, shown in figure 5.11.
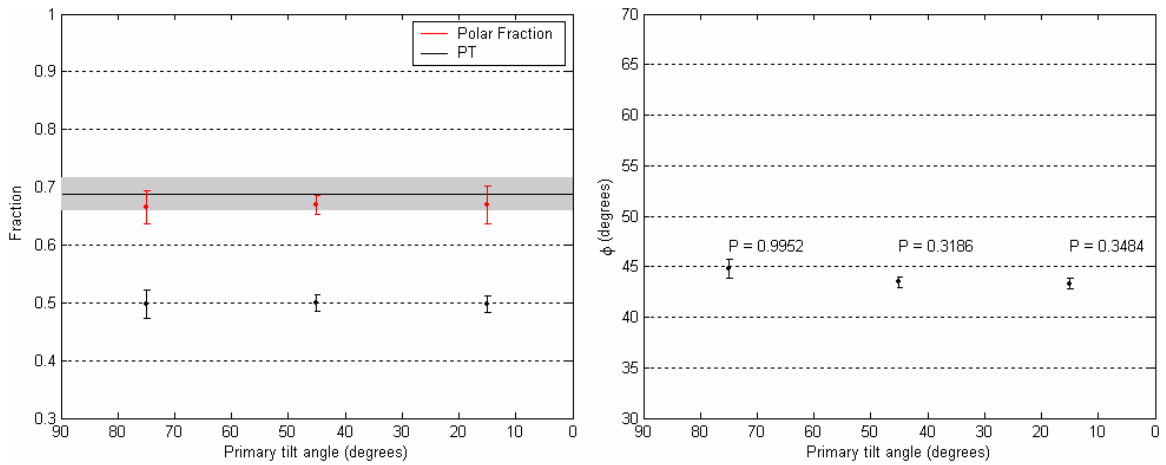
Figure 5.10: Left plot shows the fraction of satellites that appear polar along with the value of P/T for early type primary systems at different tilt angles. The solid straight line is the polar fraction determined from the model, 0.69 with errors of ± 0.03 shown as the shaded grey area. The plot one on the right shows the mean angle, ϕ, for early type primaries at different tilt angles.

The polar fraction, PT, and the mean phi angle do not depend on the tilt angle. This suggests that the satellite distributions are isotropic around late type primary galaxies. The KS test gives probabilities that are acceptable at the 5% significance level (P > 0.05).

The mean phi angle never deviates from 45 degrees by more than 3 degrees. From these plots the systems are consistent with being isotropic at angles greater than 60 degrees relative to the line of sight, and angles less than 60 degrees are consistent at a ~2σ level. The similarities between phi plots for both types of primaries and the early type primaries are likely due to the fact that early type primaries make up most of the systems in the combined sample.

68
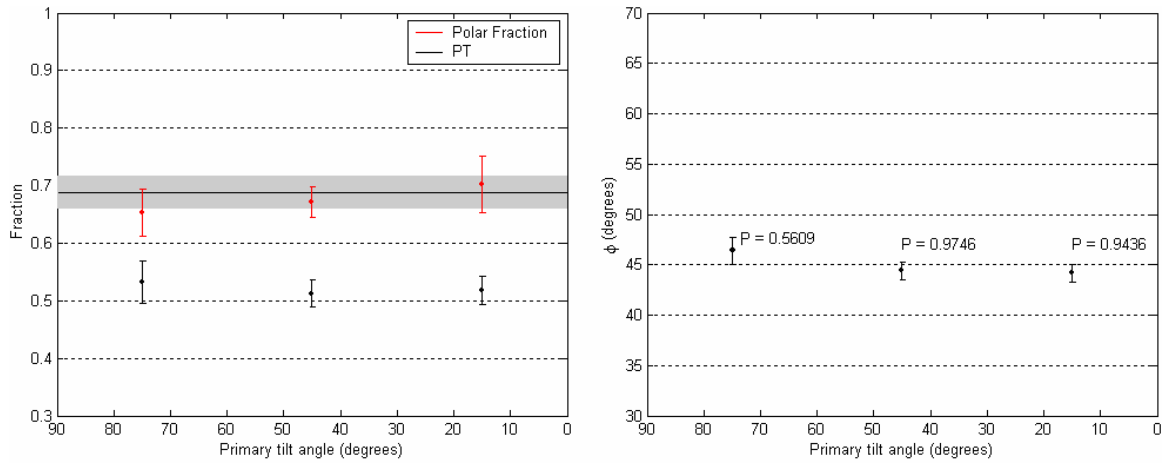
Figure 5.11: Left plot shows the fraction of satellites that appear polar along with the value of P/T for late type primary systems at different tilt angles. The solid straight line is the polar fraction determined from the model, 0.69 with errors of ± 0.03 shown as the shaded grey area. The plot one on the right shows the mean angle, ϕ, for late type primaries at different tilt angles.

I did one more analysis to see if there could be a localized anisotropy in the data by breaking up the sample into four equal radial bins. The polar plots in figure 5.12 are the same data plotted in figure 5.7 except in four radial bins. Again, we see that the fractions of polar satellites in each bin match the model for isotropy. PT is around 0.5, with the exception of bin 2. These results favor a system that is isotropically distributed.
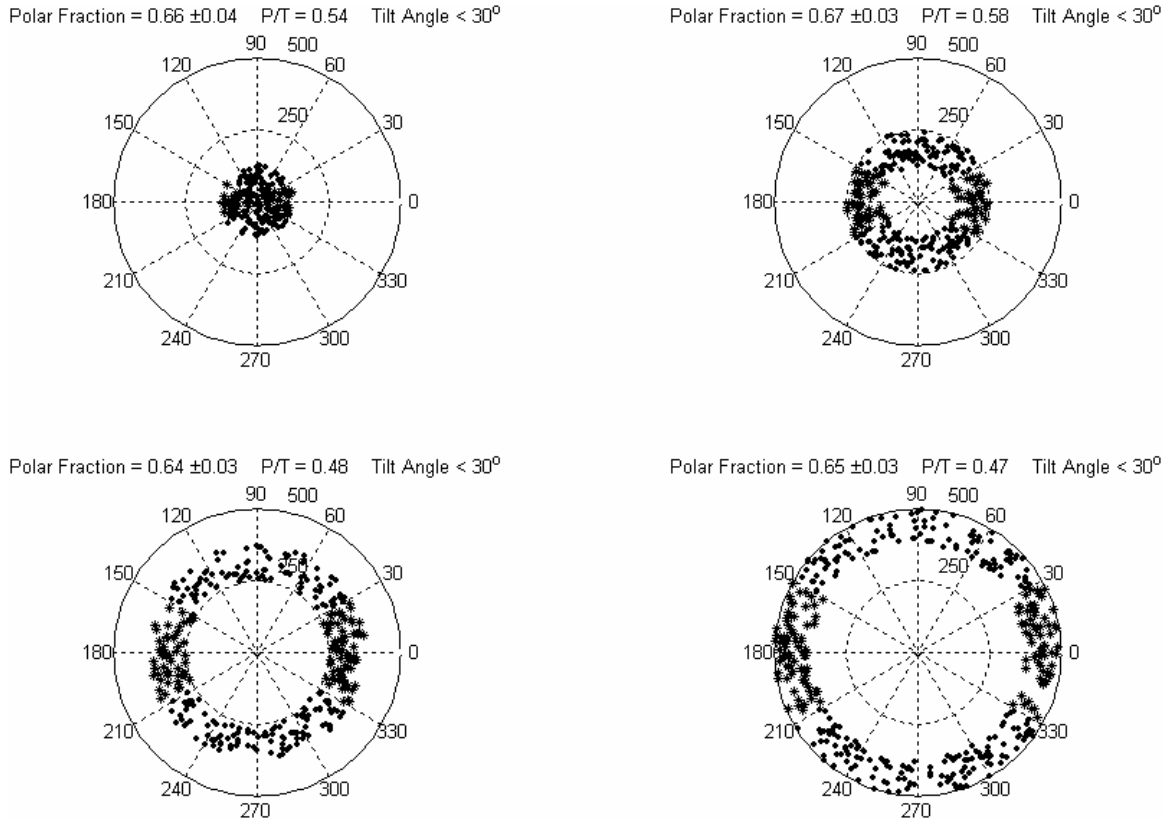
Figure 5.12: Polar plot of position angles of satellites with respect to the plane of primaries that are tilted < 30 degrees from the axis of rotation for four radial bins.

The mean ϕ angles of the four radial bins are determined and plotted in figure 5.13. From this analysis there seems to be no Holmberg Effect at any distance from the primary. The KS test for each bin in this sample was done, and the results are shown in figure 5.14 along with the cumulative probability distribution plots for each bin. These results are drastically different than what Brainerd [52] found at small projected radii. In her sample she found that an over density existed along the plane of the galaxy at small projected radii then became more isotropic at larger projected distance.
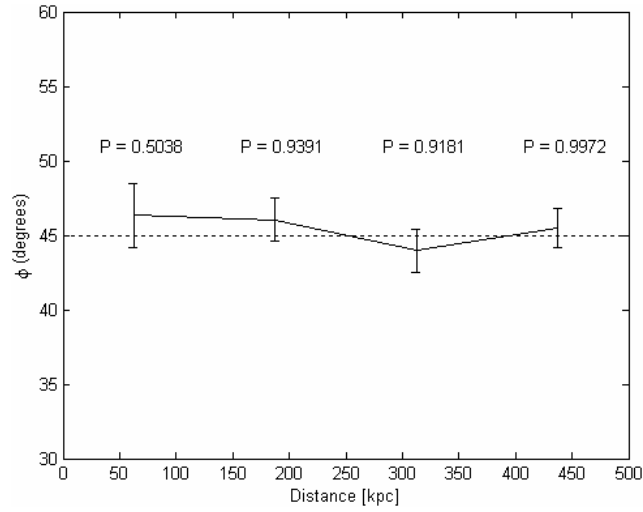
Figure 5.13: The average angle, ϕ, of satellites in the radial bins corresponding to figure 5.12.
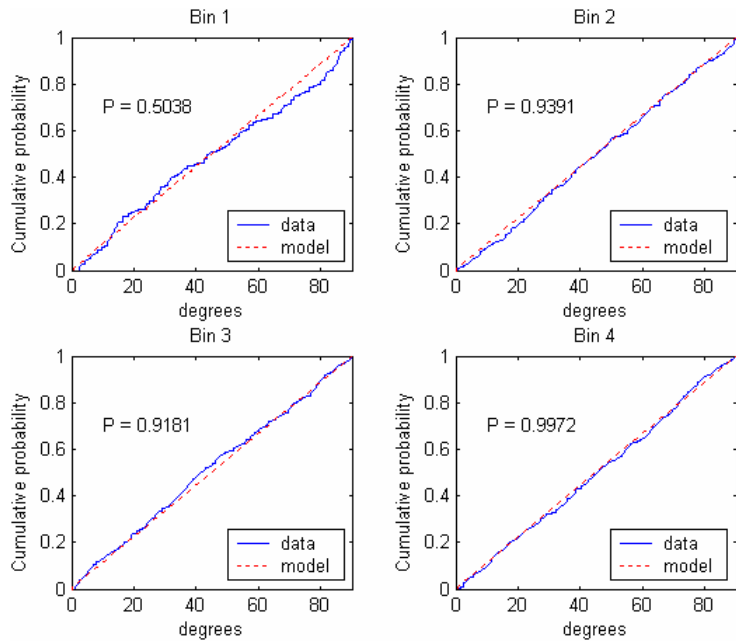
Figure 5.14: Cumulative probability distribution for the position angles of the satellites relative to the plane of the primary for the radial bins corresponding to figure 5.12. Confidence level from the KS test for the data being isotropic is shown in the figure.

71

Plots similar to figures 5.12 and 5.13 were made for primaries that had a tilt angle > 60 degree from the axis of rotation (face-on). Figure 5.15 shows the position angle of satellites relative to the plane of their primaries. These results favor a system that is isotropically distributed.
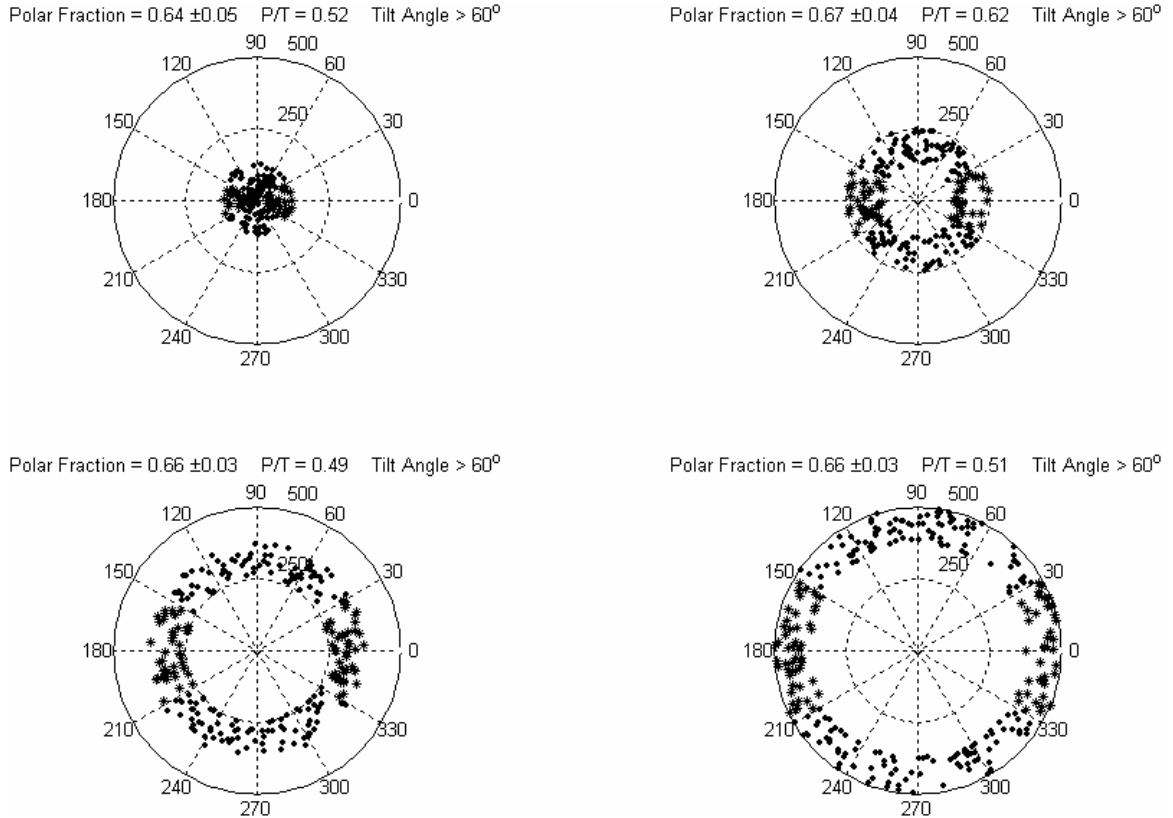
Figure 5.15: Polar plot of position angles of satellites with respect to the plane of primaries that are tilted > 60 degrees from the axis of rotation for four radial bins.

Figure 5.16 shows the average angle, ϕ, of satellites in each of the four radial bins along with the probabilities from the KS test. Systems with a tilt greater than 60

degrees from the axis of rotation (face-on) are consistent with being isotropic at a <1σ

level.
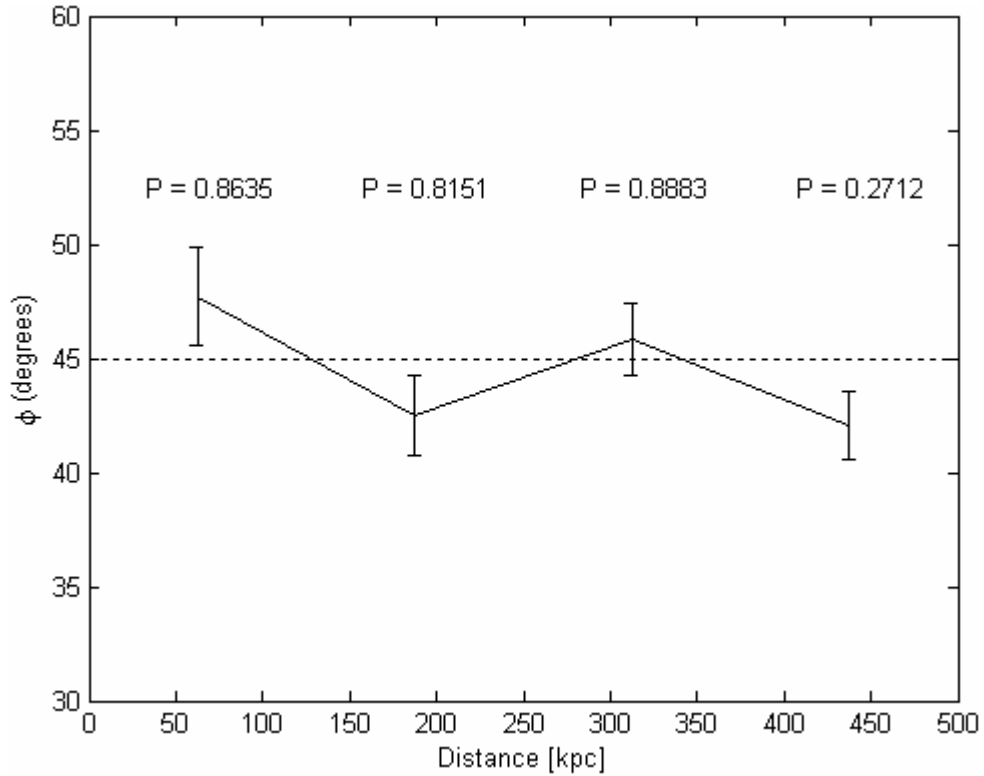
Figure 5.16: The average angle, ϕ, of satellites in each of the four radial bins in figure 5.15.

Regardless of what method I used to determine isotropy, including a similar

restriction as Sales and Lambas [38], by limiting satellites to relative velocities

< 150km/s, and finding little deviation (2σ at most) for an anisotropic distribution of

satellites, the analysis shows no Holmberg Effect. Kosh and Grebal [45] also found

evidence that satellite galaxies in the local group are isotropically distributed; that is, they find no evidence of the Holmberg Effect around M31.

Studies of the Holmberg Effect have been done by Zaritsky et al. [32, 33, 34, 36] and Sales and Lambas [38]. Zaritsky, using the same data from his mass distribution study [32], concluded that beyond $50 kpc$ there was no Holmberg Effect and believed that Holmberg's sample was too small for a definitive conclusion. Using the 2DF Galaxy Redshift Survey, Sales and Lambas found over 1000 primaries and ~800 satellites for their Holmberg study. They found more satellites in the region $> 60°$ relative to the axis of rotation of the galaxy than in the region $< 30°$ relative to the plane of the galaxy. This study found the Holmberg Effect to be present up to $500 kpc$ for satellites with relative velocities < 160km/s [38].

5.2.3 Velocity dispersion In Perpendicular Directions

From the Holmberg analysis it was a natural step to get the velocity dispersion in the plane of the disk using the planar satellites and to get the velocity dispersion in the polar region using the polar satellites. Determining the velocity dispersion in two directions will give an idea on the "shape" of the halo. Having found the satellites in both of these regions, I can plot the velocity dispersion curve for each region. In figure 5.17 the velocity dispersion of satellites in the polar region and in the planar region is plotted for all primaries with a tilt angle less than ~45 degrees from the axis of rotation. This dispersion was found, as before, using the robust fitting procedure from section 4.2.2.
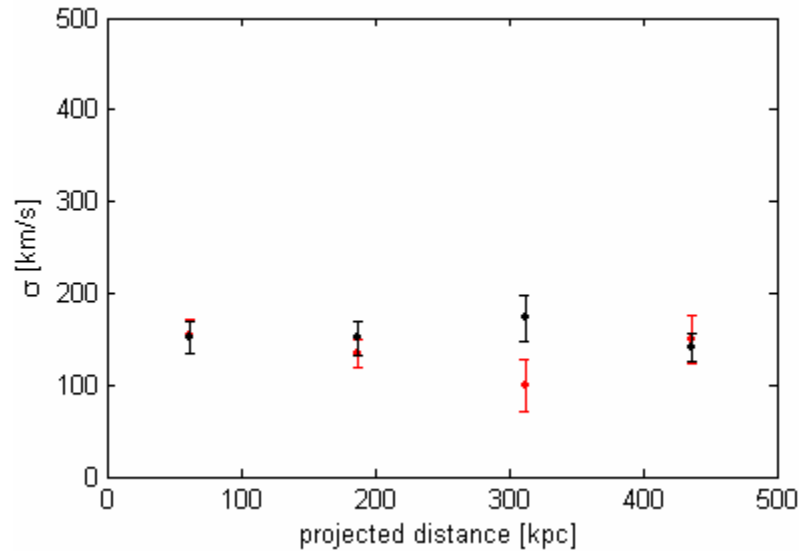
Figure 5.17: The velocity profiles for satellites in the planar region (red) and the polar region (black). These satellites belong to primaries with a tilt angle less than ~45 degrees from the axis of rotation.

The robust analysis showed that the velocity dispersion and interloper fraction were independent of bin size. The analysis also showed that the data did not always follow a Gaussian plus constant shape. The data in the third radial bin for the planar satellites, and the data in the second radial bin for the polar satellites, each dropped below the 0.01 significant level (~0.008) when the number of bins used to fit the Gaussian plus constant was equal to seven.

To date, there has been no effort to probe these regions separately, probably due to the lack of data needed for this study, so despite of the fact that these data sets fail the robust analysis, it will be informative to continue with the comparison.

In figure 5.18 a similar plot is shown for primaries with angles greater than ~45 degrees from the axis of rotation (face-on). Again, using the robust analysis, the velocity

dispersion was found and plotted. This time all the bins were greater than the 0.01

significant level.
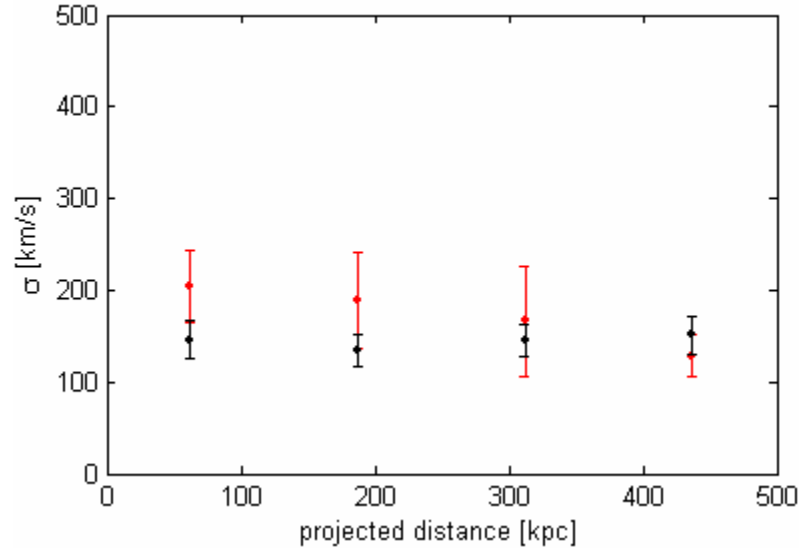
Figure 5.18: The velocity profiles for satellites in the planar region (red) and the polar region (black). These satellites belong to primaries with a tilt angle greater than ~45 degrees from the axis of rotation.

These two plots give information about the velocities of satellites in three

dimensions. When looking at the velocity profiles for the primary galaxies that were

more edge-on (figure 5.17), they exclude the more face-on galaxies. This means that most

of the velocity information came from the ϕ-direction and r-direction (not the z-direction).

The opposite is true for figure 5.18. This velocity profile excludes primaries that were

edge-on, so most of the velocity information came from the z-direction (not the ϕ-

direction or r-direction). This analysis suggests that the velocity distribution of satellites

is isotropic about the primary (which was assumed for the velocity profile analysis). A larger data set is needed to get a large number of satellites to explore this in much more detail. In particular, it would be advantageous to compare samples of nearly edge-on galaxies to near face-on galaxies in order to better separate the velocity components. These results at least show that the analysis can be done.

5.3 Tully - Fisher

The Tully-Fisher relation is a standard candle that relates the distance of a galaxy to its luminosity. Because the luminosity is related to the absolute magnitude, the Tully-Fisher relation for a system of satellites can be determined. This is an empirically-derived relation that states that the luminosity of a galaxy is directly proportional to the fourth power of its rotational velocity, $L \propto v^4$. In the following analysis this relation will be associated to the dispersion as

$$\sigma \propto L^{0.24}. \tag{15}$$

Consider that if as the stars orbit around in a galaxy, their speed were to increase, the mass of the galaxy would have to increase to keep the stars bound. Measuring the radial velocity of stars in the disk of a galaxy gives an idea of how much mass the galaxy contains. Since the galaxy's mass is related to its luminosity, the relation between luminosity and velocity exists.

In the following three figures (figure 5.19 and figure 5.20) the velocity dispersion of satellites in bin 1 that passed the robust analysis was plotted vs. the luminosity of their primary. The data points are labeled with the subset number they came from. The

velocity dispersion was taken only from the first bins that were greater than the 0.01 significant level. The luminosity was determined using the average magnitude of that subset.

In the first figure, representing early and late type primaries, the plot follows a power law in the form $\sigma \propto L^{0.37\pm0.02}$ (dotted line). This is lower than what Brainerd [18] and McKay et al. [37] determined. They determined $L^{0.45}$ and $L^{0.50}$ respectively.

Figure 5.20 was made the same way as figure 5.19 except for the late type primaries. The subsets that passed for the early type primaries all fell within the same magnitude range, as a result, they give no useful information in a velocity vs. luminosity plot. The late type primaries fit a power law of $L^{0.22\pm0.02}$, which matches the Tully-Fisher within the uncertainty.
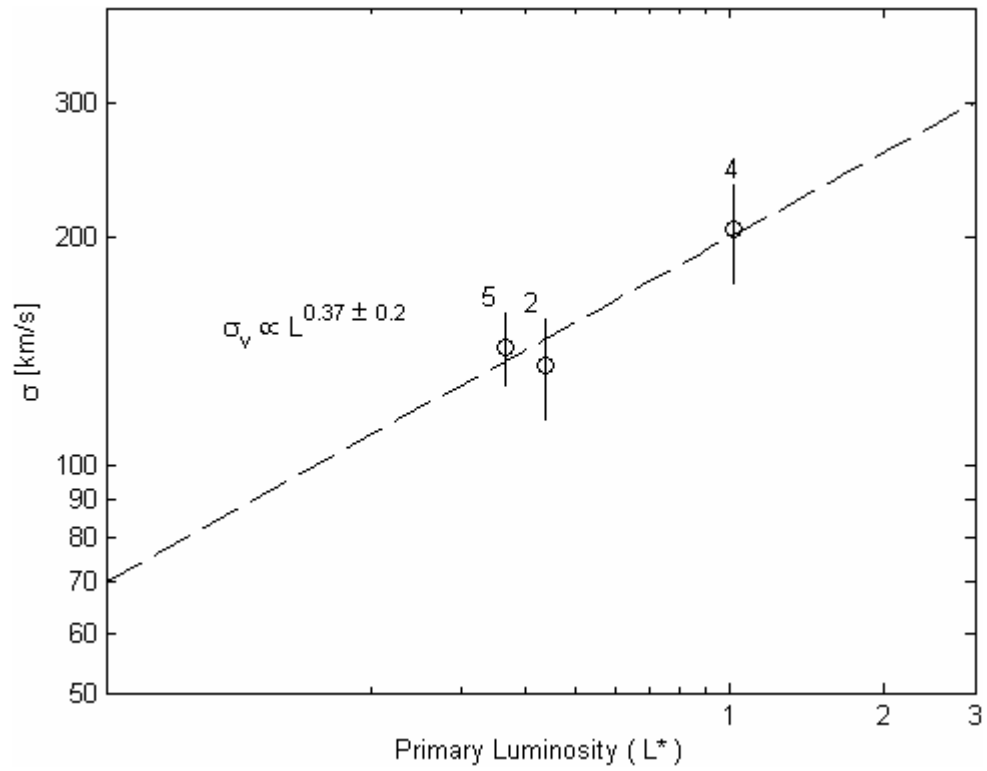
Figure 5.19 Velocity dispersion vs. primary luminosity for early and late type primaries. Dispersions are from satellites within 125*kpc* (bin 1) of the primary. The velocity dispersion was taken only from the first bin of subsets that had a probability > 0.01.
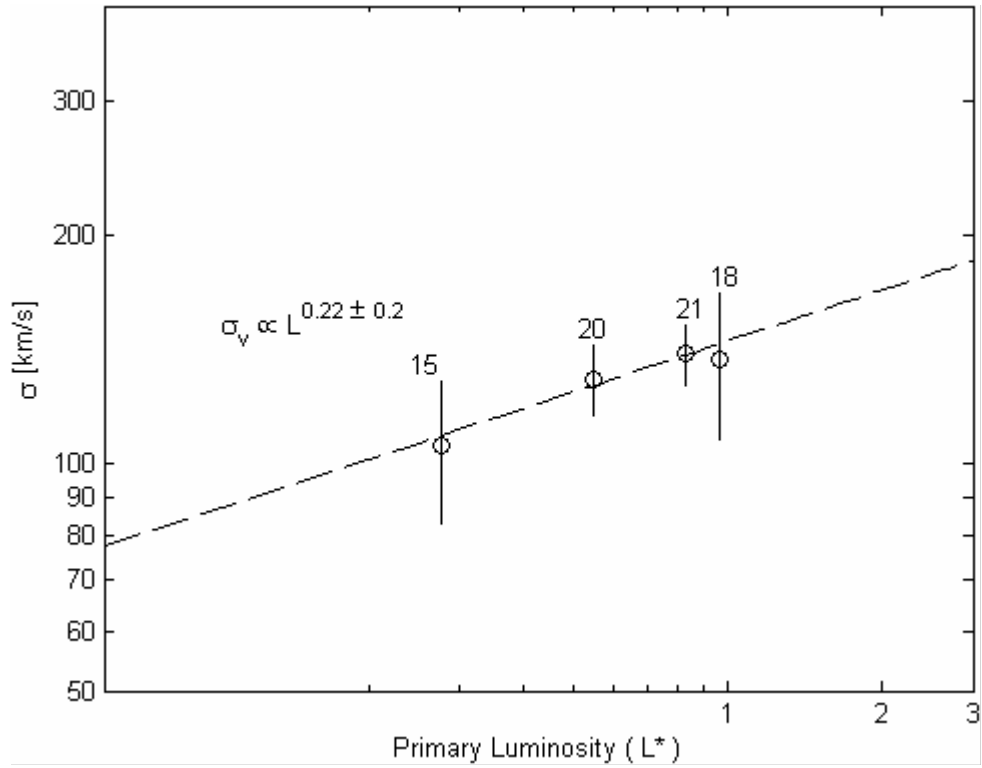
Figure 5.20: Velocity dispersion vs. primary luminosity for late type primaries. Dispersions are from satellites within 125*kpc* (bin 1) of the primary. The velocity dispersion was taken only from the first bin of subsets that had a probability > 0.01.

CHAPTER VI
CONCLUSION

By using the NYU data I was able to create a sample of isolated galaxies and related satellite galaxies. Then breaking up the sample into multiple subsets of varying absolute magnitude of the primaries, I was able to narrow the data down to a few reliable subsets. The main sample consisted of 2741 primaries between $-18.0 > M_B > -20.0$ and 4966 satellites between $-12.0 > M_B > -18.0$.

Results of a robust analysis preformed on the data showed which data is more likely to follow a Gaussian plus constant model. From the data, at a significant level of $P > 0.05$, I found that the line-of-sight velocity dispersion declines with distance indicating a dark matter halo. This trend agrees with the cosmological models of NFW and other published results that find that the density of the dark matter halo declines as $\rho \propto r^{-3}$. The neutrino model has large probabilities and cannot be completely excluded as a possible explanation of the observed velocity dispersions at the $P > 0.01$ significant level. The MOND model had small probabilities of fitting the velocity dispersion, and results of higher dispersions found for early type primaries than those found for late type primaries of the same luminosity make MOND unlikely.

Finding that the NFW model describes satellite dynamics in the local Universe ($0.005 < z < 0.05$, range in the data used in this study), and also describes satellite dynamics farther out $(0.06 < z < 0.2)$, supports the hierarchical scenario of evolution of structures in the Universe.

The line-of-site dispersion was measured in two perpendicular directions: along the plane and along the axis of rotation. There is no other work on this to compare results, but I can draw some conclusions from the analysis. I found that the magnitudes of the velocity dispersions in both directions are independent of primary tilt (within the error bars). This leads to the conclusion that the satellite velocities are distributed isotropically and suggests that the dark matter halo is spherical in shape, which some cosmological models predict. This also lends support to the initial assumption of an isotropic velocity halo.

This velocity profile analysis has provided some new insights into the study of the mass distribution of isolated galaxies beyond their optical radii. The results that early type primaries have a larger dispersion than late type primaries at the same luminosity suggest that early type primaries have a larger dark matter halo. The additional dark matter in the early type primaries is most likely from having a larger primordial dark matter halo at birth than the late type primaries. When a galaxy is forming, the infall rate of the baryonic matter depends on how large the dark matter halo is. The larger the dark matter halo, the faster the infall, and the faster the galaxy forms. By initially having a larger dark matter halo, a galaxy can evolve from a late type galaxy to an early type galaxy relatively faster than a galaxy that initially has a smaller dark matter halo.

To gain a better understanding of this phenomenon, an even larger sample of primary galaxies and their satellites is needed. Minimizing the magnitude range of primaries in an ensemble allows for the most efficient way to investigate their properties. Also, breaking up primaries by type, will give more detail of how different these systems

may be. By making samples in this manner (this was done in this study), a large number is needed to get an accurate result when determining the velocity dispersions of satellites.

I also investigated the stellar populations of the satellites surrounding isolated galaxies. I found that the distribution of satellites of low magnitude primaries (early or late) is similar. Furthermore, I find that the high magnitude primary sample shows early type satellites decline more steeply than late type satellites, indicating that the primary galaxy does have an influence on their satellites.

The satellite galaxies can be influenced by the gravitational dynamics between them and their primary. This gravitational force varies with distance from the primary. This means that the part of the satellite closer to the primary feels a stronger pull than the part of the satellite farther from the primary causing a "tidal" effect over the entire satellite. This tidal force can cause perturbations in the motion of stars and gas in the satellite galaxy inducing star formation. The total angular momentum must be conserved in the system. The interaction will increase the satellites' internal angular momentum and decreases the satellites' orbital angular momentum. This loss in orbital angular momentum causes the orbital radius of the satellite to decrease, becoming closer to the primary. This effect would be more pronounced in satellites with primaries that have a larger mass (magnitude), as shown by the results.

In this analysis a larger sample cannot hurt, but it would be of more significance to get a sample with systems (primaries of high magnitude $-19.0 > M_B > -20.0$ and fainter satellites) at a much farther distance than the one used in this study. This process in which the primary gravitationally affects its satellites takes place over a long period of

time. If this is truly the case and if we look at systems at larger z (longer ago), then we should find more late type satellites closer to the primary. This would also give support to the hierarchal scenario.

From the data I also found little deviation (1σ at most) for an anisotropic distribution of satellites, suggesting that the Holmberg Effect is not present. This anisotropy was not seen even when the tilt of the galaxy relative to the rotation axis was taken into account. From the data, satellite galaxies tend to be isotropic near the primary galaxy and at large projected distances from the primary galaxy. The only way for this analysis to be improved is to create a large sample of satellites that are very close ($< 50 kpc$) to their primary. A larger sample has been used [54], and it was found that on scales of $< 50 kpc$ satellites are preferentially aligned with the major axis of the primary.

The results show that the primordial state of these systems is isotropic and puts constraints on galaxy formation models that preferentially align satellites along filaments.

The typical size of the subsets that I used was ~1000 satellites, for a range within $500 kpc$. This would be a large sample size if they were all within $50 kpc$ and would insure that this region was probed effectively.

Finally, I found the velocity dispersion of satellites within $125 kpc$ scales with the luminosity of the primary galaxy (late) as $\sigma \propto L^{0.22 \pm .02}$.

The velocity dispersions of satellites, for late type primaries, fall within the Tully-Fisher relation. The fact that satellite dispersions are related to the luminosity of their primary even though the dispersions are driven by the dark matter halo tells us something about the matter distribution in the early Universe. There is no reason that a large dark

matter halo cannot have a small low luminous galaxy. The relationship seen in figures 5.19 and 5.20 suggests that matter was evenly distributed in the early Universe. This allowed dark matter halos to "take in" an amount of matter proportional to their size.

To obtain better results here, again, the benefit of a larger sample would make the statistics better. With a larger sample I could break up the sample into even smaller luminosity bins, which would minimize mixing of different size galaxies. Having small luminosity bins would also give more range in the primary luminosities for a better power law fit.

REFERENCES

[1]Zwicky, F., "Die Rotverschiebung von extragalaktischen Nebeln," Helvetica Phys.Acta, 6, pp. 110, (1933).

[2]Babcock, H. W., "The Rotation of the Andromeda Nebula," Lick Observatory bulletin no. 498, pp. 41-51, (1939).

[3]Roberts, M. S., and Whitehurst, R. N., "The Rotation Curve and Geometry of M 31 at Large Galactocentric Distances", Astrophysical Journal, 201, pp. 327-346, (1975).

[4]Ostriker, J. P., and Peebles, P. J. E., "A Numerical Study of the Stability of Flattened Galaxies: or, Can Cold Galaxies Survive?" Astrophysical Journal, 186, pp. 467-480, (1973).

[5]Ostriker, J. P., and Peebles, P. J. E., and Yahil, A., "The Size and Mass of Galaxies, and the Mass of the Universe", Astrophysical Journal, 193, pp. L 1-L4, (1974).

[6]Hannestad, S., Mirizzi, A., and Raffelt, G., "New Cosmological Mass Limit on Thermal Relic Axions," Journal of Cosmology and Astroparticle Physics, 7, p. 02, (2005).

[7]Desai, S et al., "Search For Dark Matter WIMPs Using Upward Through-Going Muons in Super-Kamiokande," Physical Review D, 70, id. 083523, (2004).

[8]Alcock, C. et al., "EROS and MACHO Combined Limits on Planetary-Mass Dark Matter in the Galactic Halo", Astrophysical Journal Letters, 499, p. L9, (1998).

[9]Gnedin, O., Y., "Response of Dark Matter Halos To Condensation of Baryons: Cosmological Simulations And Improved Adiabatic Contraction Model," The Astrophysical Journal, 616, Issue 1, pp. 16-26, (2004).

[10]Plionis, M., Basilakos, S., "The Cluster Substructure-Alignment Connection," Monthly Notices of the Royal Astronomical Society, 329, pp. L47-L51, (2002).

[11]Hoffman, Y., "On the Formation and Structure of Galactic Halos," Astrophysical Journal, 328, pp. 489-498, (1988).

[12]Gunn, J. E., Gott, J. R., "On the Infall of Matter Into Clusters of Galaxies and Some Effects on Their Evolution," Astrophysical Journal, 176, pp. 1-19, (1972).

[13] Navarro, J. F. and White, D. M., "The Structure of Cold Dark Matter Holos," Astrophysical Journal, 462, pp. 563-575, (1996).

[14] Navarro, J. F. and White, D. M., "A Universal Density Profile from Hierarchical Clustering," Astrophysical Journal, 593, pp. L7-L10, (1997).

[15] Navarro et al., "The inner structure of ΛCDM haloes - III. Universality and asymptotic slopes," Monthly Notices of the Royal Astronomical Society, 349, pp. 1039-1051, (2004).

[16] Zwicky, F., "On the Masses of Nebulae and of Clusters of Nebulae," Astrophysical Journal, 86, pp. 217, (1937).

[17] Brainerd, T. G., Blandford, R. D. and Smail, I., "Weak Gravitational Lensing by Galaxies," Astrophysical Journal, 466, pp.623 (1996).

[18] Brainerd, T. G., "Constraints on Field Galaxy Halos from Weak Lensing and Satellite Dynamics," arXiv:astro-ph/0411244 v1 9 Nov (2004).

[19] Faber, S. M., Gallagher, J. S., "Masses and Mass-to-Light Ratios of Galaxies," Annual review of astronomy and astrophysics, 17, p. 135-187, (1979).

[20] Sofue, Y., Rubin, V., "Rotation Curves of Spiral Galaxies," Annual Review of Astronomy and Astrophysics, 39, pp. 137-174, (2001).

[21] Wigmans, R., "On the Accelerated Expansion of the Universe," Submitted to Phys. Rev. Lett., (2004).

[22] Ringwald, A. and Wong, Y., Y., "Gravitational Clustering of relic Neutrinos and Implications for Their Detection," Journal of Cosmology and Astroparticle Physics, Issue 12, pp. 005 (2004).

[23] Wigmans, R., Personal communication. Department of Physics, Texas Tech University, Lubbock, TX).

[24] Milgrom, M., "A Modification of the Newtonian Dynamics as a Possible Alternative to the Hidden Mass Hypothesis," Astrophysical Journal, 270, pp. 365-370, (1983).

[25] Milgrom, M., "A Modification of the Newtonian Dynamics: Implications for Galaxy systems," Astrophysical Journal, 270, pp. 384-389, (1983).

[26] Sloan Digital Sky Survey (SDSS). For information, history and data from SDSS. Retrieved May 22, 2006, from the World Wide Web: http://www.sdss.org.

[27]Harvard-Smithsonian Center for Astrophysics. To access CfA Redshift Catalog, zcat. Retrieved May 22, 2006, from the World Wide Web: http://cfa-www.harvard.edu/~huchra/zcat/.

[28]Centre de Données astronomiques de Strasbourg. To access The Uppsala General Catalogue of Galaxies (UGC). Retrieved May 22, 2006, From the World Wide Web: http://cdsweb.u-strasbg.fr/viz-bin/Cat?VII/26D.

[29]The Anglo-Australian Observatory. To access 2dF Galaxy Redshift Survey (Two-degree-Field Galaxy Redshift Survey). Retrieved May 22, 2006, From the World Wide Web: http://www.aao.gov.au/2df/.

[30]Prada et al., "Observing the Dark Matter Density Profile of Isolated Galaxies," Astrophysical Journal, 598, pp.260-271, (2003).

[31]Brainerd, T. G., "Concordance between the Dynamics of Satellite Galaxies in the 2dFGRS and ΛCDM," arXiv:hep-ph/0409381 v1 7 Sep (2004).

[32]Zaritsky, Dennis, "The Asymmetric Distribution of Satellite Galaxy Velocities," Astrophysical Journal, 400, pp. 74-79, (1992).

[33]Zaritsky, D., Smith, R., Frenk, C. and White, S. D. M., "Satellites of Spiral Galaxies," Astrophysical Journal, 405, pp. 464-478, (1993).

[34]Zaritsky, D. and White, S. D. M., "The Massive Halos of Spiral Galaxies," Astrophysical Journal, 435, pp. 599-610, (1994).

[35]Zaritsky, D., Smith, R., Frenk, C. and White, S. D. M., "More Satellites of Spiral Galaxies," Astrophysical Journal, 478, pp. 39-48, (1997).

[36]Zaritsky et al., "Anisotropies in the Distribution of Satellite Galaxies," Astrophysical Journal, 478, pp. L53 - L56, (1997).

[37]McKay et al., "Dynamical Confirmation of Sloan Digital Sky Survey Weak-lensing Scaling Laws," Astrophysical Journal, 571, pp. L85, (2002).

[38]Sales, J. and Lambas, D. G., "Anisotropy in the distribution of satellites around primary galaxies in the 2df Galaxy Redshift Survey: the Holmberg Effect," Mon. Not. R. Astron. Soc., 348, pp. 1236-1240, (2004).

[39]Arp, H., "Characteristics of companion galaxies," Astrophysical Journal, 256, pp. 54-74, (1982).

[40]Blanton et al., "The Luminosity Function of Galaxies in SDSS Commissioning Data," Astrophysical Journal, 121, pp. 2358-2380, (2001).

[41]Holmberg, E., "A Study of Physical Groups of Galaxies," Arkiv för Astronomii, 5, pp.305-343, (1969).

[42]Majewski, S., R., "The Fornax-Leo-Sculptor stream revisited," The Astrophysical Journal, Part 2 - Letters, 431, pp. L17-L21, (1994).

[43]Quinn P., Goodman J., "Sinking satellites of spiral systems," Astrophysical Journal, 309, pp. 472-495, (1986).

[44]Knebe et al., "Anisotropies in the Distribution of Satellite Galaxy Orbits," Astrophysical Journal, 603, pp. 7 -11, (2004).

[45]Koch, A., and Grebel, E. K., "The Anisotropic Distribution of M31 Satellite Galaxies: A Polar Great Plane of Early-Type Companions," arXiv:astro-ph/0509258, (2006).

[46]Mathworks. For information of the program language MatLab[®]. Retrieved May 22, 2006, from the World Wide Web: http://www.mathworks.com

[47]Blanton et al., "NYU-VAGC: a galaxy catalog based on new public surveys," Astrophysical Journal, 129, pp. 2562, (2004).

[48]Adelman-McCarthy et al., "The Fourth Data Release of the Sloan Digital Sky Survey," arXiv:astro-ph/0507711, accepted to ApJ, (2005).

[49]Yasuda et al., "Galaxy Number Counts from the Sloan Digital Sky Survey Commissioning Data," The Astronomical Journal, 22, pp. 1104-1124, (2001).

[50]Strateva et al., "Color Separation of Galaxy Types in the Sloan Digital Sky Survey Imaging Data," The Astronomical Journal, 122, 4, pp.1861-1874, (2001).

[51]Lorrimer et al., "The Distribution of Satellite Galaxies," R.A.S. Monthly Notices, 269, pp. 696, (1994).

[52]Brainerd, T. G., "Anisotropic Distribution of SDSS Satellite Galaxies: Planar (Not Polar) Alignment," The Astrophysical Journal, 628, L101-L104, (2005).

[53]Agustsson, I. and Brainerd, T., "The Orientation of Satellite Galaxies: Evidence of Elongation in the Direction of the Host," The Astrophysical Journal, 644, pp. L25-L28, (2006).

APPENDIX A
MATLAB CODES

This Appendix documents the main computer programs used in this project.

<u>Galaxy Search</u>

This program takes in a text file with galaxy parameters from NYU and uses them

to obtain primary galaxies and possible satellites.

nyu_prim_sat_search.m

```
%program to read in .txt file NYU (SDSS) DR2 data

%the text file is in columns with 1.ra, 2.dec, 3.zdist,
%4.u absolute magnitude, 5.g, 6.r, 7.i, 8.z, 9.ab ratio
%and 10. phi-position angle of galaxy
%from these it finds primary galaxies and their satellites
%and prints them to file
%_____
____
clear;
clc;
tic;
%%%%%%%%%%%%%%%%%%%%%%%%%%%%%%%%%%%%%%%%%%%%
%%%%%%%%%%%%%%%%%%%%%%%%%%%%%%%%%%%%
%input parameters for primiaries_____
iso_mag = 2;              %magnitude difference to be isolated
iso_proj = 1000;           %projected distance to be isolated
iso_vel = 1000;            %velocity difference to be isolated
%%%%%%%%%%%%%%%%%%%%%%%%%%%%%%%%%%%%%%%%%%%%
%%%%%%%%%%%%%%%%%%%%%%%%%%%%%%%%%%%%
%input parameters for satellites_____
sat_mag =  2;             %magnitude difference to be sat
sat_proj = 500;            %projected distance to be sat
sat_vel = 500;            %velocity difference to be sat
%%%%%%%%%%%%%%%%%%%%%%%%%%%%%%%%%%%%%%%%%%%%
%%%%%%%%%%%%%%%%%%%%%%%%%%%%%%%%%%%%
%read in excel file of galaxy data
%file - ra, dec, zdist, u, g, r, i, z, AB ratio and phi
```

```matlab
data = textread('all_holm001.txt');
ra = data(:,1);                %ra
dec = data(:,2);               %dec
zdist = data(:,3);             %redshift z
u_mag = data(:,4);             %u absolute magnitude
g_mag = data(:,5);             %g absolute magnitude
r_mag = data(:,6);             %r absolute magnitude
i_mag = data(:,7);             %i absolute magnitude
z_mag = data(:,8);             %z absolute magnitude
AB_ratio = data(:,9);          %ab ratio
phi_angle = data(:,10);        %position angle from east of north
%%%%%%%%%%%%%%%%%%%%%%%%%%%%%%%%%%%%%%%%%%%
%%%%%%%%%%%%%%%%%%%%%%%%%%%%%%%%%%
%determining distance, velocity and B magnitude_____
H = 70;                        %hubble constant (km/s/Mpc) with h=1
c = 300000;                    %speed of light (km/s)
D = zdist.*c./H;               %distance (Mpc)
v_radial = H.*D;               %velocity (km/s)
B_mag = 0.482.*(g_mag - r_mag) + 0.169 + g_mag;     %B magnitude
%%%%%%%%%%%%%%%%%%%%%%%%%%%%%%%%%%%%%%%%%%%
%%%%%%%%%%%%%%%%%%%%%%%%%%%%%%%%%%
%possible primaries with absolute B magnitude B <= -18_____
%gathering parameters for possible primaries_____
dum = 1;
for k=1:length(B_mag);
   if (B_mag(k) < -18);
      ra_limit(dum) = ra(k);
      dec_limit(dum) = dec(k);
      u_limit(dum) = u_mag(k);
      g_limit(dum) = g_mag(k);
      r_limit(dum) = r_mag(k);
      i_limit(dum) = i_mag(k);
      z_limit(dum) = z_mag(k);
      AB_limit(dum) = AB_ratio(k);
      phi_limit(dum) = phi_angle(k);
      D_limit(dum) = D(k);
      B_limit(dum) = B_mag(k);
      v_limit(dum) = v_radial(k);
      dum = dum + 1;
   end
end
%%%%%%%%%%%%%%%%%%%%%%%%%%%%%%%%%%%%%%%%%%%
%%%%%%%%%%%%%%%%%%%%%%%%%%%%%%%%%%
%isolating possible galaxies - galaxies that have no companions within a___
```

```matlab
%projected distance (Rp) if within Rp then must have > M mag difference and
%have Vp > than specified_____
iprim = 1;
for i = 1:length(ra_limit)-1;
   pass_all = 1;
   for j = (i+1):length(ra_limit);
      if ~(((sqrt((ra_limit(i)-ra_limit(j)).^2 + (dec_limit(i)-dec_limit(j)).^2).* ...
            pi./180.*D_limit(i).*1000)) < iso_proj) & ((B_limit(j) - B_limit(i)) ...
            >= iso_mag) & (abs(v_limit(i) - v_limit(j)) > iso_vel);
         pass_all = 0;
         break
      end
   end
   if pass_all
      ra_p(iprim) = ra_limit(i);
      dec_p(iprim) = dec_limit(i);
      u_p(iprim) = u_limit(i);
      g_p(iprim) = g_limit(i);
      r_p(iprim) = r_limit(i);
      i_p(iprim) = i_limit(i);
      z_p(iprim) = z_limit(i);
      AB_p(iprim) = AB_limit(i);
      phi_p(iprim) = phi_limit(i);
      D_p(iprim) = D_limit(i);
      B_p(iprim) = B_limit(i);
      v_p(iprim) = v_limit(i);
      iprim = iprim+1;
   end
end
%%%%%%%%%%%%%%%%%%%%%%%%%%%%%%%%%%%%%%%%%%%%
%%%%%%%%%%%%%%%%%%%%%%%%%%%%%%%%%%
%clearing variables not used later_____
clear ra_limit;
clear dec_limit;
clear D_limit;
clear B_limit;
clear v_limit;
%%%%%%%%%%%%%%%%%%%%%%%%%%%%%%%%%%%%%%%%%%%%
%%%%%%%%%%%%%%%%%%%%%%%%%%%%%%%%%
%finding satellites - searching within Rs of the primaries, have to be
%>2 brighter than primary and have velocity difference of Vs
for i = 1:length(ra_p);
   isat = 1;
    for j = 1:length(ra);
```

```matlab
        if (((sqrt((ra_p(i)-ra(j)).^2 + (dec_p(i)-dec(j)).^2).*pi./180.*D_p(i).*1000)) ...
            < sat_proj) & ((B_mag(j) - B_p(i)) > sat_mag) & (abs(v_p(i) - v_radial(j)) ...
            < sat_vel) & ((sqrt((ra_p(i)-ra(j)).^2 + (dec_p(i)-dec(j)).^2).* ...
            pi./180.*D_p(i).*1000) ~= 0);
        ra_sat(i,isat) = ra(j);
        dec_sat(i,isat) = dec(j);
        u_sat(i,isat) = u_mag(j);
        g_sat(i,isat) = g_mag(j);
        r_sat(i,isat) = r_mag(j);
        i_sat(i,isat) = i_mag(j);
        z_sat(i,isat) = z_mag(j);
        AB_sat(i,isat) = AB_ratio(j);
        phi_sat(i,isat) = phi_angle(j);
        D_sat(i,isat) = D(j);
        B_sat(i,isat) = B_mag(j);
        v_sat(i,isat) = v_radial(j);
        isat = isat + 1;
      end
   end
end
%%%%%%%%%%%%%%%%%%%%%%%%%%%%%%%%%%%%%%%%%%%
%%%%%%%%%%%%%%%%%%%%%%%%%%%%%%%%%%
%clearing variables not used later_____
clear ra;
clear dec;
clear D;
clear B_mag;
clear v_radial;
%%%%%%%%%%%%%%%%%%%%%%%%%%%%%%%%%%%%%%%%%%%
%%%%%%%%%%%%%%%%%%%%%%%%%%%%%%%%%%
%finding the number of satellites per primary_____
for n = 1:size(ra_sat,1);
   NUM(n) = length(find(ra_sat(n,:)~=0));
end
%%%%%%%%%%%%%%%%%%%%%%%%%%%%%%%%%%%%%%%%%%%
%%%%%%%%%%%%%%%%%%%%%%%%%%%%%%%%%%
%text file with primary data and number of satellites with data
[xx,yy] = size(ra_sat);
fid = fopen('systemsdr4_phd012.txt','w');
for ii = 1:xx;
   if sum(ra_sat(ii,:)) ~= 0;
     info2 = [NUM(ii);ra_p(ii);dec_p(ii);u_p(ii);g_p(ii);r_p(ii);i_p(ii); ...
         z_p(ii);AB_p(ii);phi_p(ii);D_p(ii);B_p(ii);v_p(ii)];
     fprintf(fid,'%10.4f %10.4f %10.4f %10.4f %10.4f %10.4f %10.4f %10.4f ...
```

```matlab
                %10.4f %10.4f %10.4f %10.4f %10.4f\n',info2);
        end
        for jj = 1:yy;
            if ra_sat(ii,jj) ~= 0;
                info3 = [0;ra_sat(ii,jj);dec_sat(ii,jj);u_sat(ii,jj);g_sat(ii,jj); ...
                        r_sat(ii,jj);i_sat(ii,jj);z_sat(ii,jj);AB_sat(ii,jj); ...
                        phi_sat(ii,jj);D_sat(ii,jj);B_sat(ii,jj);v_sat(ii,jj)];
                fprintf(fid,'%10.4f %10.4f %10.4f %10.4f %10.4f %10.4f %10.4f ...
                %10.4f %10.4f %10.4f %10.4f %10.4f %10.4f\n',info3);
            end
        end
end
fclose(fid);
%%%%%%%%%%%%%%%%%%%%%%%%%%%%%%%%%%%%%%%%%%%%
%%%%%%%%%%%%%%%%%%%%%%%%%%%%%%%%%%%%%
t=toc
```

Gaussian Fit with ROOT

This program reads in data (peculiar velocities of satellites) and fits it to a

Gaussian plus constant function for ten different bin sizes. The program outputs the width,

height, and constant (with associated errors) of the best fit Gaussian plus constant by

minimizing chi square.

```cpp
#include <cstdlib>
#include <cstdio>
#include <iostream>
#include <fstream>
#include <TH1.h>
#include <TF1.h>
#include <TStyle.h>
#include <TROOT.h>
#include <TCanvas.h>
using namespace std;

int main(int argc, char** argv) {
  if( argv[1] == NULL ||
      argv[2] == NULL || argv[3] == NULL ||
      argv[4] == NULL || argv[5] == NULL ||
      argv[6] == NULL || argv[7] == NULL ||
      argv[8] == NULL || argv[9] == NULL ||
      argv[10] == NULL) return 1;
  else ;
  gStyle->SetOptStat(0);
  gStyle->SetOptFit(1111);
  char hname[15];
  sprintf(hname,"%d Bins",atoi(argv[2]));
  TH1F *b1 = new TH1F("b1",hname,atoi(argv[2]),0,500);
  sprintf(hname,"%d Bins",atoi(argv[3]));
  TH1F *b2 = new TH1F("b2",hname,atoi(argv[3]),0,500);
  sprintf(hname,"%d Bins",atoi(argv[4]));
  TH1F *b3 = new TH1F("b3",hname,atoi(argv[4]),0,500);
  sprintf(hname,"%d Bins",atoi(argv[5]));
  TH1F *b4 = new TH1F("b4",hname,atoi(argv[5]),0,500);
  sprintf(hname,"%d Bins",atoi(argv[6]));
  TH1F *b5 = new TH1F("b5",hname,atoi(argv[6]),0,500);
  sprintf(hname,"%d Bins",atoi(argv[7]));
  TH1F *b6 = new TH1F("b6",hname,atoi(argv[7]),0,500);
```

```
   sprintf(hname,"%d Bins",atoi(argv[8]));
   TH1F *b7 = new TH1F("b7",hname,atoi(argv[8]),0,500);
   sprintf(hname,"%d Bins",atoi(argv[9]));#include <fstream>
   TH1F *b8 = new TH1F("b8",hname,atoi(argv[9]),0,500);
   sprintf(hname,"%d Bins",atoi(argv[10]));
   TH1F *b9 = new TH1F("b9",hname,atoi(argv[10]),0,500);
   sprintf(hname,"%d Bins",atoi(argv[11]));
   TH1F *b10 = new TH1F("b10",hname,atoi(argv[11]),0,500);
   float value;
   ifstream input(argv[1]);
   while( input ) {
    input >> value;
    b1->Fill(value);
    b2->Fill(value);
    b3->Fill(value);
    b4->Fill(value);
    b5->Fill(value);
    b6->Fill(value);
    b7->Fill(value);
    b8->Fill(value);
    b9->Fill(value);
    b10->Fill(value);
   }
   for(int i = 0; i < b1->GetNbinsX(); i++) b1->SetBinError(i,sqrt(b1->GetBinContent(i)));
   for(int i = 0; i < b1->GetNbinsX(); i++) b2->SetBinError(i,sqrt(b2->GetBinContent(i)));
   for(int i = 0; i < b1->GetNbinsX(); i++) b3->SetBinError(i,sqrt(b3->GetBinContent(i)));
   for(int i = 0; i < b1->GetNbinsX(); i++) b4->SetBinError(i,sqrt(b4->GetBinContent(i)));
   for(int i = 0; i < b1->GetNbinsX(); i++) b5->SetBinError(i,sqrt(b5->GetBinContent(i)));
   for(int i = 0; i < b1->GetNbinsX(); i++) b6->SetBinError(i,sqrt(b6->GetBinContent(i)));
   for(int i = 0; i < b1->GetNbinsX(); i++) b7->SetBinError(i,sqrt(b7->GetBinContent(i)));
   for(int i = 0; i < b1->GetNbinsX(); i++) b8->SetBinError(i,sqrt(b8->GetBinContent(i)));
   for(int i = 0; i < b1->GetNbinsX(); i++) b9->SetBinError(i,sqrt(b9->GetBinContent(i)));
   for(int i = 0; i < b1->GetNbinsX(); i++) b10->SetBinError(i,sqrt(b10-
 >GetBinContent(i)));
 TF1 *fit = new TF1("fit","[0]+[1]*exp(-0.5*(x/[2])^2)",0,500);
   fit->SetParameter(0,0.);  fit->SetParName(0,"Constant");
   fit->SetParameter(1,1.); fit->SetParName(1,"Amplitude");
   fit->SetParameter(2,20.);  fit->SetParName(2,"Sigma");
   //fit->SetParLimits(0,0.,10);
   FILE *fitRes = fopen("fitResults.out","w");
   b1->Fit(fit,"Q");
   fprintf(fitRes,"%d %f %f %f %f %f %f %f %f\n",
        b1->GetNbinsX(),
        fit->GetParameter(0), fit->GetParError(0),
```

```
        fit->GetParameter(1), fit->GetParError(1),
        fit->GetParameter(2), fit->GetParError(2),
        fit->GetChisquare(), fit->GetChisquare()/fit->GetNDF());
  b2->Fit(fit,"Q");
  fprintf(fitRes,"%d %f %f %f %f %f %f %f %f\n",
        b2->GetNbinsX(),
        fit->GetParameter(0), fit->GetParError(0),
        fit->GetParameter(1), fit->GetParError(1),
        fit->GetParameter(2), fit->GetParError(2),
        fit->GetChisquare(), fit->GetChisquare()/fit->GetNDF());
  b3->Fit(fit,"Q");
  fprintf(fitRes,"%d %f %f %f %f %f %f %f %f\n",
        b3->GetNbinsX(),
        fit->GetParameter(0), fit->GetParError(0),
        fit->GetParameter(1), fit->GetParError(1),
        fit->GetParameter(2), fit->GetParError(2),
        fit->GetChisquare(), fit->GetChisquare()/fit->GetNDF());
  b4->Fit(fit,"Q");
  fprintf(fitRes,"%d %f %f %f %f %f %f %f %f\n",
        b4->GetNbinsX(),
        fit->GetParameter(0), fit->GetParError(0),
        fit->GetParameter(1), fit->GetParError(1),
        fit->GetParameter(2), fit->GetParError(2),
        fit->GetChisquare(), fit->GetChisquare()/fit->GetNDF());
  b5->Fit(fit,"Q");
  fprintf(fitRes,"%d %f %f %f %f %f %f %f %f\n",
        b5->GetNbinsX(),
fit->GetParameter(0), fit->GetParError(0),
        fit->GetParameter(1), fit->GetParError(1),
        fit->GetParameter(2), fit->GetParError(2),
        fit->GetChisquare(), fit->GetChisquare()/fit->GetNDF());
  b6->Fit(fit,"Q");
  fprintf(fitRes,"%d %f %f %f %f %f %f %f %f\n",
        b6->GetNbinsX(),
        fit->GetParameter(0), fit->GetParError(0),
        fit->GetParameter(1), fit->GetParError(1),
        fit->GetParameter(2), fit->GetParError(2),
        fit->GetChisquare(), fit->GetChisquare()/fit->GetNDF());
  b7->Fit(fit,"Q");
  fprintf(fitRes,"%d %f %f %f %f %f %f %f %f\n",
        b7->GetNbinsX(),
        fit->GetParameter(0), fit->GetParError(0),
        fit->GetParameter(1), fit->GetParError(1),
        fit->GetParameter(2), fit->GetParError(2),
```

```
        fit->GetChisquare(), fit->GetChisquare()/fit->GetNDF());
  b8->Fit(fit,"Q");
  fprintf(fitRes,"%d %f %f %f %f %f %f %f %f\n",
        b8->GetNbinsX(),
        fit->GetParameter(0), fit->GetParError(0),
        fit->GetParameter(1), fit->GetParError(1),
        fit->GetParameter(2), fit->GetParError(2),
        fit->GetChisquare(), fit->GetChisquare()/fit->GetNDF());
  b9->Fit(fit,"Q");
  fprintf(fitRes,"%d %f %f %f %f %f %f %f %f\n",
        b9->GetNbinsX(),
        fit->GetParameter(0), fit->GetParError(0),
        fit->GetParameter(1), fit->GetParError(1),
        fit->GetParameter(2), fit->GetParError(2),
        fit->GetChisquare(), fit->GetChisquare()/fit->GetNDF());
  b10->Fit(fit,"Q");
  fprintf(fitRes,"%d %f %f %f %f %f %f %f %f\n",
        b10->GetNbinsX(),
        fit->GetParameter(0), fit->GetParError(0),
        fit->GetParameter(1), fit->GetParError(1),
fit->GetParameter(2), fit->GetParError(2),
        fit->GetChisquare(), fit->GetChisquare()/fit->GetNDF());
  fclose(fitRes);

  TCanvas *c1 = new TCanvas();
  c1->Divide(5,5);
  c1->cd(1); b1->Draw("e5p");
  c1->cd(2); b2->Draw("e5p");
  c1->cd(3); b3->Draw("e5p");
  c1->cd(4); b4->Draw("e5p");
  c1->cd(5); b5->Draw("e5p");
  c1->cd(6); b6->Draw("e5p");
  c1->cd(7); b7->Draw("e5p");
  c1->cd(8); b8->Draw("e5p");
  c1->cd(9); b9->Draw("e5p");
  c1->cd(10); b10->Draw("e5p");
  c1->SaveAs("output.ps");
  return 0;
}
```

Velocity Profiles

This routine reads in the results from the Gaussian fit in ROOT and plots three graphs, velocity dispersion vs. bin number, interloper fraction vs. bin number, and χ^2 vs. bin number.

robust_results.m

```
%This program takes the results from ROOT and plots
%velocity dispersion vs. bin number, interloper fraction vs. bin number,
%and chi square vs. bin number.
clc;
clear;
tic;
sig_level = 0.05;
KK = 2;
for K = 1:1;
    write_data = 0;
    write_pass = 0;
    write_table = 0;
    pic = 0;    %close plots after plotting and saving
    allplot = 1;
    subset = K;
    if K < 10;
        name1 = 'velocity_data_00';
        name2 = '_';
        name3 = '.txt';
        nn = num2str(subset);
        file_name1 = char(strvcat([name1,nn,name2,num2str(1),name3]));
        file_name2 = char(strvcat([name1,nn,name2,num2str(2),name3]));
        file_name3 = char(strvcat([name1,nn,name2,num2str(3),name3]));
        file_name4 = char(strvcat([name1,nn,name2,num2str(4),name3]));
        %read in data
        sats = textread(file_name1);    %velocity_data_001_1.txt
        sats2= textread(file_name2);    %velocity_data_001_2.txt
        sats3 = textread(file_name3);   %velocity_data_001_3.txt
        sats4 = textread(file_name4);   %velocity_data_001_4.txt
    else
        name1 = 'velocity_data_0';
        name2 = '_';
        name3 = '.txt';
```

```matlab
    nn = num2str(subset);
    file_name1 = char(strvcat([name1,nn,name2,num2str(1),name3]));
    file_name2 = char(strvcat([name1,nn,name2,num2str(2),name3]));
    file_name3 = char(strvcat([name1,nn,name2,num2str(3),name3]));
    file_name4 = char(strvcat([name1,nn,name2,num2str(4),name3]));
    %read in data
    sats = textread(file_name1);    %velocity_data_001_1.txt
    sats2= textread(file_name2);    %velocity_data_001_2.txt
    sats3 = textread(file_name3);   %velocity_data_001_3.txt
    sats4 = textread(file_name4);   %velocity_data_001_4.txt
end
name4 = 'set';
name5 = '_bin';
name7 = '.txt';
nn = num2str(subset);
file_name5 = char(strvcat([name4,nn,name5,num2str(1),name3]));
file_name6 = char(strvcat([name4,nn,name5,num2str(2),name3]));
file_name7 = char(strvcat([name4,nn,name5,num2str(3),name3]));
file_name8 = char(strvcat([name4,nn,name5,num2str(4),name3]));
    data = textread(file_name5);    %set1_bin1.txt
    data2 = textread(file_name6);
    data3 = textread(file_name7);
    data4 = textread(file_name8);
%bin 1
    bn = [data(:,1)];
    const = [data(:,2)];
    const_err = [data(:,3)];
    amp = [data(:,4)];
    amp_err = [data(:,5)];
    sigma = abs([data(:,6)]);
    sigma_err = [data(:,7)];
    chi2 = [data(:,8)];
%determine prob from chi
    syms x;
    for i = 1:length(chi2);
    d(i) = bn(i) - 3;
    y(i) = d(i)./2;
    C(i) = 1./((2.^(y(i))).*gamma(y(i)));
    f(i) = (x.^((y(i)) - 1)).*exp((-x)./2);
    Prob(i) = C(i)*double(int(f(i),chi2(i),inf));
    end
    %interloper percent
    loper_perc = const.*bn./length(sats);
    loper_perc_err = const_err.*bn./length(sats);
```

```matlab
    perc_mean = mean(loper_perc);
    perc_mean_err = mean(loper_perc_err);
    %average sigma
    sigma_mean = mean(sigma);
    sigma_err_mean = mean(sigma_err);
    %bin 2
    bn2 = [data2(:,1)];
    const2 = [data2(:,2)];
    const_err2 = [data2(:,3)];
    amp2 = [data2(:,4)];
    amp_err2 = [data2(:,5)];
    sigma2 = abs([data2(:,6)]);
    sigma_err2 = [data2(:,7)];
    chi22 = [data2(:,8)];
    %determine prob from chi
    syms x;
    for i = 1:length(chi22);
d(i) = bn2(i) - 3;
y(i) = d(i)./2;
C(i) = 1./((2.^(y(i))).*gamma(y(i)));
f(i) = (x.^((y(i)) - 1)).*exp((-x)./2);
Prob2(i) = C(i)*double(int(f(i),chi22(i),inf));
    end
    %interloper percent
    loper_perc2 = const2.*bn2./length(sats2);
    loper_perc_err2 = const_err2.*bn2./length(sats2);
    perc_mean2 = mean(loper_perc2);
    perc_mean_err2 = mean(loper_perc_err2);
    %average sigma
    sigma_mean2 = mean(sigma2);
    sigma_err_mean2 = mean(sigma_err2);
    %bin 3
    bn3 = [data3(:,1)];
    const3 = [data3(:,2)];
    const_err3 = [data3(:,3)];
    amp3 = [data3(:,4)];
    amp_err3 = [data3(:,5)];
    sigma3 = abs([data3(:,6)]);
    sigma_err3 = [data3(:,7)];
    chi23 = [data3(:,8)];
    %determine prob from chi
    syms x;
    for i = 1:length(chi23);
d(i) = bn3(i) - 3;
```

```
y(i) = d(i)./2;
C(i) = 1./((2.^(y(i))).*gamma(y(i)));
f(i) = (x.^((y(i)) - 1)).*exp((-x)./2);
Prob3(i) = C(i)*double(int(f(i),chi23(i),inf));
    end
    %interloper percent
    loper_perc3 = const3.*bn3./length(sats3);
    loper_perc_err3 = const_err3.*bn3./length(sats3);
    perc_mean3 = mean(loper_perc3);
    perc_mean_err3 = mean(loper_perc_err3);
    bb3 = (perc_mean3);
    %average sigma
    sigma_mean3 = mean(sigma3);
    sigma_err_mean3 = mean(sigma_err3);
    %bin 4
    bn4 = [data4(:,1)];
    const4 = [data4(:,2)];
    const_err4 = [data4(:,3)];
    amp4 = [data4(:,4)];
    amp_err4 = [data4(:,5)];
    sigma4 = abs([data4(:,6)]);
    sigma_err4 = [data4(:,7)];
    chi24 = [data4(:,8)];
    %determine prob from chi
    syms x;
    for i = 1:length(chi24);
d(i) = bn4(i) - 3;
y(i) = d(i)./2;
C(i) = 1./((2.^(y(i))).*gamma(y(i)));
f(i) = (x.^((y(i)) - 1)).*exp((-x)./2);
Prob4(i) = C(i)*double(int(f(i),chi24(i),inf));
    end
    %interloper percent
    loper_perc4 = const4.*bn4./length(sats4);
    loper_perc_err4 = const_err4.*bn4./length(sats4);
    perc_mean4 = mean(loper_perc4);
    perc_mean_err4 = mean(loper_perc_err4);
    %average sigma
    sigma_mean4 = mean(sigma4);
    sigma_err_mean4 = mean(sigma_err4);

  sigma_data = [sigma_mean;sigma_mean2;sigma_mean3;sigma_mean4];
  sigma_err_data =
[sigma_err_mean;sigma_err_mean2;sigma_err_mean3;sigma_err_mean4];
```

```matlab
    tot_per = [perc_mean perc_mean2 perc_mean3 perc_mean4];
        tot_per_err = [perc_mean_err perc_mean_err2 perc_mean_err3 perc_mean_err4];
        %%%%%%%%%%%%%%%%%%%%%%%%%%%%%%%%%%%%%%%%
%%%%%%%%%%%%%%%%%%%%%%%%%%%%%%%%%%%%%%%%
        %write to file sigma and its error, and loper percent and its errors
        if write_data == 1;
    fid = fopen('sigma_data03.txt','a');
    info = [sigma_data';sigma_err_data';tot_per;tot_per_err];
    fprintf(fid,'%10.4f %10.4f %10.4f %10.4f\n',info);
    fclose(fid);
        end
        if write_table == 1;
    %sigma_data = [sigma_mean;sigma_mean2;sigma_mean3;sigma_mean4];
    %sigma_err_data =
[sigma_err_mean;sigma_err_mean2;sigma_err_mean3;sigma_err_mean4];
    fid = fopen('data_table04.txt','w');

    info = [bn';sigma';sigma_err';loper_perc';loper_perc_err';chi2';Prob];
    fprintf(fid,'%10.4f %10.4f %10.4f %10.4f %10.4f %10.4f %10.4f\n',info);
    info_err = [0;sigma_mean;sigma_err_mean;perc_mean;perc_mean_err;0;0];
    fprintf(fid,'%10.4f %10.4f %10.4f %10.4f %10.4f %10.4f%10.4f\n\n',info_err);

    info2 = [bn';sigma2';sigma_err2';loper_perc2';loper_perc_err2';chi22';Prob2];
    fprintf(fid,'%10.4f %10.4f %10.4f %10.4f %10.4f %10.4f %10.4f\n',info2);
    info_err2 = [0;sigma_mean2;sigma_err_mean2;perc_mean;perc_mean_err2;0;0];
    fprintf(fid,'%10.4f %10.4f %10.4f %10.4f %10.4f %10.4f %10.4f\n\n',info_err2);

    info3 = [bn';sigma3';sigma_err3';loper_perc3';loper_perc_err3';chi23';Prob3];
    fprintf(fid,'%10.4f %10.4f %10.4f %10.4f %10.4f %10.4f %10.4f\n',info3);
    info_err3 = [0;sigma_mean3;sigma_err_mean3;perc_mean3;perc_mean_err3;0;0];
    fprintf(fid,'%10.4f %10.4f %10.4f %10.4f %10.4f %10.4f %10.4f\n\n',info_err3);

    info4 = [bn';sigma4';sigma_err4';loper_perc4';loper_perc_err4';chi24';Prob4];
    fprintf(fid,'%10.4f %10.4f %10.4f %10.4f %10.4f %10.4f %10.4f\n',info4);
    info_err4 = [0;sigma_mean4;sigma_err_mean4;perc_mean4;perc_mean_err4;0;0];
    fprintf(fid,'%10.4f %10.4f %10.4f %10.4f %10.4f %10.4f %10.4f\n\n',info_err4);
    fclose(fid);
        end
    if write_table == 1;
        %write data to xl file
        xldata = textread('data_table04.txt');
        colnames = {'bin number','sigma','sigma error','fraction','fraction
error','chi2','probability'};
        xlname = 'subset';
```

```matlab
    nn = num2str(subset);
    xlfilename = char(strvcat([xlname,nn]));
    xlswrite(xldata,'subset data',colnames,xlfilename)
  end


%%%%%%%%%%%%%%%%%%%%%%%%%%%%%%%%%%%%%%%%%
%%%%%%%%%%%%%%%%%%%%%%%%%%%
  if allplot == 1;
    %sigma plots
    %plot bin 1
               H = figure;
               subplot(2,2,1);
               errorbar(bn,sigma,sigma_err,'k.')
               hold on;
    if max(sigma-sigma_err) <= min(sigma+sigma_err);
       y_fit = max(sigma-sigma_err);
       Pass1 = 1;
    else
       y_fit = mean(sigma);
       Pass1 = 0;
    end
    plot([min(bn) max(bn)],[y_fit y_fit],'r-')
    title(['Radial Bin 1     Pass = ',int2str(Pass1)]);
               if max(sigma+sigma_err) > 300;
       ylim([0 max(sigma+sigma_err)]);
               else
       ylim([0 300]);
               end
    xlabel('Number of bins per Histogram')
               ylabel('\sigma [km/s]')
               grid on;
               hold off;
               %plot bin 2
               subplot(2,2,2);
               errorbar(bn2,sigma2,sigma_err2,'k.')
               hold on;
    if max(sigma2-sigma_err2) <= min(sigma2+sigma_err2);
       y_fit2 = max(sigma2-sigma_err2);
       Pass2 = 1;
    else
       y_fit2 = mean(sigma2);
       Pass2 = 0;
    end
    plot([min(bn) max(bn)],[y_fit2 y_fit2],'r-')
```

```
title(['Radial Bin 2      Pass = ',int2str(Pass2)]);
if max(sigma2+sigma_err2) > 300;
   ylim([0 max(sigma2+sigma_err2)]);
          else
   ylim([0 300]);
          end
xlabel('Number of bins per Histogram')
          ylabel('\sigma [km/s]')
          grid on;
          hold off;
          %plot bin 3
          subplot(2,2,3);
          errorbar(bn3,sigma3,sigma_err3,'k.')
          hold on;
if max(sigma3-sigma_err3) <= min(sigma3+sigma_err3);
   y_fit3 = max(sigma3-sigma_err3);
   Pass3 = 1;
else
   y_fit3 = mean(sigma3);
   Pass3 = 0;
end
plot([min(bn) max(bn)],[y_fit3 y_fit3],'r-')
title(['Radial Bin 3      Pass = ',int2str(Pass3)]);
          if max(sigma3+sigma_err3) > 300;
   ylim([0 max(sigma3+sigma_err3)]);
          else
   ylim([0 300]);
          end
          xlabel('Number of bins per Histogram')
          ylabel('\sigma [km/s]')
          grid on;
          hold off;
          %plot bin 4
          subplot(2,2,4);
          errorbar(bn4,sigma4,sigma_err4,'k.')
          title('Radial Bin 4')
          hold on;
if max(sigma4-sigma_err4) <= min(sigma4+sigma_err4);
   y_fit4 = max(sigma4-sigma_err4);
   Pass4 = 1;
else
   y_fit4 = mean(sigma4);
   Pass4 = 0;
end
```

```matlab
plot([min(bn) max(bn)],[y_fit4 y_fit4],'r-')
title(['Radial Bin 4      Pass = ',int2str(Pass4)]);
            if max(sigma4+sigma_err4) > 300;
    ylim([0 max(sigma4+sigma_err4)]);
            else
    ylim([0 300]);
            end
            xlabel('Number of bins per Histogram')
            ylabel('\sigma [km/s]')
            grid on;
            hold off;
text(-2.5,760,['SUBSET ',int2str(subset)],'FontSize',20)
            set(H,'Color','White');
orient landscape
pre_file = 'sigma0';
nfile = num2str(subset);
file_name = (strvcat([pre_file,nfile,'.ps']));
print('-dpsc',file_name);
movefile(file_name,'C:\matlab_sv13\work\psplots\passfailplots2\')

            if pic == 1;
    close;
            end
sigma_pass = [Pass1;Pass2;Pass3;Pass4];

    %%%%%%%%%%%%%%%%%%%%%%%%%%%%%%%%%%%%%%%
%%%%%%%%%%%%%%%%%%%%%%%%%%%%%%%%%%%%%
            %constant plot
            H=figure;
            %bin 1
            subplot(2,2,1);
            errorbar(bn,loper_perc,loper_perc_err,'k.')
            title('Radial Bin 1')
            hold on;
    if max(loper_perc-loper_perc_err) <= min(loper_perc+loper_perc_err);
    y_fit5 = max(loper_perc-loper_perc_err);
    Pass5 = 1;
    else
    y_fit5 = mean(loper_perc);
    Pass5 = 0;
    end
    plot([min(bn) max(bn)],[y_fit5 y_fit5],'r-')
    title(['Radial Bin 1      Pass = ',int2str(Pass5)]);
    hold off;
```

```matlab
        if max(loper_perc+loper_perc_err) > 1;
    ylim([0 max(loper_perc+loper_perc_err)]);
        else
    ylim([0 1]);
        end
        xlabel('Number of bins per Histogram')
        ylabel('Interloper Fraction')
        grid on;
        %bin 2
        subplot(2,2,2);
        errorbar(bn2,loper_perc2,loper_perc_err2,'k.')
        title('Radial Bin 2')
        hold on;
        if max(loper_perc2-loper_perc_err2) <=
min(loper_perc2+loper_perc_err2);
    y_fit6 = max(loper_perc2-loper_perc_err2);
    Pass6 = 1;
else
    y_fit6 = mean(loper_perc2);
    Pass6 = 0;
end
plot([min(bn) max(bn)],[y_fit6 y_fit6],'r-')
title(['Radial Bin 2      Pass = ',int2str(Pass6)]);
if max(loper_perc2+loper_perc_err2) > 1;
    ylim([0 max(loper_perc2+loper_perc_err2)]);
        else
    ylim([0 1]);
        end
        xlabel('Number of bins per Histogram')
        ylabel('Interloper Fraction')
        grid on;
hold off;
        %bin 3
        subplot(2,2,3);
        errorbar(bn3,loper_perc3,loper_perc_err3,'k.')
        title('Radial Bin 3')
        hold on;
if max(loper_perc3-loper_perc_err3) <= min(loper_perc3+loper_perc_err3);
    y_fit7 = max(loper_perc3-loper_perc_err3);
    Pass7 = 1;
else
    y_fit7 = mean(loper_perc3);
    Pass7 = 0;
end
```

```matlab
plot([min(bn) max(bn)],[y_fit7 y_fit7],'r-')
title(['Radial Bin 3      Pass = ',int2str(Pass7)]);
        hold off;
        if max(loper_perc3+loper_perc_err3) > 1;
    ylim([0 max(loper_perc3+loper_perc_err3)]);
        else
    ylim([0 1]);
        end
        xlabel('Number of bins per Histogram')
        ylabel('Interloper Fraction')
        grid on;
        %bin 4
        subplot(2,2,4);
        errorbar(bn4,loper_perc4,loper_perc_err4,'k.')
        title('Radial Bin 4')
        hold on;
if max(loper_perc4-loper_perc_err4) <= min(loper_perc4+loper_perc_err4);
    y_fit8 = max(loper_perc4-loper_perc_err4);
    Pass8 = 1;
else
    y_fit8 = mean(loper_perc4);
    Pass8 = 0;
end
plot([min(bn) max(bn)],[y_fit8 y_fit8],'r-')
title(['Radial Bin 4      Pass = ',int2str(Pass8)]);
        if max(loper_perc4+loper_perc_err4) > 1;
    ylim([0 max(loper_perc4+loper_perc_err4)]);
        else
    ylim([0 1]);
        end
        xlabel('Number of bins per Histogram')
        ylabel('Interloper Fraction')
        grid on;
hold off;
text(-2.5,2.521,['SUBSET ',int2str(subset)],'FontSize',20)
        set(H,'Color','White');
orient landscape
pre_file = 'loper0';
nfile = num2str(subset);
file_name = (strvcat([pre_file,nfile,'.ps']));
print('-dpsc',file_name);
movefile(file_name,'C:\matlab_sv13\work\psplots\passfailplots2\')

        if pic == 1;
```

```matlab
        close;
    end
    loper_pass = [Pass5;Pass6;Pass7;Pass8];

        %%%%%%%%%%%%%%%%%%%%%%%%%%%%%%%%%%%%%%
%%%%%%%%%%%%%%%%%%%%%%%%%%%%%%%%%%%%%%%
    %plot Prob Bin 1
            H=figure;
            subplot(2,2,1);
            plot(bn,Prob,'k.')

            if Prob >= sig_level;
    Pass9 = 1;
    else
        Pass9 = 0;
    end
    title(['Radial Bin 1      Pass = ',int2str(Pass9)]);
            hold on;
            h=plot([0 15],[0.05 0.05],'k-');
            hh=plot([0 15],[0.01 0.01],'k-.');
            xlim([0 15]);
            ylim([0 1]);
            xlabel('Number of bins per Histogram')
            ylabel('Probability from \chi^{2}')
            grid on;
            legend([h(1) hh(1)],'0.05','0.01');
            hold off;
            %plot bin2
            subplot(2,2,2);
            plot(bn2,Prob2,'k.')

    if Prob2 >= sig_level;
        Pass10 = 1;
    else
        Pass10 = 0;
    end
    title(['Radial Bin 2      Pass = ',int2str(Pass10)]);
            hold on;
            h2=plot([0 15],[0.05 0.05],'k-');
            hh2=plot([0 15],[0.01 0.01],'k-.');
            xlim([0 15]);
            ylim([0 1]);
            xlabel('Number of bins per Histogram')
            ylabel('Probability from \chi^{2}')
```

```matlab
            grid on;
            legend([h2(1) hh2(1)],'0.05','0.01');
            hold off;
            %plot bin3
            subplot(2,2,3);
            plot(bn3,Prob3,'k.')

            if Prob3 >= sig_level;
   Pass11 = 1;
else
   Pass11 = 0;
end
title(['Radial Bin 3     Pass = ',int2str(Pass11)]);
            hold on;
            h3=plot([0 15],[0.05 0.05],'k-');
            hh3=plot([0 15],[0.01 0.01],'k-.');
            xlim([0 15]);
            ylim([0 1]);
            xlabel('Number of bins per Histogram')
            ylabel('Probability from \chi^{2}')
            grid on;
            legend([h3(1) hh3(1)],'0.05','0.01');
            hold off;
            %plot bin4
            subplot(2,2,4);
            plot(bn4,Prob4,'k.')

            if Prob4 >= sig_level;
   Pass12 = 1;
else
   Pass12 = 0;
end
title(['Radial Bin 4     Pass = ',int2str(Pass12)]);
            hold on;
            h4=plot([0 15],[0.05 0.05],'k-');
            hh4=plot([0 15],[0.01 0.01],'k-.');
            xlim([0 15]);
            ylim([0 1]);
            xlabel('Number of bins per Histogram')
            ylabel('Probability from \chi^{2}')
            grid on;
            legend([h4(1) hh4(1)],'0.05','0.01');
            hold off;
text(-5.7,2.5,['SUBSET ',int2str(subset)],'FontSize',20)
```

```
            set(H,'Color','White');
        orient landscape
        pre_file = 'chi0';
        nfile = num2str(subset);
        file_name = (strvcat([pre_file,nfile,'.ps']));
        print('-dpsc',file_name);
        movefile(file_name,'C:\matlab_sv13\work\psplots\passfailplots2\')
        if pic == 1;
            close;
        end

        chi_pass = [Pass9;Pass10;Pass11;Pass12];
        if write_pass == 1;
            fid = fopen('pass_data007.txt','a');
            info = [sigma_pass';loper_pass';chi_pass'];
            fprintf(fid,'%d %d %d\n',info);
            info = [8;8;8];
            fprintf(fid,'%d %d %d\n',info);
            fclose(fid);
        end
    end
    K
end
t=toc
```

This is a C++ program that uses ROOT to fit the three cosmological models to the data.

```
//fit routine for three cosmological models
gROOT->Reset();
c1 = new TCanvas("c1","Cosmological Model Fits");
c1->SetGrid();

// draw a frame to define the range
TH1F *hr = c1->DrawFrame(0,0,500,300);
hr->SetYTitle("Velocity Dispersion [km/s]");
hr->SetXTitle("Projected Distance [kpc]");

// create first graph
Int_t n1 = 4;
Double_t x1[]  = {62.4675,187.4024,312.3374,437.2723};
Double_t y1[] = {203.81    ,  184.98    ,  158.09    ,  134.7};
Double_t ex1[] = {.0,.0,.0,.0};
Double_t ey1[] = {29.9496 ,  22.6787 ,  15.9465 ,  16.1188};
gr1 = new TGraphErrors(n1,x1,y1,ex1,ey1);
gr1->Draw("LP");
//fit
gStyle->SetOptStat(0);
gStyle->SetOptFit(1111);
//fit data with neutrino model
TF1 *fit = new TF1("fit","0.001202*(sqrt((10^[0])/x) +  sqrt(10^[1])*x^(1/4))",0,500);
fit->SetMarkerColor(45);
fit->SetParameter(0,1.);  fit->SetParName(0,"Mass_g");
fit->SetParameter(1,1.);  fit->SetParName(1,"Mass_n");
//fit data with mond model
TF1 *fit2 = new TF1("fit2","0.20536*(10^[0])^(1/4)",0,500);
fit2->SetMarkerColor(45);
fit2->SetParameter(0,5.);  fit2->SetParName(0,"Mass_mond");
//fit data with NFW model
TF1 *fit3 = new TF1("fit3","sqrt(((((4.3*10^-3))*((((((200/3)*(([0]^3)/((log(1 + [0]) -
([0]/(1 + [0]))))))*(280.7176))/((x\
/(((((1.63*10^-2)*((1*10^[1])^(1/3))))/[0]))*(1+(x/(((((1.63*10^-
2)*((1*10^[1])^(1/3))))/[0])))^2))*((4/3)*pi*x^3)))/((x*10\
00)))",0,500);
fit3->SetParameter(0,2.);  fit3->SetParName(0,"Concentration");
fit3->SetParLimits(0,2,12);
```

```
fit3->SetParameter(1,5.);  fit3->SetParName(1,"Mass_NFW");
gr1->Fit(fit,"Q");
FILE *fitRes = fopen("fitResults.out","w");
fprintf(fitRes,"%f %f %f %f %f %f\n",
     fit->GetParameter(0), fit->GetParError(0),
     fit->GetParameter(1), fit->GetParError(1),
     fit->GetChisquare(), fit->GetChisquare()/fit->GetNDF());
gr1->Fit(fit2,"Q+");
fprintf(fitRes,"%f %f %f %f\n",
     fit2->GetParameter(0), fit2->GetParError(0),
     fit2->GetChisquare(), fit2->GetChisquare()/fit2->GetNDF());
gr1->Fit(fit3,"Q+");
fprintf(fitRes,"%f %f %f %f %f %f\n",
     fit3->GetParameter(0), fit3->GetParError(0),
     fit3->GetParameter(1), fit3->GetParError(1),
     fit3->GetChisquare(), fit3->GetChisquare()/fit3->GetNDF());
fclose(fitRes);
//save graph as .ps file
c1->Print("output.ps");
```

Rotation Curves

This program uses the results from the C++ program above and plots the rotation curve and interloper fraction for a data set.

model_fit.m

```
%model fits
clc;
clear;
%enter subset
for K = 1;
    subset = K;
    subset2 =01;
    i = 4*(subset-1);
    pre_name = 'model_fit0';
    suf_name = '.txt';
    nn = num2str(subset);
    file_name = char(strvcat([pre_name,nn,suf_name]));
    %read in data
    %Neutrino Model-
Mass_galaxy;Mass_galaxy_err;Mass_DM;Mass_DM_err;chi2;chi2/d
    %Mond Model- Mass_DM;Mass_DM_err;chi2;chi2/d
    %NFW Model- Mass_DM;Mass_DM_err;chi2;chi2/d
    data = textread(file_name);
    data2 = textread('sigma_data03.txt');
    x = [62.4675 187.4024 312.3374 437.2723];
    sigma = data2(1+i:4+i,1);
    sigma_err = data2(1+i:4+i,2);
    const = data2(1+i:4+i,3);
    const_err = data2(1+i:4+i,4);
    %prob for models
    syms Y;
    d = data(1,5)./data(1,6);
    y = d/2;
    C = 1/((2^(y))*gamma(y));
    f = (Y^((y) - 1))*exp((-Y)/2);
    Prob1 = C*double(int(f,data(1,5),inf));
    %prob for models
    syms Y;
    d = data(2,3)./data(2,3);
    y = d/2;
    C = 1/((2^(y))*gamma(y));
```

114

```matlab
        f = (Y^((y) - 1))*exp((-Y)/2);
        Prob2 = C*double(int(f,data(2,3),inf));
        %prob for models
        syms Y;
        d = data(3,5)./data(3,6);
        y = d/2;
        C = 1/((2^(y))*gamma(y));
        f = (Y^((y) - 1))*exp((-Y)/2);
        Prob3 = C*double(int(f,data(3,5),inf));
        %neutrino plot data
        mass_g = data(1,1);
        mass_n = data(1,3);
        r = 30:500;
        sigma_n = 0.001202*(sqrt((10.^[mass_g])./r) +  sqrt(10.^[mass_n]).*r.^(1/4));
        sigma_n_maxr = 0.001202*(sqrt((10.^[mass_g])./500) +
    sqrt(10.^[mass_n]).*500.^(1/4));
        mass_tot_n = 3*500*1000*sigma_n_maxr^2/(4.3.*10.^-3);
        %mond plot data
        mass_m = data(2,1);
        sigma_m = 0.2334.*(10.^[mass_m]).^(1./4);
        %NFW plot data
        conc = data(3,1);
        mass_nfw = data(3,3);
        sigma_nfw = sqrt(((((4.3.*10.^-3)).*(((((200./3).*(([conc].^3)./((log(1 + [conc]) - ...
            ([conc]./(1 + [conc])))))).*(280.7176)) ./ ((r./(((1.63.*10.^-2).* ...
            ((1.*10.^[mass_nfw]).^(1./3)))./[conc])).*(1+(r./(((1.63.*10.^-2).* ...
            ((1.*10.^[mass_nfw]).^(1./3)))./[conc]))).^2)).*((4./3).*pi.*r.^3)))./((r.*1000)));
        %interloper chi2 fit
        loper_predict = [0.06 .19 .31 .44];
        chi2 = sum((loper_predict' - const).^2./const_err);
        syms X;
        d = data(3,5)./data(3,6);
        y = d/2;
        C = 1/((2^(y))*gamma(y));
        f = (X^((y) - 1))*exp((-X)/2);
        Prob = C*double(int(f,chi2,inf));
        %plot data with models
        H = figure;
        subplot(2,2,1);
        errorbar(x,sigma,sigma_err,'k.');
        hold on;
        h=plot(r,sigma_n,'k-');
        h2=plot([min(r) max(r)],[sigma_m sigma_m],'k:');
        h3=plot(r,sigma_nfw,'k-.');
```

```matlab
if max(sigma + sigma_err) > 500;
   ylim([0 max(sigma+sigma_err)]);
else
   ylim([0 500]);
end
     xlabel('projected distance [kpc]');
     ylabel('\sigma [km/s]');
     legend([h(1) h2(1) h3(1)],['Neutrino',' Prob = ',num2str(Prob1,2)], ...
   ['MOND',' Prob = ',num2str(Prob2,2)], ...
   ['NFW',' Prob = ',num2str(Prob3,2)]);
     title(['subset ',num2str(subset)]);
     hold off;

     %plot interloper
     subplot(2,2,2);
     h=errorbar(x,const,const_err,'k.');
     hold on;
     h2=plot(x,loper_predict,'kd');
     xlabel('projected distance[kpc]');
     ylabel('Interloper Fraction');
     title(['subset ',num2str(subset)]);
     ylim([0 1]);
     xlim([0 500])
     legend([h(2) h2(1)],'data','expected',['Prob = ',num2str(Prob,2)],2);
     hold off;
     set(H,'Color','White');
     orient landscape
     pre_file = 'subset0';
     suf_file = '_model.ps';
     nfile = num2str(subset);
     file_name = (strvcat([pre_file,nfile,suf_file]))
     %print -r100 -dpsc2 C:\matlab_sv13\work\psplots\modelplots\file_name
     print('-dpsc',file_name);
     %close;
     movefile(file_name,'C:\matlab_sv13\work\psplots\modelplots\')
                                        end
```

Holmberg

This program analyzes the data as projected on the sky and determines the

number of polar satellites and planar satellites.

Holmberg_v3

%holmberg program

```
tic;
clear;
clear;
warning off MATLAB:divideByZero;
clc;
print = 0;
tropic_print = 1;
bin_hist_plot = 0;
polar_plot = 0;
hist_plot = 0;
color_plot = 0;
print_velocity = 0;
print_PT = 0;
velocity_plot2D = 1;
brainerd_plot = 0;
plot_sigma = 0;      %planar gauss test
plot_sigma2 = 0;     %polar gauss test
%takes in ra, dec and position angle and determines position around host
data = textread('systemsdr4_phd09.txt');
NUM = data(:,1);
ra = data(:,2);
dec = data(:,3);
u_mag = data(:,4);              %u absolute magnitude
g_mag = data(:,5);              %g absolute magnitude
r_mag = data(:,6);              %r absolute magnitude
i_mag = data(:,7);              %i absolute magnitude
z_mag = data(:,8);              %z absolute magnitude
ab_ratio = data(:,9);
position_angle = data(:,10).*pi./180;
distance = data(:,11);
B_mag = data(:,12);             %B absolute magnitude
vel = data(:,13);              %radial velocity from Hubble's
color = u_mag - r_mag;
type = 2;   %%1 = (early >= 2.22)   2 = (late < 2.22)    0 = both
```

```matlab
%%%%%%%%%%%%%%%%%%%%%%%%%%%%%%%%%%%%%%%%%%%%
%%%%%%%%%%%%%%%%%%%%%%%%%%%%%%%%%%%
%adjusting position angles to 0 - 180
for i = 1:length(position_angle);
   if (position_angle(i) >= 0) & (position_angle(i) <= pi);
      position_angle(i) = position_angle(i);
   elseif position_angle(i) < 0;
      position_angle(i) = pi - abs(position_angle(i));
   elseif position_angle(i) > pi;
      position_angle(i) = position_angle(i) - pi;
   end
end
%finding primaries and satellites at polar and planar region_____
min_mag = [-18];
max_mag = [-20];
ab_number = [0.0 0.1 0.2 0.3 0.4 0.5 0.6 0.7 0.8 0.9];
angle_norm = acos(ab_number).*180./pi;
iter = 1;
nbin = 2;   %number of bins to break sample
nbinfit = 7;    %number of bins do fit of each nbin.
bin_size = 500/nbin;
for L = 1;
   for M = 10;%6:length(ab_number);
      for K = 1:iter;
         for N = 1:nbin;
            if polar_plot == 1;
               if nbin ~= 1 & polar_plot == 1;
                  subplot(2,2,N)
               end
               polar(0,500,'w.');
               hold on;
            end
            planar_count = 1;
            polar_count = 1;
            dum = 1;
            prim_count = 0;
            sat_count = 0;
            tropi_count = 1;
            for i = 1:length(ra);
               if ((NUM(i) ~=0) & (ab_ratio(i) < ab_number(M)) ...
                     & (B_mag(i) > max_mag(L)) & (B_mag(i) < ...
                     min_mag(L))) & ((color(i)) < 2.22));
                  prim_count = prim_count + 1;
                  for k = (i+1):(i+NUM(i));
```

```
if (sqrt((ra(i) - ra(k)).^2 + (dec(i) - dec(k)).^2).*(pi./180) ...
   .*distance(i).*1000 >= bin_size*(N-1)) & ...
      (sqrt((ra(i) - ra(k)).^2 + (dec(i) - dec(k)).^2).*(pi./180) ...
      .*distance(i).*1000 < bin_size*N);
   vert_dist = ((dec(k) - dec(i)));
   horz_dist = ((ra(k) - ra(i)));
   proj_radii = sqrt((ra(i) - ra(k)).^2 + (dec(i) - dec(k)).^2). ...
      *(pi./180).*distance(i).*1000;
   sat_color = color(k);
   sat_vel = (vel(k)-vel(i));        %radial velocity from Hubble's
   tropic(tropi_count) = atan(vert_dist./horz_dist); %rads
   tropi_count = tropi_count + 1;
   if ((vert_dist > 0) & (horz_dist > 0));
      alpha = atan(vert_dist./horz_dist); %rads
      beta = (pi/2 - alpha);
      holm_angle = -(beta + position_angle(i));
      if abs(holm_angle) > pi;
         holm_angle = pi -(abs(holm_angle) - pi);
      else
         holm_angle = holm_angle;
      end
      if ((holm_angle > pi/6) & (holm_angle < 5*pi/6)) ...
            | ((holm_angle > 7*pi/6) & (holm_angle < 11*pi/6)) ...
            | ((holm_angle <= -pi/6) & (holm_angle >= -5*pi/6)) ...
            | ((holm_angle <= -7*pi/6) & (holm_angle >= -11*pi/6));
         if polar_plot == 1;
            polar(holm_angle,proj_radii,'r.');
         end
         polar_vel(polar_count) = sat_vel;
         polar_radii(polar_count) = proj_radii;
         hist_pol_angle(polar_count) = holm_angle;
         polar_count = polar_count + 1;
      else
         if polar_plot == 1;
            polar(holm_angle,proj_radii,'b.');
         end
         planar_vel(planar_count) = sat_vel;
         planar_radii(planar_count) = proj_radii;
         hist_plan_angle(planar_count) = holm_angle;
         planar_count = planar_count + 1;
      end
   end
   if ((vert_dist > 0) & (horz_dist < 0));
      alpha = atan(vert_dist./horz_dist); %rads
```

```matlab
        beta = pi/2 - abs(alpha);
        holm_angle = (beta - position_angle(i));
        if ((holm_angle > pi/6) & (holm_angle < 5*pi/6)) ...
            | ((holm_angle > 7*pi/6) & (holm_angle < 11*pi/6)) ...
            | ((holm_angle <= -pi/6) & (holm_angle >= -5*pi/6)) ...
            | ((holm_angle <= -7*pi/6) & (holm_angle >= -11*pi/6));
          if polar_plot == 1;
            polar(holm_angle,proj_radii,'r.');
          end
          polar_vel(polar_count) = sat_vel;
          polar_radii(polar_count) = proj_radii;
          hist_pol_angle(polar_count) = holm_angle;
          polar_count = polar_count + 1;
        else
          if polar_plot == 1;
            polar(holm_angle,proj_radii,'b.');
          end
          planar_vel(planar_count) = sat_vel;
          planar_radii(planar_count) = proj_radii;
          hist_plan_angle(planar_count) = holm_angle;
          planar_count = planar_count + 1;
        end
    end
    if ((vert_dist < 0) & (horz_dist < 0));
        alpha = atan(vert_dist./horz_dist) + pi/2;  %rads
        holm_angle = (alpha - position_angle(i));
        if ((holm_angle > pi/6) & (holm_angle < 5*pi/6)) ...
            | ((holm_angle > 7*pi/6) & (holm_angle < 11*pi/6)) ...
            | ((holm_angle <= -pi/6) & (holm_angle >= -5*pi/6)) ...
            | ((holm_angle <= -7*pi/6) & (holm_angle >= -11*pi/6));
          if polar_plot == 1;
            polar(holm_angle,proj_radii,'r.');
          end
          polar_vel(polar_count) = sat_vel;
          polar_radii(polar_count) = proj_radii;
          hist_pol_angle(polar_count) = holm_angle;
          polar_count = polar_count + 1;
        else
          if polar_plot == 1;
            polar(holm_angle,proj_radii,'b.');
          end
          planar_vel(planar_count) = sat_vel;
          planar_radii(planar_count) = proj_radii;
          hist_plan_angle(planar_count) = holm_angle;
```

```
                     planar_count = planar_count + 1;
                  end
               end
            if ((vert_dist < 0) & (horz_dist > 0));
               alpha = (atan(vert_dist./horz_dist) + pi/2);  %rads
               holm_angle = -(alpha + position_angle(i));
               if holm_angle > pi;
                  holm_angle =  pi -(abs(holm_angle) - pi);
               else
                  holm_angle = holm_angle;
               end
               if ((holm_angle > pi/6) & (holm_angle < 5*pi/6)) ...
                     | ((holm_angle > 7*pi/6) & (holm_angle < 11*pi/6)) ...
                     | ((holm_angle <= -pi/6) & (holm_angle >= -5*pi/6)) ...
                     | ((holm_angle <= -7*pi/6) & (holm_angle >= -11*pi/6));
                  if polar_plot == 1;
                     polar(holm_angle,proj_radii,'r.');
                  end
                  polar_vel(polar_count) = sat_vel;
                  polar_radii(polar_count) = proj_radii;
                  hist_pol_angle(polar_count) = holm_angle;
                  polar_count = polar_count + 1;
               else
                  if polar_plot == 1;
                     polar(holm_angle,proj_radii,'b.');
                  end
                  planar_vel(planar_count) = sat_vel;
                  planar_radii(planar_count) = proj_radii;
                  hist_plan_angle(planar_count) = holm_angle;
                  planar_count = planar_count + 1;
               end
            end
         sat_count = sat_count + 1;
      end
   end
end
p_r_mot = [planar_vel polar_vel];
PT(N) = length(find(p_r_mot>0))/length(p_r_mot);
if polar_plot == 1;
   title(['Fraction Polar = . . .
',num2str(polar_count/(polar_count+planar_count),2), ...
         '   P/T = ',num2str(PT(N),2),'    Tilt Angle < ',num2str( ...
         (90-acos(ab_number(M)).*180/pi),4),'^{o}']);
```

121

```
            end
            %sigma_fit planar
            velocity_data = abs(planar_vel);
            x_min = min(planar_radii);
            x_max = max(planar_radii);
            [sigma_fit,loper_frac,sigma_upper,sigma_lower,chi_fit,pass] = ...

holmberg_gaussian_constant_fit(N,nbinfit,velocity_data,x_min,x_max,plot_sigma);
            sigma_planar(N) = sigma_fit;
            error_planar(N) = abs(sigma_fit-sigma_upper);
            passing1(N) = pass;
            loper_F(N) = loper_frac;
            %sigma_fit polar
            velocity_data2 = abs(polar_vel);
            x_min = min(polar_radii);
            x_max = max(polar_radii);
            [sigma_fit2,loper_frac2,sigma_upper2,sigma_lower2,chi_fit2,pass2] = ...

holmberg_gaussian_constant_fit(N,nbinfit,velocity_data2,x_min,x_max,plot_sigma2);
            sigma_polar(N) = sigma_fit2;
            error_polar(N) = abs(sigma_fit2 - sigma_upper2);
            passing2(N) = pass2;
            loper_F2(N) = loper_frac2;
            %polar planar counts
            bin_tot_polar(N) = polar_count;
            bin_tot_planar(N) = planar_count;
            bin_tot_polar./(bin_tot_polar + bin_tot_planar);
            %get mean holmberg angle per brainerd
            if tropic_print == 1;
                tropic_degrees = abs(tropic.*180./pi);
                for Ntp = 1:length(tropic_degrees);
                    if tropic_degrees(Ntp) > 90;
                        tropic_degrees2(Ntp) = 180 - tropic_degrees(Ntp);
                    else
                        tropic_degrees2(Ntp) = tropic_degrees(Ntp);
                    end
                end
                trop_mean(N) = mean(tropic_degrees2);
                trop_std(N) = std(tropic_degrees2)./sqrt(length(tropic_degrees2));
            end
        end
        max_dist = 500;
        bin_size = max_dist/(nbin);
        for i = 1:nbin;
```

```matlab
      bin_loc(i) = bin_size/2 + bin_size*(i-1);
   end

      frac_bin = bin_tot_polar./(bin_tot_polar + bin_tot_planar);
      sum_bin_polar = sum(bin_tot_polar);
      sum_bin_planar = sum(bin_tot_planar);
      figure;
      errorbar(bin_loc,trop_mean,trop_std,'b');
      hold on;
      plot([0 500],[45 45],'k:');
      axis([0 500 30 60]);
      xlabel('Distance [kpc]');
      ylabel('\phi (degrees)');
      hold off;

end
if brainerd_plot == 1;
   figure;
   errorbar(bin_loc,trop_mean,trop_std./length(tropic_degrees2));
   xlabel('Distance [kpc]');
   ylabel('\phi (degrees)');
   axis([0 500 30 70]);
end
%plot histogram
_____
            hist_angle = abs([hist_pol_angle hist_plan_angle]).*180./pi;
hist_count = 1;
for i = 1:length(hist_angle);
   if hist_angle(i) >= 0 & hist_angle(i) <= 90;
      angle_hist(hist_count) = abs(hist_angle(i));
      hist_count = hist_count + 1;
   elseif (hist_angle(i) > 90) & (hist_angle(i) <= 180);
      angle_hist(hist_count) = 180 - hist_angle(i);
      hist_count = hist_count + 1;
   elseif (hist_angle(i) > 180) & (hist_angle(i) <= 360);
      angle_hist(hist_count) = abs(hist_angle(i) - 180);
      hist_count = hist_count + 1;
   end
         end
%histogram
if hist_plot == 1;
   figure;
   hist(angle_hist)
   xlabel('angle from the galactic plane (degrees)');
```

123

```
    ylabel('Number of satellites');
end
%write velocity data to file
if print_velocity == 1;
    fid = fopen('polar_velocity001.txt','w');
    info_pol = [polar_vel];
    fprintf(fid,'%10.4f\n',info_pol);
    fclose(fid);
                    fid = fopen('planar_velocity001.txt','w');
    info_plan = [planar_vel];
    fprintf(fid,'%10.4f\n',info_plan);
    fclose(fid);
end
%write fraction data to file
if print_PT == 1;
    fid = fopen('polar_frac018.txt','a');
    info_pol = [frac_bin(1)];%;frac_bin(2);frac_bin(3);frac_bin(4)];
    fprintf(fid,'%10.4f\n',info_pol); %10.4f %10.4f %10.4f\n',info_pol);
    fclose(fid);
    fid2 = fopen('brain018.txt','a');
    info_brain = [trop_mean(1)];%;trop_mean(2);trop_mean(3);trop_mean(4)];
    fprintf(fid2,'%10.4f\n',info_brain); %10.4f %10.4f %10.4f\n',info_brain);
    fclose(fid2);
    fid3 = fopen('PT018.txt','a');
    info_pt = [PT];%;trop_mean(2);trop_mean(3);trop_mean(4)];
    fprintf(fid3,'%10.4f\n',info_pt); %10.4f %10.4f %10.4f\n',info_brain);
    fclose(fid3);
end
%plot velocity profile
bin_size = x_max/nbin;
for i = 1:nbin;
    bin_loc(i) = bin_size/2 + bin_size*(i-1);
end
if velocity_plot2D == 1;
    figure;
    h = errorbar(bin_loc,sigma_planar,error_planar,'r.-');
    text(10,400,['loper % = ',num2str(loper_F,2)],'color','r');
    text(10,380,['pass = ',num2str(passing1,2)],'color','r');
    hold on;
    hh = errorbar(bin_loc,sigma_polar,error_polar,'b.-');
    text(10,350,['loper % = ',num2str(loper_F2,2)],'color','b');
    text(10,330,['pass = ',num2str(passing2,2)],'color','b');
    xlabel('Distance [kpc]');
    ylabel('velocity [km/s]');
```

```matlab
        axis([0 500 0 500])
        title(['Tilt angle < ',num2str((90-acos(ab_number(M)).*180/pi),4),'^{o}'])
        legend([h(1) hh(1)],'planar satellites','polar satellites',2);
    end
  end
%    clear tropic_degrees2;clear tropic; clear tropic_degrees;clear Ntp;
%    clear sigma_planar; clear error_planar; clear sigma_polar; clear error_polar;
end
t = toc
```

The plots on the left show the rotation curves of the data along with the three cosmological models and the probabilities that they fit the data. The plots on the right show the expected interloper fraction (diamonds) per bin compared to the interloper fractions found in the data. The data points with error bars in both graphs are the average values found in each radial bin of the robust analysis described in section 4.2.3.
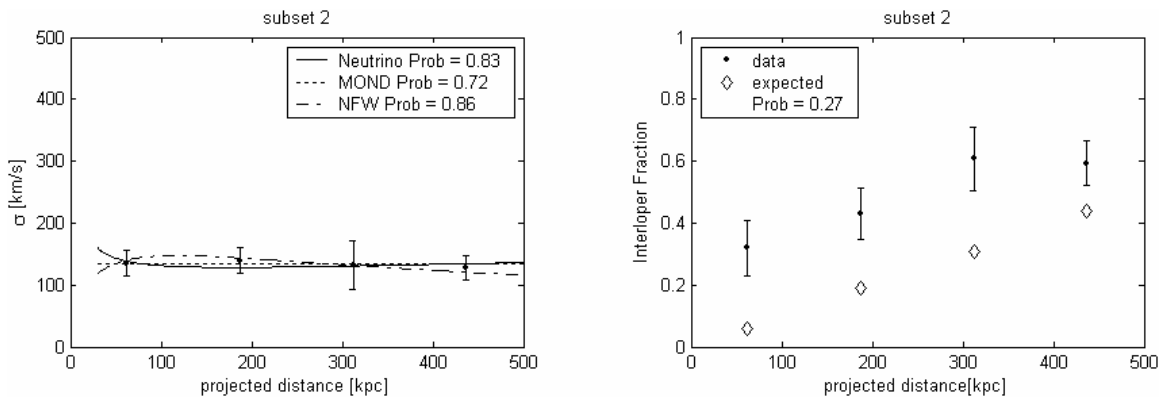
Figure B.1: Velocity dispersion profile plotted with the three cosmological models and interloper fraction of subset 2.
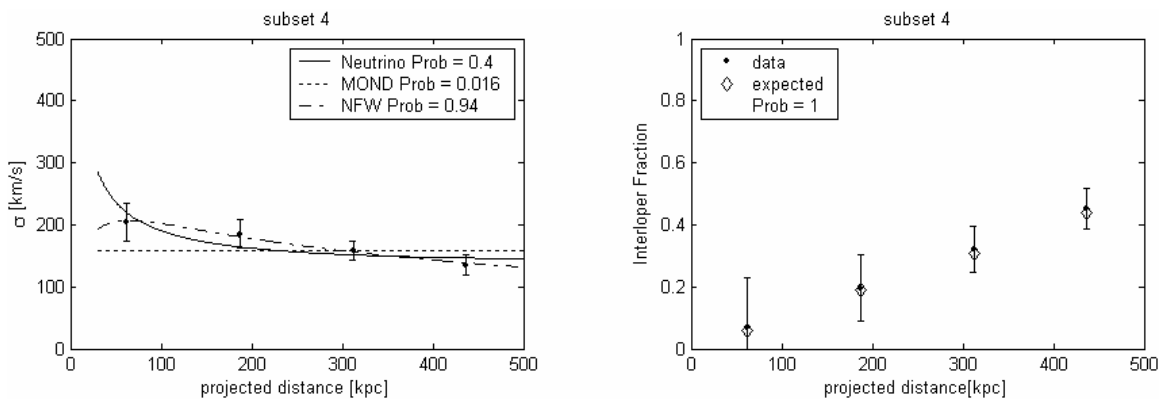
Figure B.2: Velocity dispersion profile plotted with the three cosmological models and interloper fraction of subset 4.
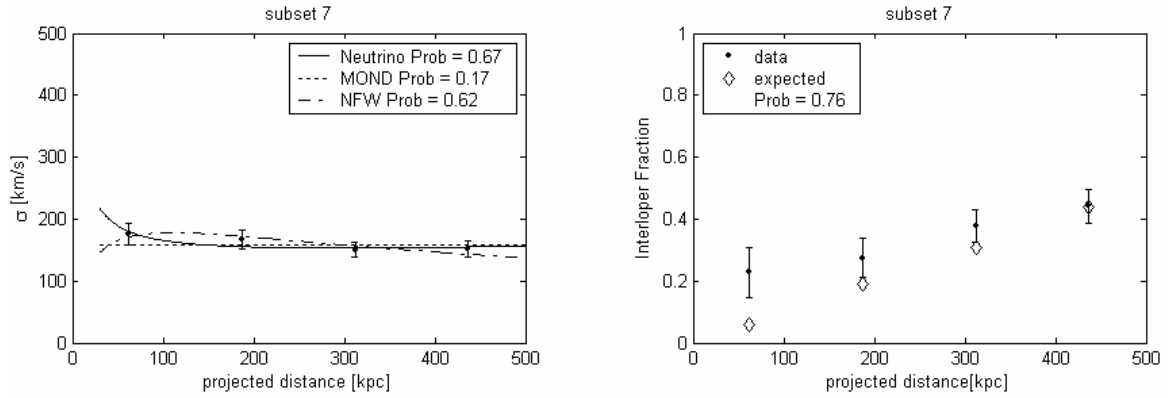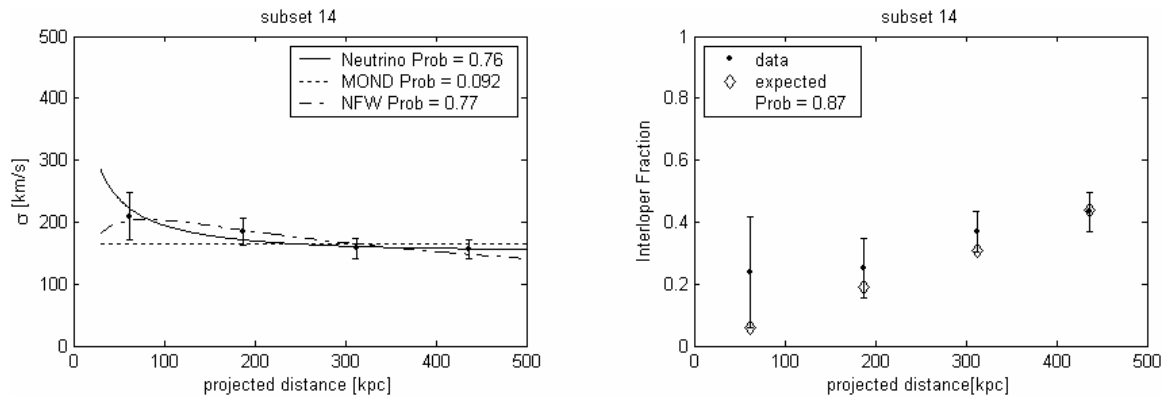
Figure B.3: Velocity dispersion profile plotted with the three cosmological models and interloper fraction of subset 7.
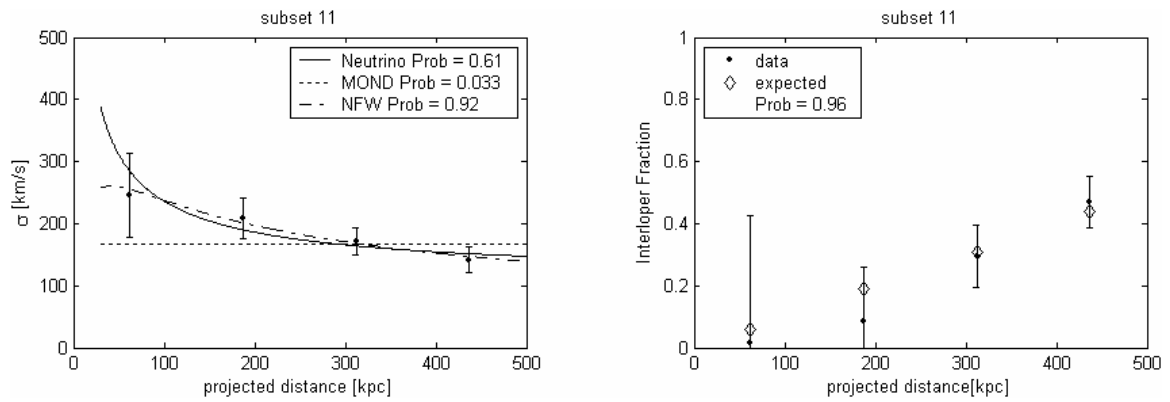
Figure B.4: Velocity dispersion profile plotted with the three cosmological models and interloper fraction of subset 11.

Figure B.5: Velocity dispersion profile plotted with the three cosmological models and interloper fraction of subset 14.

The plots on the left show the rotation curves of the data along with the three

cosmological models and the probabilities that they fit the data. The velocity dispersions

in red represent the planar region, and the velocity dispersions in blue represent the polar

region. The plots on the right show the expected interloper fraction (diamonds) per bin

compared to the interloper fractions found in the data. The data points with error bars in

both graphs are the average values found in each radial bin of the robust analysis

described in section 4.2.3.
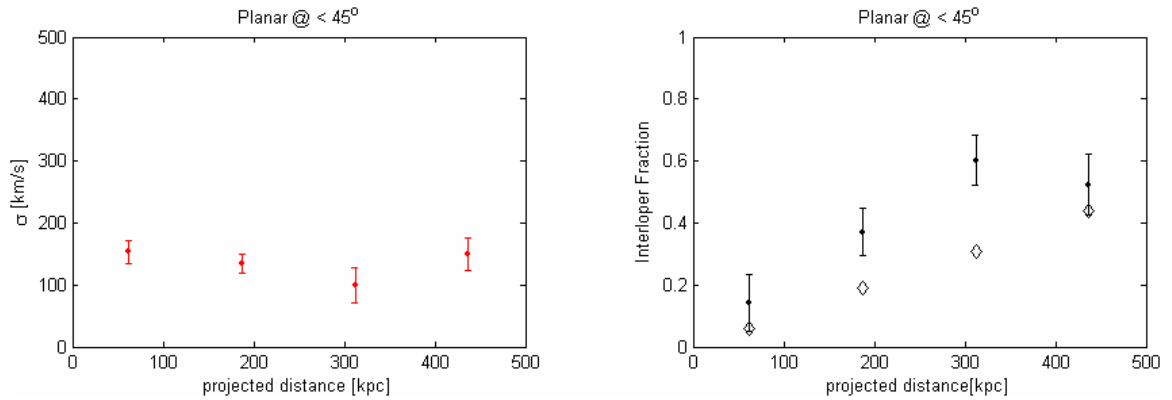
Figure C.1: Results for satellites in the planar region with primaries at tilt angle less than or equal to ~45 degrees relative to the axis of rotation.
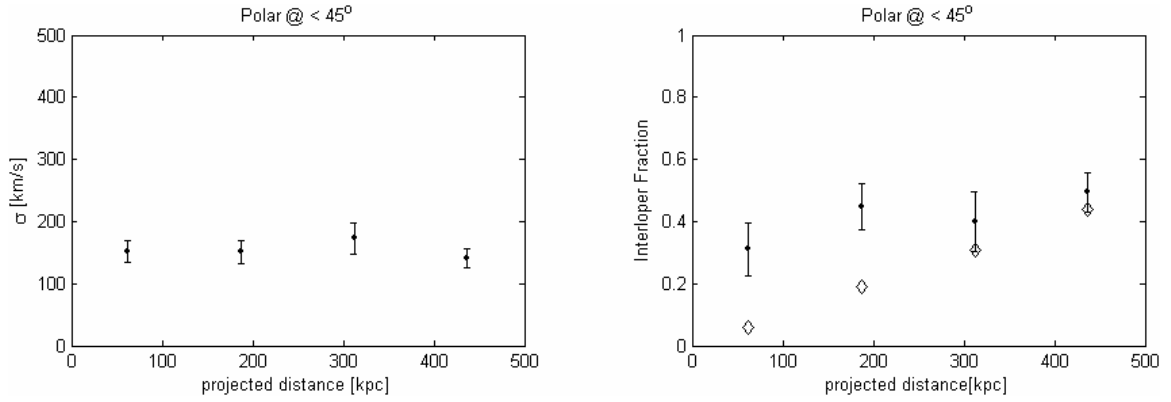
Figure C.2: Results for satellites in the polar region with primaries at tilt angle less than or equal to ~45 degrees relative to the axis of rotation.
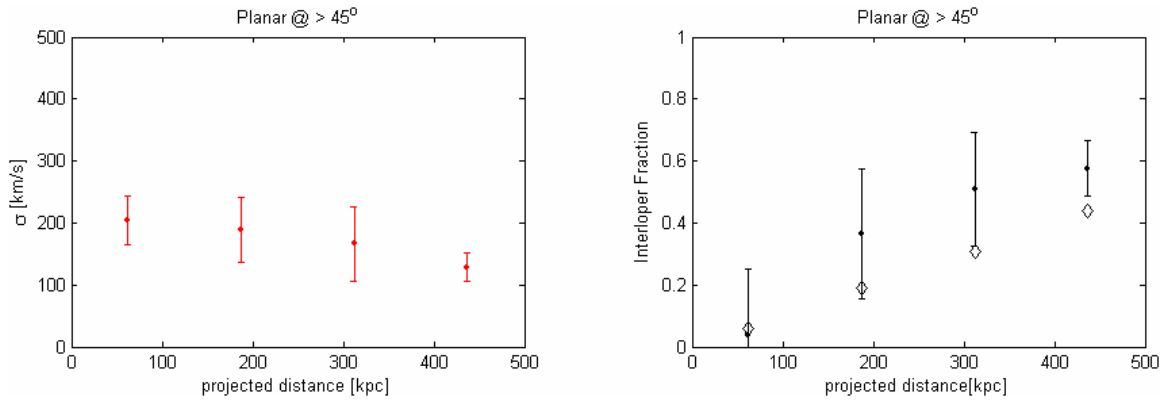

Figure C.3: Results for satellites in the planar region with primaries at tilt angle greater than or equal to ~45 degrees relative to the axis of rotation.
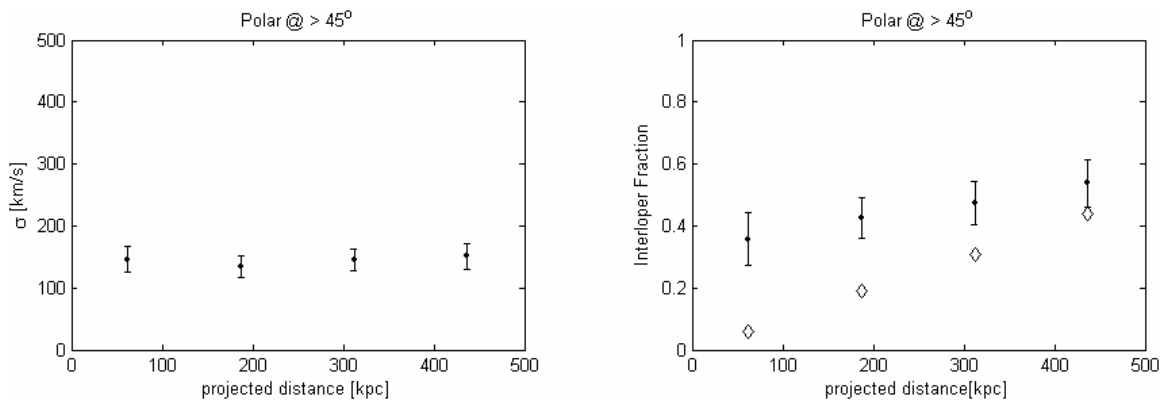

Figure C.4: Results for satellites in the polar region with primaries at tilt angle greater than or equal to ~45 degrees relative to the axis of rotation.